

Politecnico di Torino

---

Facoltà di Ingegneria



Electronic Engineering

Master's Thesis  
in  
Micro&Nano systems

**Design and fabrication of  
flexible wearable triboelectric  
nanogenerators**

Supervisor:  
Prof. Stefano STASSI

Candidate Author:  
Francesco MARRANO

DECEMBER 2020



---

# Abstract

An increasing demand for power sources accessible everywhere and at anytime led to the development of harvesting technologies to convert directly mechanical energy from the surrounding environment into electrical energy. A huge step forward in this field comes in 2006 with the invention of nanogenerators (NG). These devices can convert mechanical energy into electrical one, generating power of the order of some milliwatts. This low level, with the development of modern devices, is enough to directly supply some simple devices or to store energy into capacitors. The most promising type of nanogenerators is based on triboelectric effect. Triboelectric NGs can transform any type of mechanical movement into electrical energy utilizing the mutual movement of two materials. The simplicity of their working mechanism made triboelectric nanogenerators (TENGs) good candidates to develop wearable devices able to produce energy by everyday actions. The countless fields in which these types of devices can be applied range from the civil to the military environment, bringing numerous advantages in terms of equipment's lightness and size. This work's goal is to design a flexible, bio-compatible and with low environmental impact TENG in view of wearable use. To do this, transparent and conductive hydrogels were used as electrodes. They are cellulose-based and exploit ions coming from a dissolved salt to conduct electricity. Different salt concentrations have been investigated in order to have the best output performance. Furthermore, various conditioning circuits have been tested to understand which is the best way to manage power and to store energy into capacitors.



---

# Table of contents

<b>1</b>	<b>Background information</b>	<b>1</b>
1.1	Energy harvesting . . . . .	1
1.2	Triboelectric Nanogenerators . . . . .	2
1.2.1	Contact separation mode . . . . .	4
1.2.2	Linear sliding . . . . .	5
1.2.3	Single electrode . . . . .	6
1.2.4	Free standing . . . . .	6
1.3	Maximize TENG's output . . . . .	6
1.3.1	Charge generation . . . . .	7
1.3.2	Contact surface . . . . .	7
1.3.3	Avoid recombination . . . . .	8
1.4	Wearable TENG . . . . .	9
1.4.1	Challenges . . . . .	10
1.4.2	Types of wearable TENGs . . . . .	11
1.5	Military application . . . . .	13
<b>2</b>	<b>Device production</b>	<b>17</b>
2.1	Materials choice . . . . .	17
2.1.1	PDMS . . . . .	18
2.1.2	Hydrogel . . . . .	19
2.2	Device structure . . . . .	23
2.3	PDMS shell . . . . .	25
2.4	Photosensible cellulose-based ionogel . . . . .	26
2.4.1	Photopolymerization . . . . .	28
2.4.2	Ionogel production . . . . .	28
2.5	Assemblage . . . . .	30
<b>3</b>	<b>Influence of ionic-hydrogel on TENG's performances</b>	<b>32</b>
3.1	Performed tests . . . . .	32
3.1.1	Instrumentation . . . . .	32

3.1.2	Working mode . . . . .	34
3.2	Voltage and current outputs . . . . .	34
3.2.1	Voltage analysis . . . . .	34
3.2.2	Current analysis . . . . .	40
3.3	Power analysis . . . . .	41
<b>4</b>	<b>Conditioning circuit</b>	<b>50</b>
4.1	Power management . . . . .	50
4.2	TENG lumped model . . . . .	51
4.3	Full wave rectifier . . . . .	53
4.4	Half wave rectifier . . . . .	57
4.5	Bennet's circuit . . . . .	58
4.6	Comparison among different circuits . . . . .	64
<b>5</b>	<b>Material influence on TENG's performances</b>	<b>69</b>
5.1	Triboelectric effect . . . . .	69
5.2	Analysis on triboelectric properties of materials . . . . .	74
5.2.1	Single electrode mode . . . . .	74
5.2.2	Double electrode mode . . . . .	79
	<b>Conclusion</b>	<b>84</b>
	<b>Bibliography</b>	<b>85</b>

---

# List of figures

1.1	Power densities generation of different power sources. . . . .	2
1.2	Example of triboelectric series. . . . .	3
1.3	Operating Modes of TENGs. . . . .	5
1.4	Example of TENG treated with ions injection. . . . .	8
1.5	Example of TENG with a charge-trapping layer. . . . .	9
1.6	Examples of wearable TENGs. . . . .	10
1.7	Examples of 1D TENGs. . . . .	12
1.8	Examples of 2D TENGs. . . . .	13
1.9	Examples of wearable devices. . . . .	15
1.10	Example of military energy harvesting equipment. . . . .	16
2.1	PDMS Sylgard©184 (Dow Corning Corporation) . . . . .	18
2.2	Structure of PDMS. . . . .	19
2.3	Examples of dehydration of an hydrogel without (a) and with (b) salt in it. . . . .	20
2.4	Cellulose's unit. . . . .	22
2.5	Cellulose in amorphous and crystalline form . . . . .	22
2.6	Chemical structure of CMC sodium salt. . . . .	23
2.7	Hydrogel dehydration with and without elastomer layer. . . . .	24
2.8	Mold used to create a PDMS shell. . . . .	25
2.9	PDMS shell component (a) and complete shell (b). . . . .	26
2.10	Carboxymethyl cellulose. . . . .	27
2.11	Schematic of BAPO (a) and BAPO-OH (b) molecule. . . . .	28
2.12	Pictures of the mixing phase. . . . .	30
2.13	Ionogel's photopolymerization. . . . .	31
2.14	Single electrode triboelectric device. . . . .	31
3.1	Used setup for measurements. . . . .	33
3.2	Schematic of open circuit configuration. . . . .	34
3.3	Voltage graphs in open circuit mode. . . . .	35
3.4	Voltage trends of different samples in open circuit configuration. . . . .	36

3.5	Voltage variation in time. . . . .	37
3.6	Comparison between voltage outputs by different molar concentration ionogels. . . . .	39
3.7	LiCl 1mol/L voltage behavior. . . . .	39
3.8	Peak-to-peak voltage vs molar concentration. . . . .	40
3.9	Schematic of close circuit configuration. . . . .	40
3.10	Peak current vs molar concentration. . . . .	41
3.11	Schematic of resistor circuit configuration. . . . .	42
3.12	Voltage peak values for different ionogels. . . . .	43
3.13	Examples of output voltage waves using different resistors. . . . .	44
3.14	Schematic of resistor circuit configuration . . . . .	44
3.15	Current peak values for different ionogels. . . . .	45
3.16	Current and Voltage peak values for different ionogels. . . . .	46
3.17	Power density values for different ionogels. . . . .	48
3.18	Power density peaks versus molar concentration. . . . .	49
4.1	Schematic of TENG with parameters. . . . .	53
4.2	Full wave bridge rectifier. . . . .	54
4.3	Schematic (a) and output voltage (b) of the used Full wave rectifier. . . . .	55
4.4	Voltage using Full wave rectifier. . . . .	56
4.5	Stored energy using Full wave rectifier. . . . .	56
4.6	Schematic (a) and output voltage (b) of the used Half wave rectifier. . . . .	58
4.7	Voltage using Half wave rectifier. . . . .	59
4.8	Stored energy using Half wave rectifier. . . . .	59
4.9	Bennet's circuit . . . . .	60
4.10	Voltage using Bennet's circuit. . . . .	62
4.11	Stored energy using Bennet's circuit. . . . .	63
4.12	Stored energy using Bennet's circuit. . . . .	65
4.13	Voltage and energy stored using different conditioning circuits. . . . .	66
4.14	Led lighting via TENG. . . . .	68
5.1	Triboelectrification example. . . . .	70
5.2	Quantified triboelectric series. . . . .	72
5.3	Quantified triboelectric series. . . . .	73
5.4	Triboelectric series containing ITO. . . . .	75
5.5	Charging behaviors of PDMS using different materials. . . . .	76
5.6	Single-electrode TENG voltage output using different materials. . . . .	77
5.7	Comparison among peak-to-peak voltage values. . . . .	78
5.8	Aluminum (a) and PDVF (b) current wave. . . . .	79
5.9	Comparison among peak-to-peak current values. . . . .	80

5.10	Conductive foil made of PET and ITO. . . . .	81
5.11	Double-electrode TENG voltage output using different materials. . . . .	82
5.12	Comparison among voltage (a) and current (b) output values using double-electrode TENG. . . . .	83

---

---

## CHAPTER 1

---

# Background information

### 1.1 Energy harvesting

The growing requirement of accessible power due to a wide spread of portable electronics has immediately urged scientists to find new clean and portable energy sources. Until now, all the electronic devices are supplied by electric current taken directly by power grids or by batteries which represent not only an additional weight but also a waste difficult to dispose of. Moreover, batteries have limited life and need to be substituted, so it is necessary that they are placed in easily accessible positions. However, this is not always possible, especially talking of biomedical applications. It appears clear that batteries have a lot of issues that would be better to overcome. Another important trouble of a massive using of electronics is that the majority of consumed energy, today, comes from natural nonrenewable resources. Obviously, they are limited and impossible to be generate artificially. A lot of researches are focused on looking at alternative ways to overcome a possible energy crisis. An interesting solution can be represented by energy harvesting characterized by clean and self-sufficient power sources. The expression "energy harvesting" refers to the capability of electronic devices to obtain energy directly from the environment where they are situated. Thanks to energy harvesting devices it is possible to recover a lot of energy that otherwise would be wasted. In fact there are a lot of sources of energy like solar light, vibration, wind, water wave, human motions and vehicle motions that cannot be efficiently harvested using a conventional approach. This is due to the fact that these sources are characterized by very low frequencies and so it is necessary a new technology to store the energy produced by them. This new technology came in 2006 with the invention of nanogenerators (NGs). Different kind of nanogenerators have been produced during the last years basing their working principle on particular properties of materials. There are devices that exploit piezoelectric effect (PNG) [41], triboelectric effect (TENG), thermoelectric effect (TEG) [13] and pyroelectric effect (PYG). However NGs

are able to provide only few milliwatts (mW) of power which, until some years ago, were too low for a practical using. In order to have an idea about the density of power produced by energy harvesting devices, could be useful to take a look at Fig. 1.1. Observing the

Energy Source	Types	Energy-Harvesting Method	Power density
Radiant	Solar	Solar cells (indoors)	$<10\mu W/cm^2$
		Solar cells (outdoors, sunny days)	$15mW/cm^2$
	RF	Electromagnetic conversion	$0.1\mu W/cm^2$ (GSM)
		Electromagnetic conversion	$0.01\mu W/cm^2$ (WiFi)
Mechanical	Wind Flow and Hydro	Electromechanical conversion	$16.2\mu W/cm^3$
	Acoustic Noise	Piezoelectric	$960nW/cm^3$
	Motion	Piezoelectric	$330\mu W/cm^3$
Thermal	Body heat	Thermoelectric	$40\mu W/cm^2$

Figure 1.1: Power densities generation of different power sources [23].

values in Fig. 1.1, it appears clear that the use of all these kind of alternative sources of energy is interesting only if associated to very low-power devices. In fact, a nanogenerator can supply an electronic tool in real time only if the requested power is not excessive. Moreover, it is important to take into account that the mentioned sources are not able to provide a continuous and stable generation of energy. This means that it is necessary to consider solutions where different alternative sources work together or even hybrid solutions. Another option could be to store energy when it is not requested, in way to use that in the right time. For this last choice it is needed to think about an appropriate storage circuit and overall an appropriate storage device. Good candidates for this role are supercapacitors which have a very high versatility thanks to an excellent reversibility, a very long cycle life and less problems than batteries due to Joule heating. They also enjoy an easy integration in electronics and can be made in such a way to be flexible. On the other hand, devices that exploits energy harvesting can be used also as self-powered and real time sensors. This type of sensors does not require any kind of power supply and so could replace all that sensors that today are powered by external power-sources. There are a lot of environments where these sensors could be extremely useful, for example, they can be used to keep track of body parameters during sports or to monitor vital activities in biomedical or military applications. Also smart tools that everyone frequently uses can be rebuilt using energy harvesting devices, allowing an important reduction in power consumption. One of this smart devices already realized as prototype is a keyboard that does not need any power supply [26].

## 1.2 Triboelectric Nanogenerators

One of the most interesting nanogenerator is without any doubt the triboelectric one. TENG devices are able to transform almost any kind of mechanical motion into electricity.

The sources can be different: pressure, vibrations, wind, rain or body motion. The principle behind these devices is to exploit at the same time both the triboelectric effect and the electrostatic induction. TENGs based their mechanism in the generation of charges that once moved thanks to a difference of tension, produce a current. A very important step for the design of a triboelectric nanogenerator is the choice of materials. In fact a TENG can work if there are at least two different materials put in contact. Thanks to the mutual movement of the the two materials, static opposite charges appear on their surfaces and as a consequence on the back side of the materials it is possible to find the same amount of charges but with opposite sign. The difference in polarity of the charges present on the surfaces lead to an huge potential difference that is the base of the working principle of TENGs. Based on the characteristics of the material chosen more or less charges are generated. In order to know in advance the properties of the materials, they are categorized depending on polarity and intensity of acquired charge. Positive triboelectric materials tend to accumulate a positive charge on the contact surface and vice-versa for negative triboelectric ones. An example of triboelectric series is reported in Fig.1.2. Usually the more positive triboelectric materials are placed on the top of the list and the

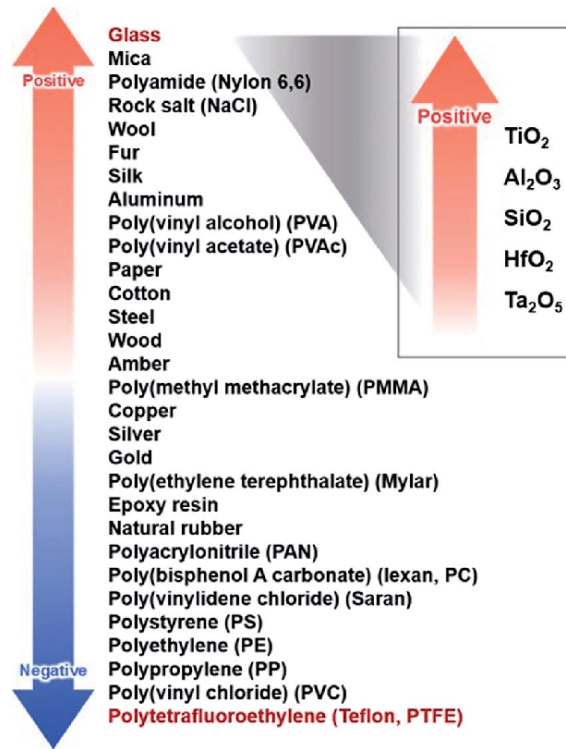


Figure 1.2: Example of triboelectric series [28].

more negative on the bottom. This means that the materials are listed in order of polarity from the top to the bottom. To maximize the generation of charges it is better to put in

contact materials that are far each other in the triboelectric series. In fact if materials with similar polarity are put in contact there is not any generation of charges or those generated are not sufficient for any kind of application. Triboelectric series are constantly updated so that new materials can be used to produce triboelectric devices. An interesting aspect is that human skin is one of the most positive triboelectric materials, so it is possible to create very simple devices that exploit directly the human body as part of the structure. Since triboelectric materials can be indifferently conductive or non conductive, in this second case must be ensured that charges are free to move in order to generate a current. Usually happens that the chosen materials are dielectric and so it is necessary to attach two conductive electrodes to their back side. Each electrode have the same charge of the back side triboelectric material to which is attached. This expedient allows a free movement of charges inside the electrode and, in this way, they are no more confined in the material as superficial distribution. Once that the two materials of the device are charged positively or negatively, a huge potential difference is created between them and, obviously, the same variation in potential can be observed between the two electrodes. At this time, to generate a movement of charges it is necessary to connect one or both the electrodes to an external circuit. The configuration changes based on the type and on the working mode of device built. In fact the triboelectric nanogenerator can be realized exploiting at least 4 different operating modes:

- contact separation;
- linear sliding;
- single electrode;
- free standing.

All the considerations made until this point are valid for every used configuration, but between them there are some differences about the mechanical movement and the external circuit. The mentioned modes are represented schematically in Fig.1.3 and are explained more in details in the following sections.

### 1.2.1 Contact separation mode [1]

As suggested by the name, this operating mode is based on the contact separation process of two different triboelectric materials. At the begin the two layers are separated and neutral, once they touch, the more triboelectrically positive left electrons in favor to the more triboelectrically negative but, since the two materials are attached, the whole system is still neutral. When the two parts of the device are separated again, both inner surfaces present an equal and opposite surface charge. To maintain the electric equilibrium, equivalent and opposite charges appear in the corresponding electrode and as a

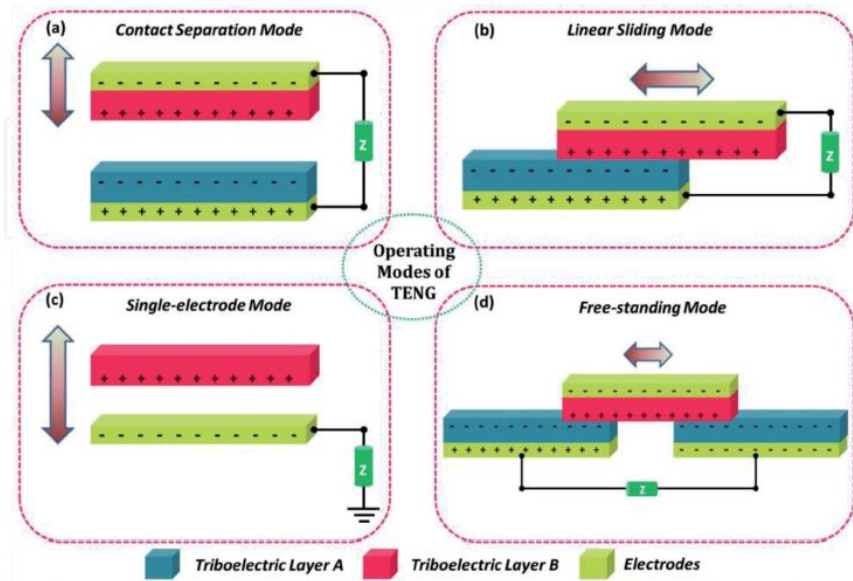


Figure 1.3: Operating Modes of TENGs [1].

consequence there is a voltage difference between electrodes. The maximum voltage difference is reached in correspondence of the maximum displacement. The resultant system appears as an open circuit, so it is necessary to add an external circuit which connects the two electrodes. Thanks to the potential difference between them, electrons start to flow in order to balance the electrostatic field. It is necessary that the actions described until now do not happen only one time, but they must be repeated with a certain frequency. In fact once the two triboelectric materials touch again, the surface charges in the inner surfaces disappear and electrons flow back. This mechanism allows to produce an alternate current of some mA and an alternate potential difference between electrodes with peaks of the order of hundred of Volts.

### 1.2.2 Linear sliding [1]

This model is similar in geometry to the contact separation one. In fact, also this is composed of 2 different triboelectric materials face to face which are in contact and their back parts are connected to two electrodes. The two electrodes are connected each other by an external circuit, similarly to the contact separation case. This time the charges on the surfaces are created by a relative sliding in parallel of the two components. In a similar manner to the previous case, the two materials are polarized and so also on the electrodes appear charges and obviously a potential difference. In order to fully balance the created electric field, electrons start to flow across the external circuit. Thanks to the periodicity of the sliding movement an alternate output is generated. One clarification can be useful:

the sliding movement is not only a planar motion but can be also a cylindrical or disc rotation.

### 1.2.3 Single electrode [1]

In the two modes illustrated until now, the parts composing the device are linked each other thanks to an external circuit, but it exist another configuration that does not require the connection of both the elements to a circuit. In fact the single electrode method has only one electrode connected to ground and the other triboelectric material is free, so does not require any electrode. Once that the triboelectric material is properly charged, the connection to ground allows the flux of electrons. Also this time the current generated is AC. The structure of this type of TENG is very simple, but the performances are not very good. Since one of the two triboelectric material is unconnected, this solution is particularly indicated for movable object that can use the floor as mechanical part of the device. Moreover, this method makes possible to use materials on which is impossible to attach an electrode. An interesting example can be the human skin that, as already mentioned, is a very good triboelectrically positive material. The possibility to use human body as structural component of the TENG leads to a very simple fabrication of nanogenerators since they need only one material and also the geometry obtained is thinner.

### 1.2.4 Free standing [1]

This last method to implement a TENG is based on one free movable layer of triboelectric material which is used to charge two different pieces of another triboelectric material respectively connected to two electrodes. These last parts are very close each other and so when they polarize, since charges of the same species tends to reject, an asymmetric charge distribution is achieved in each piece. The two electrodes are linked by an external circuit, so electrons start to flow to balance the local potential distribution.

## 1.3 Maximize TENG's output

As it is possible to appreciate from the previous analysis, TENGs are very simple devices in which materials properties assume a lot of relevance in order to have an appreciable output. In fact, a figure of merit of TENGs is the square of the surface charge density [35] and therefore the goal of researches is to maximize this parameter. There are some measures that allow to improve the surface quantity of charge:

- improving of charge generation;
- increasing of contact surface;
- avoiding of recombination.

### 1.3.1 Charge generation

The main strategy to improve TENGs' outputs is to increase the charge generation. In fact, having an increase in total charges, obviously a bigger charge density is achieved. To have the maximum polarization, the choice of the triboelectric materials became fundamental. As already said, bigger is the distance between the two material in the triboelectric series and big is the amount of charges generated. However, there are some processes that allow to change the properties of a substance, increasing the capability to take or leave electrons. Changing the intrinsic characteristics of a material, it can become more triboelectrically positive or negative based on the kind of used doping ions. It could be also interesting to consider that the increase in dielectric constant can be an advantage because high dielectric constant materials usually have an high-density charge generation. Ion injection, plasma treatment or radical injection are three powerful methods to strongly improve the output performances of TENGs. A big advantage of these methods is that charge density can be manually controlled. Some experimental studies empathize that these processes are particularly useful for TENGs which exploit the contact- separation mode, instead do not seem particularly interesting for linear-sliding and are completely useless for single electrode one. To understand how a TENG treated with one of the mentioned techniques works, it can be helpful to see Fig.1.4. The example reported in this figure is about a triboelectric material treated with ions injection. The bottom part of the system is composed by a triboelectric material attached to an electrode. During the negative ions implantation the electrode is connected to ground (Fig.1.4a). In this way, since the triboelectric matter is negatively charging, electrons tends to transfer to ground from the electrode, making it positively charged (Fig.1.4b). Once that the implantation process is finished, the electrode is ready to be connected to another one by an external circuit (Fig.1.4c). When the top electrode goes close to the bottom part, positive charges move from the bottom electrode to the top one (Fig.1.4d). When the two components are fully in contact, all the charges that were present in the bottom electrode are gone into the top one (Fig.1.4e). During all this time a current flow is measurable into the external circuit. When the top electrode leave the bottom part, a created potential difference between the two electrodes causes a back transferring of positive charges from the top electrode to the bottom one producing again a flux of current but, this time, in the opposite direction (Fig.1.4f).

### 1.3.2 Contact surface

Charge density is directly proportional to the contact surface, so a good idea to increment the generation of charge is to increase the number of contact points in the device. In order to do this, avoiding to have a large TENG, a good solution is to fabricate nanoscale or microscale surface structures. This means that a rough surface is much more performing than a flat one. There are a lot of methods to increase the roughness of a plane, for example

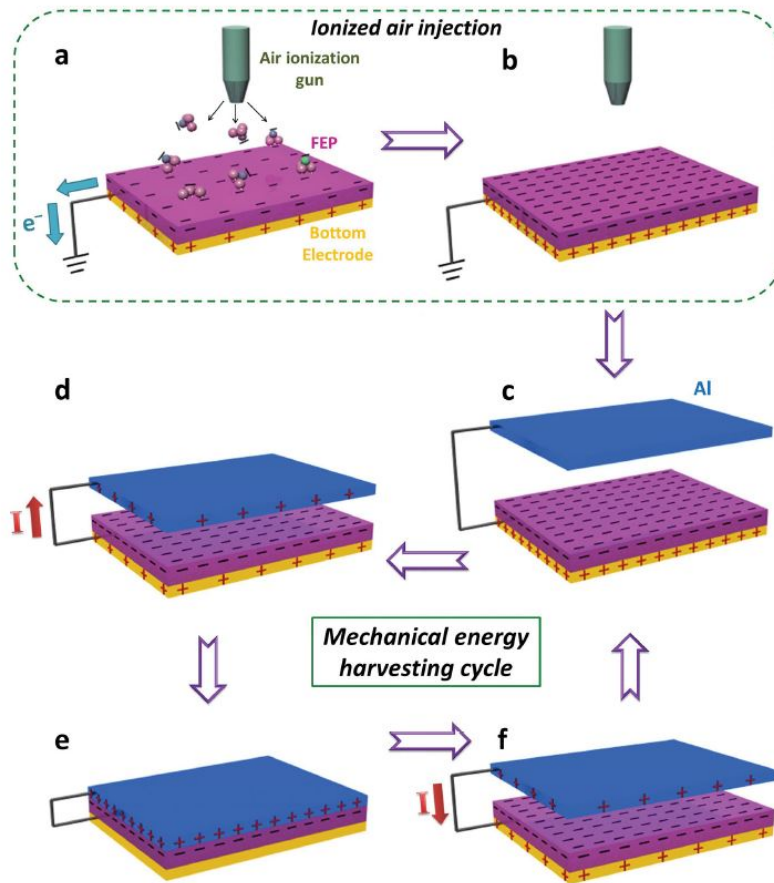


Figure 1.4: Example of TENG treated with ions injection [43].

lithography, plasma etching, wet etching but also other low cost techniques like using sandpaper as a mold for the triboelectric layer. Moreover the presence of microstructures improves the performances in humid environments of TENGs which exploit hydrophobic surfaces. This aspect is not of little importance considering that humidity is one of the most important issues for TENGs. Another significant feature in TENGs is the adhesion energy. In fact, this is a point different to the roughness and also difficult to investigate. Nevertheless, some researches have reported that viscoelasticity and contact adhesion can have a big impact in charge generation.

### 1.3.3 Avoid recombination

An interesting aspect which is not always taken into account is the effect of charges recombination. In fact, once that the triboelectric material's surface is charged, the same amount of charge, but with opposite sign, is present on the back side of the material. This

charge configuration leads to the creation of an electric field inside the matter. Thanks to that field, charges can move and recombine causing a reduction of the charge density on the surface. Thus became important trying to block the recombination of charges in favor of an accumulation of them. In order to achieve this task, some charge-trapping layers are been studied. These structures are not always new materials, but can be also particular conformations of the matter itself that are able to act as insulators. For example in polymers, a good charge-trapping layer is constituted by physical defects such as chemical defects or imperfections in the lattice. Aromatic polymers, in particular, are characterized to have the main chains with nonuniform energy levels and this correspond to have a lot of trapping site. This means that, adding an aromatic substance between the triboelectric material and the electrode, it leads to a remarkable increment of TENG's output. Another very good material which can be used as charge-trapping layer is the polydimethylsiloxane (PDMS) which has the additional characteristic to be extremely stretchable.

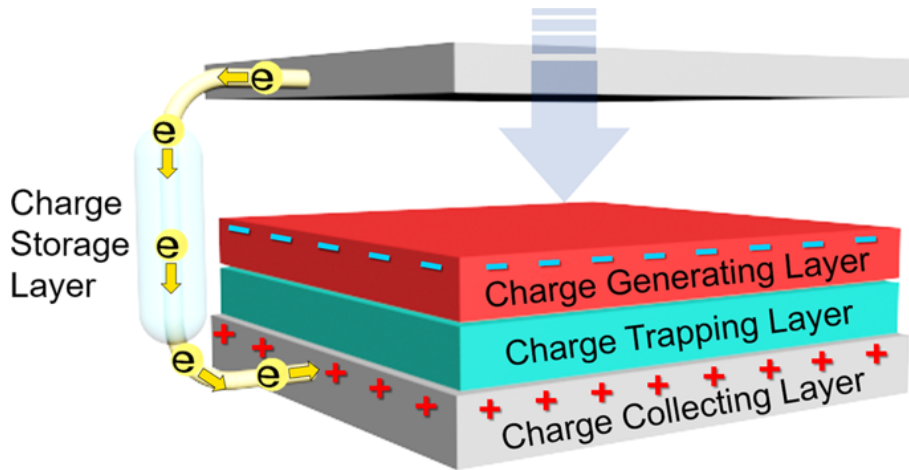


Figure 1.5: Example of TENG with a charge-trapping layer [6].

## 1.4 Wearable TENG

The simplicity that characterize TENGs led early to think about wearable devices based on TENGs. In fact body motion is one of the sources of energy that can be used to store energy. The best way to exploit this type of energy is to built a wearable device which can transform each movement into electricity. It is impressive to think how much energy is wasted during a walking or a running. Thanks to each movement of the body, clothes stretch and relax and these variations can be exploited to stimulate a TENG device. In this way the everyday outfit will became a power source like a battery able to power body-sensors or to act themselves as sensors. However, wearable TENGs are not so simple to design. In fact, there are a lot of factors that it is necessary to take into account.

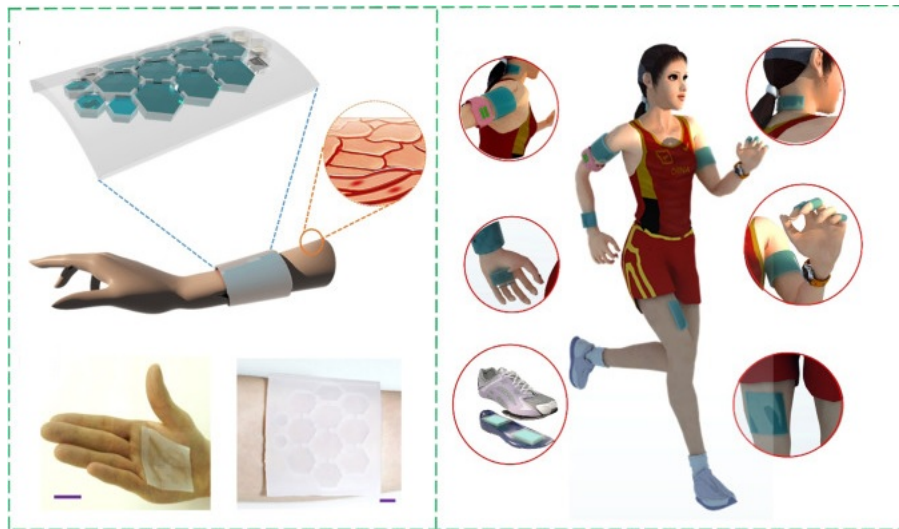


Figure 1.6: Examples of wearable TENGs [27].

### 1.4.1 Challenges

The first requirement for a wearable device is obviously the flexibility. In fact, since the TENG must be on the human body it is necessary that it does not obstacle any movement and follows all the actions without resistance. The aim of these tools is to facilitate the everyday life and not to make it harder. So it's important that wearable TENGs are able to extend and to deform according to the own use. Definitely, they must assure the maximum comfort because they are built in order to be dressed for long periods. Since these kind of devices are thought to be in contact with the skin it is needed that the used materials are biocompatible and do not cause any disease both in short and long period. Another important point for wearable TENGs is the weight. TENGs have to be projected in order to be portable and to substitute clothes, so they must be lightweight and do not have to add load. Despite the used materials must be stretchable and lightweight, the device must be also robust, able to support stresses for years. In fact the wanted TENGs must be durable in time and capable to be used several times. This means that they should be also washable, so they could stay in water without any damage. Since the created device will be a cloth, it should be breathable so as not to hurt the skin. All the consideration made until now do not concern only the triboelectric materials, but also the electrodes. In particular, it is important to study a conductive material that is able to stretch and deform allowing the maximum degree of freedom for movements. Extensive studies are been made in order to find some good flexible electrodes. One of the most employed solution was metal electrodes with particular shape as metal nanosheets or metal flakes. Other interesting solutions could be to use liquid metals, in fact some metals are liquid at room temperature and can be injected into microchannels of elastomer. These proposals

are surely shape adaptive, but it should be checked out if they are usable in wide areas like that of a shirt or a pants. Another interesting option is given by gels like hydrogels and ion gels. These materials are characterized to very good mechanical properties and an high biocompatibility. The last issue that is not considered a lot, talking about wearable devices, is the necessity to have an external circuit flexible and adaptable like the triboelectric materials which form the TENG. In fact, the external circuit, consisting of wires, rectifier and device of storage, is an integral part of the TENG and cannot be considered as a separated component. To obtain good results from this point of view, it is necessary to investigate new type of materials. This is the reason why a lot of researches are about flexible supercapacitors in order to replace ceramic capacitors which are limiting. To sum up, the main challenges to overcome in order to create a wearable TENG are:

- flexibility;
- stretchability;
- comfortability;
- washability;
- breathability;
- lightweight;
- robustness to continuous stress.

#### 1.4.2 Types of wearable TENGs

Following the goal of achieving wearable TENGs, different ways to obtain the wanted result are been thought. Remembering the fabrication's process of clothes, starting from natural or synthetic fabrics, TENGs based on fibers and yarns (1D TENGs) are born. In parallel, 2D TENGs are been studied with the aim of overcome the issues of 1D TENGs. These last devices are realized in situ and tends to be more feasible than the fiber based ones. In the following sections are described the two mentioned methods to produce wearable TENGs.

**1D TENGs** In 1D TENGs each fiber is designed in order to be a single and independent nanogenerator. After their production, they have to be weaved in order to form a fabric. The single 1D TENG can be made in different ways, the two main solutions are coaxial cables and twisted yarns. The first ones see usually a polymer used to encapsulate the triboelectric materials. Internally there is a core formed by two triboelectric materials, the electrodes, instead, can be found as coil or in straight form. Anyway during the last years a lot of solutions are been studied and 1D TENGs are been invented both with the core

of electrode or of triboelectric material and in the same way the shell. For what concern yarns, instead, they are built twisting together two or more fibers. Their working principle is the contact-separation or the friction between the fibers that compose the yarn. Thanks to the characteristic of exploiting two separated fibers, yarns are more versatile in terms of choice of materials and working mode. Fig1.7 reports some examples of 1D TENGs. All the 1D TENGs are extremely flexible and could be useful both as power sources and sensors, but there are also a lot of issues that must be considered. Electrically speaking, despite each fiber is a complete device, the power density produced is very low and so it is necessary to link together different fibers in order to have an appreciable output. This is not always simple and the connection in parallel of a lot of TENGs must be managed in a correct way. It is also important to remember that 1D TENGs are not the finished device but they must be weaved in order to become cloths. Thus they have to pass an industrial process of transformation, so it is necessary that fibers are able to support mechanical stresses due to industrial processes. They have to be sufficiently robust and capable to resist to traction. Remembering that these devices will be used as clothes, the prerequisites of resistance to usury and washability remain. Also the length of fibers is a big issue, in fact now it is not simple to produce long TENG fibers ready to be processed. Another big problem is the diameter of these devices. In fact, due to the presence of a lot of layers to compose a single fiber, the final result is thick and this made it difficult to manage. The last important issue to consider is the large scale production of these TENGs that at the moment is not possible or, anyway, difficult to implement.

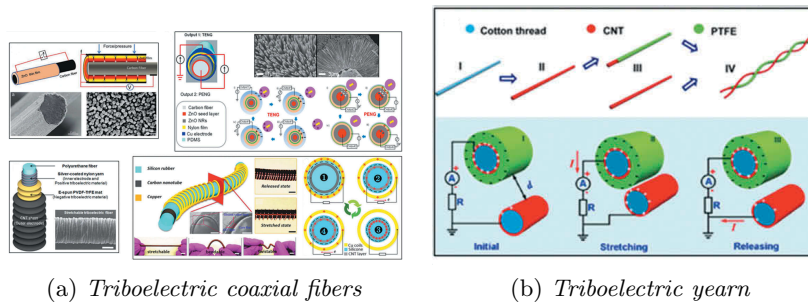


Figure 1.7: Examples of 1D TENGs[8].

**2D TENGs** With regard to 2D wearable TENGs, they are nanogenerators created by the superposition of different flexible and stretchable triboelectric materials. If two layers of triboelectric materials have the required mechanical properties and exploit also a good bio-compatibility they are optimal candidate to be triboelectric materials for 2D TENGs. In fact, associated with a stretchable electrode they can easily form a wearable triboelectric device. It is possible also to coat existing cloths with wanted triboelectric material in order to create a TENG, this is the case of textile fabricated by "in situ" technique. These kind

of devices are characterized to have a lot of advantages but also some issues. They are extremely easy to fabricate, the cost of production is not high and a production in large scale is possible too. There is not the problem of connecting various fibers each other, typical of 1D TENGs, because the finished product is already an area that can be modeled to assume the wanted shape. 2D TENGs assure a wide choice of materials that can be used and the mechanical properties of the finished product derive directly to those of the fabric employed. Since the covered area by these type of smart textiles can be relatively big, the choice of electrodes able to flex and to not be heavy is important and not so simple. Some big issues due to 2D TENGs are comfortability and breathability. In particular since they usually are not porous structures, they tends to loose the natural skill of tissues to be air-permeables.

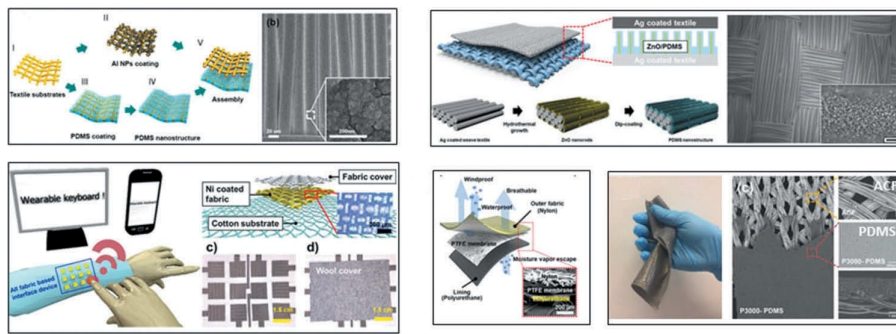


Figure 1.8: Examples of 2D TENGs [8].

## 1.5 Military application

Devices based on TENGs are very versatile and, together with others energy harvesting systems, are destined to see a lot of progresses and a wide spread in many environment. The particular development of the Internet of things (IoT) has made particularly easy to have systems of tools interconnected and able to interact each other. In the near future wearable electronics are called to assume a predominant role and the necessity to have flexible and comfortable devices is becoming increasingly urgent. Obviously, one of the most issue of IoT is the need to power all these devices and in particular to easily integrate the power sources. The solutions to this problem is not always immediate and a big help can comes from energy harvesting. In fact, as already said, wearable nanogenerators are good candidates to replace batteries, in particular if associated with devices of energy storage like flexible supercapacitors. TENGs, for example, can be integrated in a lot of everyday objects and can become an ordinary system of power production. However, the two field where TENGs could be markedly interesting are the biomedical and the military one. In this thesis some aspects will be explored in order to evaluate their introduction as

powerful resource for Army.

All the governments across the world are giving ever greater importance to equip soldiers with state-of-the-art devices in order to have the maximum military performance associated with the maximum comfort. A constant program of modernization is in place for all troops and wearable devices are the protagonists. In fact, they enjoy of an easy integration with the uniform, an adaptability to harsh environment and a very good comfortability. In front of this scenario which sees the use on the battlefield of smart watches, GPS, advanced helmets, wearable computers and various type of sensors, nano-technology assume a role of predominance. The concept of wearable electronics owes its birth to military field tanks to a researcher team of the Georgia Institute of Technology, granted by US Defense Advanced Research Project Agency, that invented a smart T-shirt considered one of the best invention in 2001. Smart textiles are now considered the next frontier in Defense. These systems are now thought to detect the health status in a non-intrusive way, to manage stress, to catch external information like temperature or the presence of toxic gases, to provide power or to charge batteries and devices of storage. The presence of all these systems of monitoring is justified by the necessity to pay more attention to the external environment but in particular to track constantly the vital parameters of a soldier in order to provide the right alerts. The possibility to collect all the data in a central computer is also a substantial help to the management of both operations on the battlefield and emergency's situations like the necessity to have medical treatment. To understand the importance of these type of innovations just think that the U.S. army has allocated 50 million of dollars to MIT in order to create the uniform of the future. Moreover the market of smart textiles is estimated to reach the size of 5.5 billion of dollars by 2025. In front of a so massive use of electronic devices, power become soon an issue. The problem of army energy supply is on the table of many countries' future projects. In U.S.A, for example, George W. Bush signed a law, in 2007, in order to obtain 25% of electricity consumed by military buildings from renewable energy by 2025. Barack Obama reinforced this agreement and wanted that Army opened a laboratory to develop energy technologies for combat vehicles. The research in new energy supply technologies did not stop to stationary projects to be located on buildings or vehicles, but arrived on the battlefield by the examination of new systems capable to be carried by soldiers. Today, batteries are the only sources of portable power, but they add an huge amount of weight to the soldier equipment compromising the mobility and making the warfighter more vulnerable on the battlefield. Soldiers are incredibly dependent to batteries and power sources in general, every time these are not available or must be delivered, the life of the soldier is in danger. New compact power sources able to support long runtime missions are needed. Energy harvesting devices are a possible very interesting solution to have always energy ready to be used. In fact, kinetic and solar energy harvesting can store energy or supply devices on-the-go. For example, a TENG could be able to power continuously the troops on the ground exploiting the constant oscillation of legs. Another interesting solution can be also exploiting hybrid solution

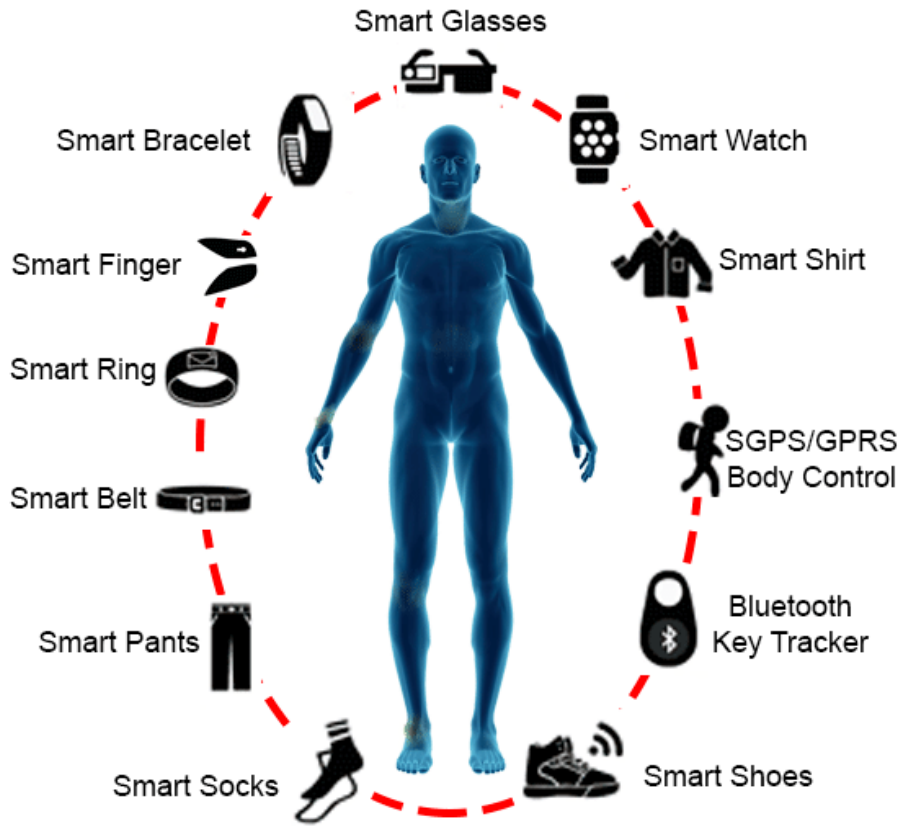


Figure 1.9: Examples of wearable devices [31].

utilizing different combination of energy harvesting devices in order to produce power in different type of situations. For example, a hybrid solution which exploits solar cells and triboelectric textiles together is able to provide electricity both when there is the sun and when the soldier moves. The U.S. Army’s Communications-Electronics Research, Development and Engineering Center, or CERDEC, has already developed energy harvesting technologies which converts soldier’s movements into usable energy ready to supply wearable devices like night vision goggles or radios. Thanks to these inventions, the warfighter can bring fewer batteries and, also, he is independent from power supplies for long time. Energy harvesting solutions, like TENGs, are lightweight, perfectly integrable with the uniform and compatible with the life on the battlefield. Nanogenerators, indeed, can be embedded into the uniform or even replace some of its parts, freeing up space for water, ammunition and food. In fact, should be considered that the soldier is often called to act in harsh environment for long period of time. Thus, the comfortability of the equipment is

imperative and the possibility to reduce until the 40% of the weight giving up on batteries is surely attractive. It is important to keep in mind that wearing uncomfortable and heavy uniform compromises the performances of a warfighter putting his life at risk. Another big advantages brought by energy harvesting devices is the reduction in terms of time needed to substitute batteries. In fact since in a war scenario the failure due to forgetfulness and distractions is not contemplated, before to start a mission all the batteries are changed. This operation leads to a loss of time that can reach over 40 minutes. These waste of time can be reduced or even canceled if systems like TENGs were adopted. In order to understand an additional situation in which energy harvesting devices can be very useful it is possible to think to a battery lost during a military operation, nowadays there are no way to use the relative equipment in that situation. However, this problematic can be avoided if nanogenerators were used just as a support system to power the electronic kit. Energy harvesting applications are countless and very powerful, so the study of one particular type of nanogenerator results to be extremely attractive. For this reason, a deep investigation about the design of a possible wearable triboelectric nanogenerator is extremely valid.



Figure 1.10: Example of military energy harvesting equipment [3].

---

---

## CHAPTER 2

---

# Device production

### 2.1 Materials choice

The goal of this thesis is the production of a new type of triboelectric nanogenerator which is wearable, soft, stretchable, low cost, compliant with human tissue and resistant to stress due to frequent motion. Another important characteristic that could be useful for this type of device is the transparency which is an interesting feature for most of bio-compatible sensors because allows a visual transmission of informations. The developed device, obviously, is not timeless but have a natural life cycle like every cloth. This problem must be taken into account, in fact, in future, TENGs could generate a massive electronic waste with a consequent environmental issue due to the non-degradability of employed materials. It appear clear that the choice of materials for the wanted device must guarantee a good compromise between all the previous considerations. The first decision to made is about the operating mode of the final system. The single electrode mode seems to be a good choice. In fact, talking about a wearable device, it is easy to think of human skin as the second triboelectric material. Moreover with the single electrode configuration, the final device results much more simple in structure and easy to made, but also able to work properly and so to produce power. According to the made choice, there are necessary only two different materials: a triboelectric one and a conductive electrode. Taking inspiration from various papers [18, 29, 22], as first material the polymethylsiloxane (PDMS) has been chosen. Instead, following an innovative and promising way, hydrogels have been chosen as electrodes. Both these materials are characterized to an high bio-compatibility, a good stretchability and also transparency. PDMS is a very common elastomer, easy to find and to use. Hydrogels are not so popular but they can be make in a simply way. This means that the industrial production of the designed TENG can be easy and competitive.

### 2.1.1 PDMS

The polymethylsiloxane (PDMS) is a silicone elastomer with a lot of interesting properties that make it a very common material for many application, especially in biomedical environment. PDMS is an organic polymer and its chemical formula is  $\text{CH}_3[\text{Si}(\text{CH}_3)_2\text{O}]_n\text{Si}(\text{CH}_3)_3$ . The PDMS used for this application is PDMS Sylgard©184 (Dow Corning Corporation), purchased as a kit of two component: a co-polymer and a cross-linker. The first one is the base and contains vinyl groups. The second one is the curing agent, it has 3 silicon hybrid bond for each molecule and also an amount of platinum that works like a catalyst. When the two components are mixed, the double bond that links the vinyl group to the rest of the molecule breaks and thanks to the -Si-H group of the curing agent, there is the formation of -Si-CH<sub>2</sub>-CH<sub>2</sub>-Si- part. According to the manufacturer, the weight ratio of the co-polymer and the cross-linker must be in the order of 10:1. The base is a viscoelastic material, instead, the curing agent is liquid. After the mixing the compound results to be viscoelastic at the begin, but the cross-linking process started and in almost 24h at room temperature a completely reticulated silicon rubber is obtained. The reticulation process can be accelerated if the mixed solution is put into a furnace at 60°C for an hour. It is possible to see the used PDMS kit in Fig.2.1. PDMS, it is chemically inert, permeable to



Figure 2.1: PDMS Sylgard©184 (Dow Corning Corporation)

gases, thermally stable, hydrophobic and it is also simple to manipulate exploiting the fact that the curing is not instantaneous. In fact the uncured version of PDMS can be easily handled and assumes easily the form of any kind of mold. After the curing, the elastomer is a solid rubber that can be stretched, compressed and bent in all directions. PDMS is also cheaper if it is compared to other silicones and it is largely used for micro-structures, in particular for biomedical applications. In fact, this material is bio-compatible, nontoxic and transparent, all characteristic that are extremely useful in bio-systems. The easy availability and the low cost of this material, associated to its compatibility with Micro

Electro-Mechanical Systems (MEMS) and with bio-systems, make the PDMS one of the most promising elements for Bio-MEMS applications and in particular it comes as very good choice for the aim of this thesis.

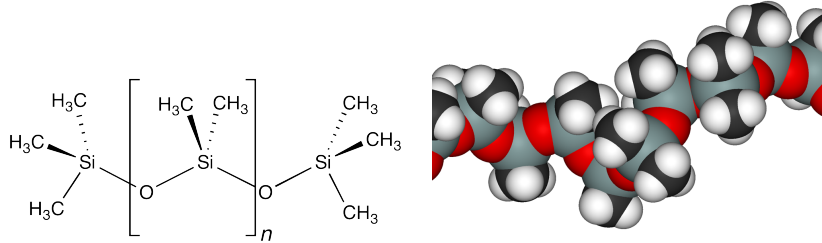


Figure 2.2: Structure of PDMS [49].

## 2.1.2 Hydrogel

### Hydrogels' overview

The first hydrogel as we know appears in literature in 1960 with the aim to use it for a permanent application in contact with biological tissues. Since that moment, hydrogels have fascinated scientists all over the world because they seem to have a great potential for a lot of application, especially in biomedical one. Hydrogels consist in 3D and self-supporting polymeric matrices, they swell in water but do not dissolve. Hydrogels have a high thermodynamical affinity for the solvent itself. Changing the concentrations of monomer or cross-linker it is possible to modify the hydrogel's structure. Moreover if a solute is added, also chemical and physical properties change. A first classification of hydrogels divides them into two categories: natural and synthetic. The first ones are made using derivatives of natural materials and are more suitable for a bio-use. On the other hand, they are characterized by some difficulties to control their reproducibility. Synthetic hydrogels, instead, are more reproducible but it is needed a rigorous control of external conditions during the preparation in order to have always the same result. Hydrogels need to be cross-linked and this process can be occurred by heating, irradiation or using a cross-linker. A big drawback of hydrogels is the dehydration along with time. In fact, since these materials contain a big amount of water, if they are exposed to high temperature, they can lose water by evaporation. This means that hydrogels have a range of temperature in which they can be used, but a slow evaporation is always present also at room temperature. Therefore, it is necessary to study a way to reduce this effect. As a mixture of polymer network and water, hydrogel is not only a transparent and elastic solid but could be a conductive one, exploiting the chemical and physical properties of water. Hydrogel, indeed, can be a good ionic conductor if a salt is added into the solution. In fact, it must be considered that electricity can be conducted both with electrons and ions. Living matter, for example,

uses mostly ions to conduct electricity, instead, machines use mainly electrons. This means that it is sufficient that a salt is dissolved into a solution and, after the consequent splitting into ions, the solution became conductive [15]. If this solution is used to make an hydrogel, also this last will be conductive. In addition, thanks to the hygroscopic properties of salts, the hydrogel's vapor pressure decreases[21]. As a consequence, hydrogels with hygroscopic salts swell and deflate in response to variations in the ambient humidity, but they can be used in a wide range of temperature. Nevertheless, evaporation of water is not stopped and with the deterioration of the hydrogel, the conductive properties are get worse. Fig.2.3 shows clearly how dehydration affects differently a common hydrogel and a hydrogel obtained from a ionic solution. The first one lost a lot of its water after only two days, instead the second one is obviously more durable in time and, indeed, after a month appears sufficiently swollen. As last interesting aspect about hydrogels, it can be

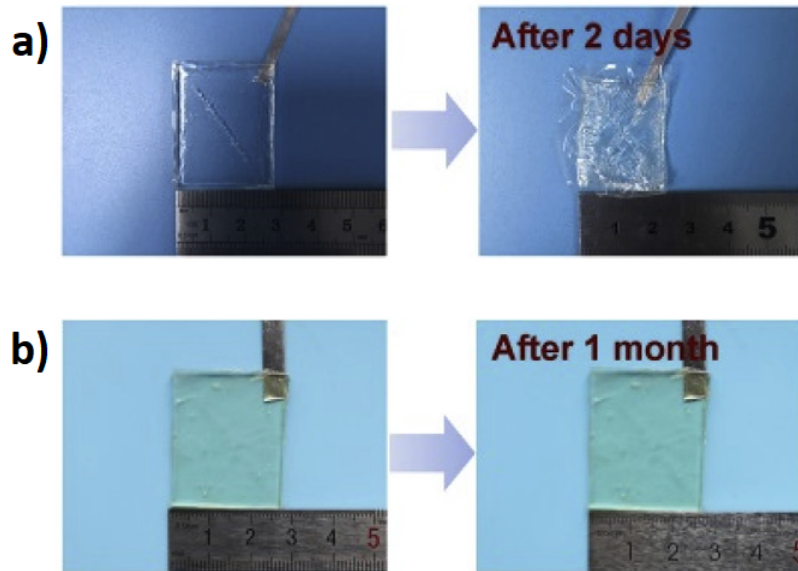


Figure 2.3: Examples of dehydration of an hydrogel without (a) and with (b) salt in it [15].

interesting to mention that there are not a lot of studies about its resistance to fatigue, but in literature it is possible to find some papers about the production of self-healable hydrogel [16]. In fact, since electrical performance of a triboelectric device drastically reduces when the electrode layer is broken or damaged, having the possibility to repair it in an easy way is a very big advantage.

## Natural and eco-friendly hydrogel

Thinking about the future application of the device developed in this thesis, it is necessary to find materials that are extremely bio-compatible and also eco-friendly. In fact in view of a massive production, it is needed that the consequent disposal does not become a big issue for the environment. Natural materials come in aid to these problems. Three different categories of bio-material can be of particular interest for energy harvesting: plant's parts, plant products and biodegradable materials like spider silk. In particular, natural products, like cellulose, can be used to produce hydrogels in order to have a very bio-compatible material that is also flexible and stretchable. One of the goal of this work of thesis is to understand if it is possible to make a recyclable, bio-compatible and eco-friendly triboelectric device. To reach this purpose a natural hydrogel has been chosen as electrode because it does not cause immunological and inflammatory reactions.

To make a natural hydrogel, it is necessary to use polysaccharides or proteins. The choice is wide for both of them. Collagen, silk-fibroin, gelatin and fibrin are mainly used for protein-based hydrogels. Hyaluronic- acid, alginate, cellulose, chitosan and agarose, instead, are often used to prepare polysaccharides-based hydrogels. Polysaccharides are widely diffused in plants and are characterized by a repeating saccharide units linked with O-glycosidic bonds. The difference between two polysaccharides is determined by the groups that substitute the saccharide units, the weight of the molecule and the linkage type. All these features contribute to change the physical properties of the final material. In this thesis a natural polysaccharides-based hydrogel will be developed starting from cellulose.

## Cellulose-based hydrogel

Talking about polysaccharides, one of the most easily available is, without no doubt, cellulose. This means that the exploitation of cellulose could be the faster and cheapest way to produce hydrogels. In particular, cellulose can be used as constituent polymer or only as nano-support. In fact, adding nanocellulose particles into a hydrogel matrix it is obtained an improvement of mechanical properties. In order to produce a cellulose-based hydrogel it is necessary to follow two steps:

- dissolution of cellulose powder or fibers into a solvent;
- cross-linking in a chemical or physical manner.

An important observation is that varying the amount of cross-linker into the cellulose solution, different mechanical properties are obtained. Consequently, in order to obtain the stronger three-dimensional network with the best swelling capability, it is necessary to tune correctly the ratio between cross-linker and used cellulose [40]. Cellulose hydrogels are not particularly investigated in literature, especially in a triboelectric context. They

appears to be extremely versatile, but there are not a lot of works about their properties as electrode. So this thesis can be an interesting starting point to understand something more about these type of material and maybe can open the way for future researches.

**Cellulose** Cellulose is the most abundant polysaccharides of glucose. All the glucose units are linked together by 1,4- $\beta$ -glucosidic bonds and are organized into cellulose fibrils. Cellulose have good mechanical properties, low density, hydrophilicity and a significant inclination to different chemical modifications [40]. It is characterized to the presence of

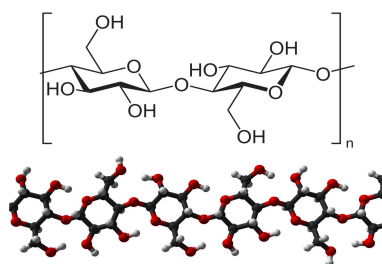


Figure 2.4: Cellulose's unit [50].

a big amount of hydroxyl groups that can easily interact with water or adjacent polymer molecules through hydrogen bonds. Cellulose presents in the first case amorphous regions and in the second crystalline domains. The strong presence of crystalline regions makes the cellulose insoluble in water, but improves its mechanical strength. Since cellulose

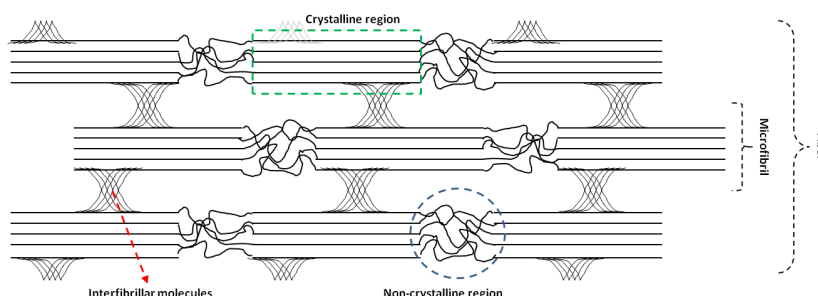


Figure 2.5: Cellulose in amorphous and crystalline form [42].

is easily available, environmentally-friendly and low cost, it is a very good candidate to produce a valid hydrogel. On the other hand, both bacteria's and plant's cellulose have a big percentage (between 40% and more than 60%) of crystalline structures. The dissolution of cellulose has immediately proved to be one of the most challenging issue to be overcome, so it became the subject of an intense activity of research. Only in the past few years ionic liquids have been proved good green solvents. Can be interesting to note that with solubilization and the consequent reduction of crystalline region, the

biodegradation rate is improved a lot. To obtain a water-soluble cellulose, it is needed to separate the molecules of a cellulose fiber and to derivate a sufficient amount of their hydroxyl groups. Following these steps molecules cannot rearrange exploiting hydrogen bonds, so the final structure results more soluble. A valid technique to produce soluble cellulose is etherification, where the degree of cellulose dissolution depends on the average number of hydroxyl groups substituted in the glucose units.

**Cellulose nanocrystal** The first step to manage cellulose is the extraction of cellulose nanocrystals (CNCs) by acid hydrolysis. For this purpose is often used the sulfuric acid that, reacting with cellulose's -OH groups, allows the linking of anionic sulfate ester group to the nanoparticles surface. This guarantees a stable spread of CNCs into the solution. In fact nanocrystals results to be negatively charged and so tends to repulse each other. Thanks to this process, glycosidic bonds are cleaved leading to the degradation of amorphous regions and the release of cellulose's nanocrystals. Centrifugation, dialysis and ultrasonication are the next steps.

**Carboxymethyl cellulose** The protagonist of this work is the carboxymethyl cellulose (CMC), a cellulose ether derived from the substitution of some 2,3 and 6 hydroxyl groups with hydrophilic carboxymethyl groups. CMCs appears as a white, tasteless, odorless powder that is also soluble in water [5]. Carboxymethyl cellulose is characterized by hydrophilicity, bioadhesion and obviously non toxicity. It can be interesting to underline that the nonocellulose can be obtained starting from various sources like wood, animal, palm oil, bacteria and, of course, plants.

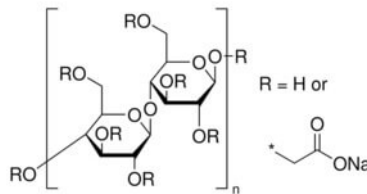


Figure 2.6: Chemical structure of CMC sodium salt [5].

## 2.2 Device structure

In this thesis project, the produced device will work in a single electrode mode, so it has a simpler structure than other types of triboelectric devices (e.g., contact separation mode). Furthermore, since the chosen electrode is an hydrogel, its dehydration problem must be taken into account. In order to solve this issue, it has been decided to package the hydrogel in a PDMS shell. In fact, it has been proved that an hydrogel located into

an environment at 30°C and about 26% of relative humidity, can reduce its dehydration rate of more than 73.3% if it is covered with a thin elastomer layer [18]. As reported

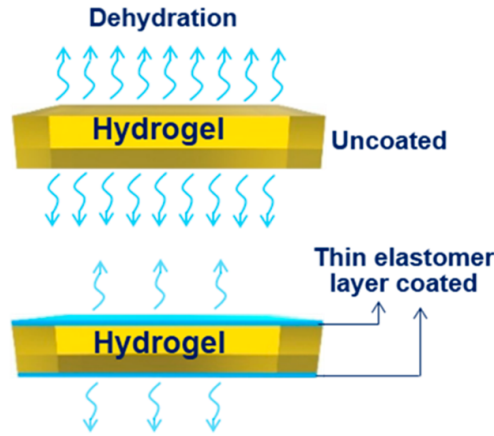


Figure 2.7: Hydrogel dehydration with and without elastomer layer [18].

by [18] after 72h an uncoated hydrogel loses 85.5% of its weight, instead covering the hydrogel with a layer of PDMS the dehydration rate reduces of 78.6%. Remembering that a ionic-hydrogel is less affected by the dehydration effect, if it is sandwiched with PDMS the evaporation of water is mostly reduced. In [29] is underlined as a LiCl-hydrogel coated with PDMS, exposed at 30°C and about 30% of average relative humidity, showed an improvement in water holding of 5%. At a first look, this percentage can seem small, but if it is considered that in this way the hydrogel reached a weight retention of 95% is not so small anymore. Thanks to coating, another important result is reached on the range of temperature that the device can stand without a significant deterioration. In fact, [29] proved that the same ionic-hydrogel, subjected to a temperature of 80°C, had a weight retention of 95,6% when packaged into a PDMS and of only 68.6% when uncoated. To summarize, the two main improvements introduced by the use of a PDMS shell are:

- greater durability;
- improved resistance to high temperatures.

Once that the ionic-hydrogel (also called ionogel) is packaged into an elastomer like PDMS, the resulted structure can be just considered a triboelectric device. In fact, it presents both the two fundamental components of a single mode TENG: a triboelectric material (PDMS) and an electrode (ionogel). Moreover, since the hydrogel is encapsulated into the elastomer, it is able to collect the charges generated in each part of the device. Especially if is considered a flat device, where, both of the two big faces are useful to generate energy. The designed TENG, indeed, is symmetric, so it is able to produce energy in any case. The

only condition that must be respected is that the TENG must be touched by a triboelectric material different to PDMS. At this point, the only missing thing is a small piece of metal which connects the hydrogel to the external world. This sort of wire acts as a bridge from a ionic world to an electronic one. In fact, the TENG is connected to an external circuit where the current is due to the movement of electrons, instead into the hydrogel, current exploits ions. In conclusion, the final structure of the single electrode TENG is a flat and thin box containing a ionogel connected to the outside by a narrow steel foil.

### 2.3 PDMS shell

In light of the above, it appears clear that the first thing to do is the PDMS support. The shell must be thin enough to be managed in view of a wearable application, but on the same time, it must be sufficiently robust in order to bear the tensions due to stretching and bending. The structure must have a cavity of defined dimension in which finds place the hydrogel. In order to have a sort of reproducibility, a mold was made. Fig.2.8 shows the used mold, it is a rectangular block made of poly(methyl methacrylate) (PMMA) where there have been patterned two structures by mechanical milling.

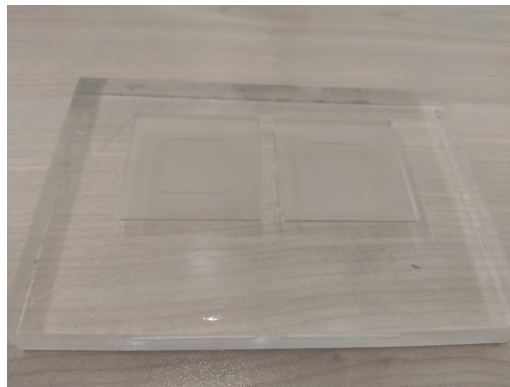


Figure 2.8: Mold used to create a PDMS shell.

PDMS into the mold, the latter is put into a oven for an hour at the temperature of 60°C. During this time, the PDMS hardens and became an elastic silicone ready to be used. The mold allows to produce two different PDMS samples. Each of them is a squared 3D structure whose dimensions are 4x4 cm. In the center there is a 2x2 cm cavity that acts as container for the ionogel. For the depth of the cavity it is possible to choose between two options: 0.5 mm and 1 mm. In the obtained samples, the hollow for the ionogel is opened to the air in the upper part. This means that the structure is not complete and it is necessary an extra layer of PDMS to cover the cavity as a roof. Fig.2.9 is a picture of the PDMS structure just detached from the mold. A trivial plastic container has been used to make the extra PDMS layer. Pouring a small amount of liquid PDMS on the bottom of

the container and baking it for the same time and temperature previously indicated, it is obtained a very thin foil of elastomer. The two main components of the PDMS shell are now completed and ready to be bonded. The liquid PDMS is used now as glue in order to attach together the thin foil of PDMS to the structure with the cavity in the center. During this operation, a thin and narrow piece of steel is located between the elastomer foil and the PDMS structure. A small part of this piece of steel is placed inside the cavity, in this way it will be in contact with the hydrogel. Obviously the steel plate sticks out sufficiently from the PDMS, so that it can be connected to an electronic circuit. Another factor to take into account is to assure that on one side the two shell's components must not be attached, leaving free a small corridor and allowing the access to the cavity from the extern. At the end, the shell appears like a PDMS box with a rectangular cavity in the center which is reachable from the external world by a tiny passage. Fig.2.9 shows the finished PDMS structure.

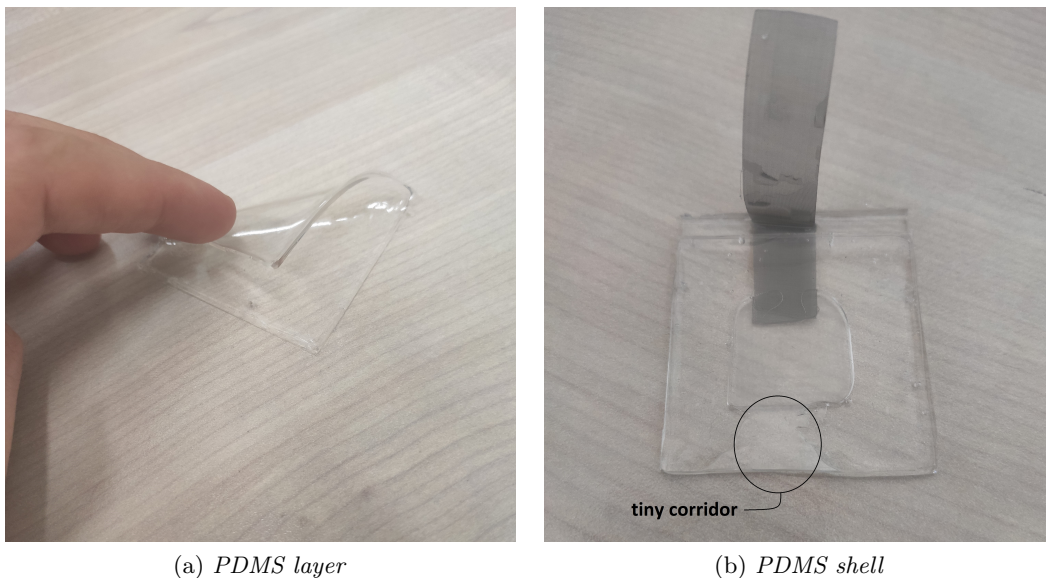


Figure 2.9: PDMS shell component (a) and complete shell (b).

## 2.4 Photosensible cellulose-based ionogel

The cellulose-based ionogel has been made starting from a carboxymethyl cellulose (CMC) synthesized into the Politecnico di Torino. A sample of CMC can be seen in Fig.2.10.

The required ingredients to make the ionogel are:

- water;
- salt;
- photoiniziator.

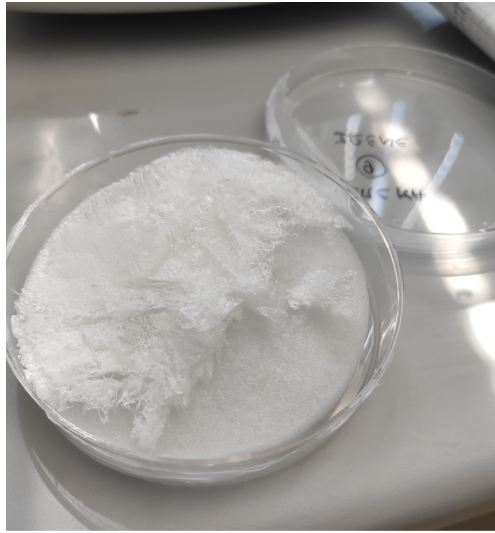


Figure 2.10: Carboxymethyl cellulose.

**Salt choice** Different type of salt can be indifferently used to reach the goal of this work of thesis. Looking in literature, in order to make ionic hydrogels, the salt choice often fall on lithium chloride (LiCl) and sodium chloride (NaCl). The first, used in the majority of papers, should have a better water retention respect to the latter but the sodium chloride is expected to have better biocompatibility. This thesis aims to deepen the use of a ionogel made with the NaCl trying also to underline a possible conductive difference with the LiCl one. Since one of the goals of this work is to highlight how the percentage of salt dissolved into the hydrogel influences the performances of the triboelectric device, different ionogel samples have been made exploiting various molar concentrations. The investigated ones are 0.5mol/L, 0.75mol/L, 1mol/L, 2mol/L, 3mol/L as regards NaCl and 1mol/L for the LiCl. For the sake of completeness, it could be useful to define the concept of molar concentration. It is also called molarity and is defined as the measure of the solute concentration in a solution, it is expressed as the quantity of substance's moles per unit volume of solution.

**Photoiniziator** The used photoiniziator is the bismesitoylphosphinic acid BAPO-OH. It is obtained by the functionalization of phenylbis(2,4,6-trimethylbenzoyl)phosphine oxide (also called BAPO) with an OH group. Products that use this molecule are used for UV-curable applications, so it can be used to obtain the photopolymerization of the hydrogel. This means that adding this substance to the hydrogel solution and simply exposing this to UV light, a the 3D solid structure is obtained [5]. The schematic of BAPO and BAPO-OH molecules are shown in Fig.2.11.

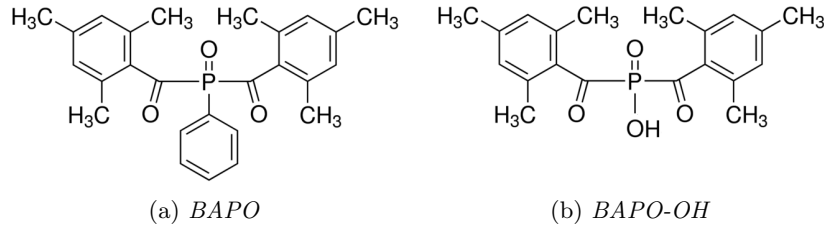


Figure 2.11: Schematic of BAPO (a) and BAPO-OH (b) molecule.

### 2.4.1 Photopolymerization

The word photopolymerization refers to the photochemical process that uses light in order to harden a liquid monomer producing a thermoplastic polymer. In a simple way, the photopolymerization is based on the absorption of radiations by a substance. This phenomenon happens when the energy gap between the excited and unexcited state of a molecule is equal to the wavelength of the radiation hitting the molecule itself. In the laboratory, to achieve this aim, UV radiation are usually used because they are more powerful than visible and IR radiations. Since in the majority of cases monomers are not able to absorb UV radiation, a photoinitiator is needed to start the curing reaction. Absorbing radiations, this molecule forms a reactive specie that initiates a thermal chain reaction called polymerization. At the end of the reaction, a polymer is obtained. The polymerization rate and the final resolution of the polymer depend on the type of used photoinitiator. The main advantage of photopolymerization is the high speed of fabrication, moreover, thanks to this technique it is possible to have an high production rate and a very good resolution. In fact, compared with photopolymerization, a very common process like extrusion is definitely time consuming and less precise.

### 2.4.2 Ionogel production

Once chosen the type of cellulose, the salts and the photoinitiator, it is possible to mix them together in order to obtain the liquid base of the ionogel, ready to be cured by photopolymerization. In the following there are indicated the quantities of each element for each investigated sample.

- Ionogel with NaCl, 0.5mol/L:
  - 3.5g of H<sub>2</sub>O;
  - 0.07g of CMC;
  - 101.5mg of NaCl;
  - 1.4mg of BAPO-OH (2% in weight of CMC).
- Ionogel with NaCl, 0.75mol/L:
  - 3.5g of H<sub>2</sub>O;
  - 0.07g of CMC;
  - 152.25mg of NaCl;
  - 1.4mg of BAPO-OH (2% in weight of CMC).
- Ionogel with NaCl, 1mol/L:
  - 3.5g of H<sub>2</sub>O;
  - 0.07g of CMC;
  - 203mg of NaCl;
  - 1.4mg of BAPO-OH (2% in weight of CMC).
- Ionogel with NaCl, 2mol/L:
  - 3.5g of H<sub>2</sub>O;
  - 0.07g of CMC;
  - 406mg of NaCl;
  - 1.4mg of BAPO-OH (2% in weight of CMC).
- Ionogel with NaCl, 3mol/L:
  - 3.5g of H<sub>2</sub>O;
  - 0.07g of CMC;
  - 609mg of NaCl;
  - 1.4mg of BAPO-OH (2% in weight of CMC).
- Ionogel with LiCl, 1mol/L:
  - 3.5g of H<sub>2</sub>O;
  - 0.07g of CMC;
  - 147.7mg of NaCl;

- 1.4mg of BAPO-OH (2% in weight of CMC).

The first thing to do after having weighted the different components is mixing them. The solvent is the water that is poured into a small container, then, into the same it is placed the required amount of treated cellulose. To allow the dissolution of the last into the water, a mechanical movement is exploited. Thus, a magnetic stir bar is used to mix continuously the solution for almost 10 minutes. After that, the salt is added and at the end also the photoinitiator. When this one is inserted, the container is covered with a thin aluminum foil to avoid that the light can launch the polymerization process. The blend is still mixed for some other minutes. Fig.2.12 shows the liquid compound during the mixing phase.



(a) *Solution not containing BAPO-OH*      (b) *Solution containing BAPO-OH*

Figure 2.12: Pictures of the mixing phase.

## 2.5 Assemblage

Once made the PDMS shell and the ionic solution, the only thing that remains to do is to join them in order to have a single device. Since the blend for the ionogel is in a liquid form, it can be taken with a syringe. Then using a thin needle, it is put into the cavity of the PDMS shell passing through the tiny empty corridor. Filled the cavity, it is possible to pass to the curing phase. In fact, exploiting the transparency of the PDMS, the hydrogel can be hardened even if it is inserted into the shell. Thus, the device is exposed to UV light for 5 minutes. In Fig.2.13 it is possible to see how this operation is performed. During this time the photopolymerization takes place and the ionogel is formed directly

inside the PDMS package. The last step to do now is sealing the hydrogel inside closing



Figure 2.13: Ionogel's photopolymerization.

the corridor. To do this, PDMS is used once again. Thus, the semi-complete structure is located into a trivial container and liquid PDMS is poured on its edge where is located the corridor. This time the PDMS is not baked in order to avoid a fast and unwanted evaporation of the hydrogel. So, the sample is left at room temperature for 24h and after this time the device is complete. Since the PDMS is a simple elastomer, it is possible to cut the device in the wanted shape taking care only to maintain the hydrogel packaged. The final device is shown in Fig.2.14.

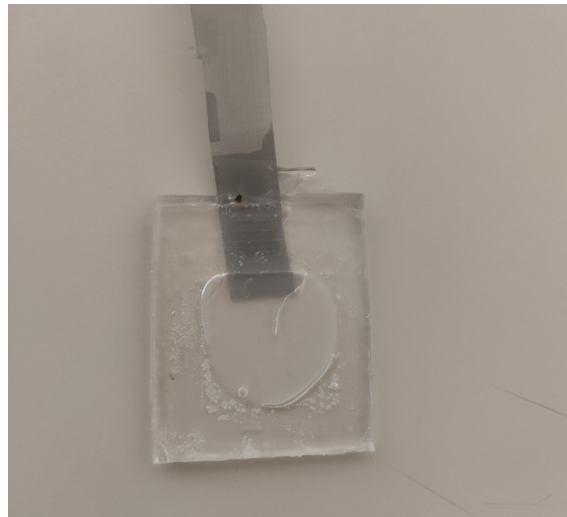


Figure 2.14: Single electrode triboelectric device.

---

---

## CHAPTER 3

---

# Influence of ionic-hydrogel on TENG's performances

### 3.1 Performed tests

Before presenting the obtained experimental results, it is useful to understand the conditions in which the tests have been performed. Thus, the following description have a double purpose: to inform the reader about the working mode and to give the possibility to repeat the tests in order to obtain similar reported results.

#### 3.1.1 Instrumentation

The equipment used includes few but fundamental instruments:

- an electromechanical shaker;
- an electrometer;
- some resistors;
- some wires;
- some cables.

**Shaker** The shaker is an electromechanical structure where on top there is an oscillating plate. It is connected to a power amplifier and to a computer by which is possible to set oscillation frequency, acceleration and displacement. Obviously these three parameters are connected to each other so it is necessary to set only two of them while the third is automatically computed. The shaker used in this thesis work is the Vibration Test System

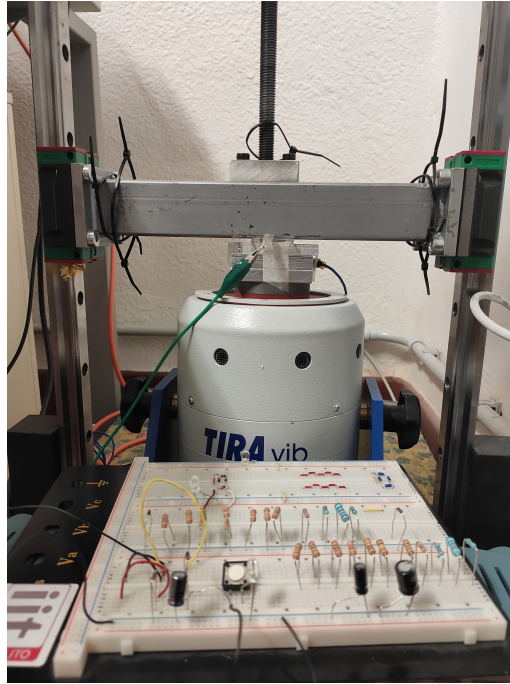


Figure 3.1: Used setup for measurements.

TV 51110 by TIRA Schwingtechnik that have a frequency range 2-7000Hz and a maximum peak-to-peak displacement of 13mm. An accelerometer is fixed on the oscillating plate in order to have a continuous feedback.

**Electrometer** The used electrometer is the Model 6517B by KEITHLEY. It is an high-resistance meter capable to detect voltage, current, amount of charge, resistance, surface resistivity, volume resistivity, external temperature and also humidity. In this thesis work it has been used only as voltage and current meter. It is connected to a computer that allows to set all the parameters in a very easy way, thanks to a video interface based on Labview software. This machine is particularly indicated to detect electrical parameters of high impedance devices like TENGs thanks to its input impedance on voltage measurements higher than  $200T\Omega$ . This feature is a peculiarity of the instrument because typically the oscilloscopes input resistance is much lower. Since the percent error due to loading is inversely proportional to the input resistance, the electrometer results to be particularly accurate. In fact, during high-impedance voltage measurements, comparing the values detected by a common oscilloscope with that taken using this electrometer, it is possible to see that the former need to be corrected by almost a factor 10.

### 3.1.2 Working mode

In order to simulate a continuous contact with another material, the triboelectric device is attached by a double-sided tape to the shaker's top plate. The tape is used to strongly link the device to the shaker and avoid any movement that would involve unwanted noise in the electrical outputs. A suspended still bar is placed above the oscillating plate at a well defined height. Once the oscillation starts, the shaker plate hits the bar, in this way the TENG under measurement touches the bar with a defined force. The frequency of touching is the same set for the shaker. This continuous movement allows a repeated stimulation of the triboelectric device with a consequent production of potential difference. Through the thin steel foil, the TENG is connected to a breadboard where are located the circuits that will be tested. All the tested triboelectric devices have been subjected to a frequency of 5Hz and a maximum acceleration  $60m/s^2$ .

## 3.2 Voltage and current outputs

### 3.2.1 Voltage analysis

Directly connecting the TENG to the electrometer, used as voltmeter, it is possible to see the generated voltage in real time. Since the built triboelectric device works in single electrode mode, it has only one output terminal. Thus, in this first experimental section, the last has been connected to the positive cable of the electrometer, instead the negative one has been connected to the ground. The schematic of the circuit is drawn in Fig.3.2. In

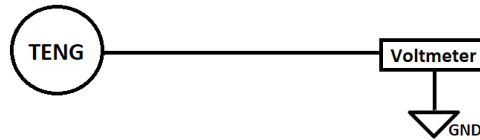
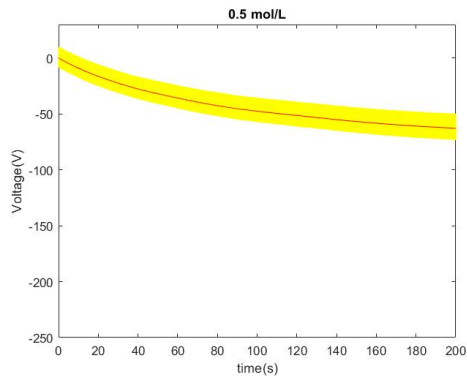
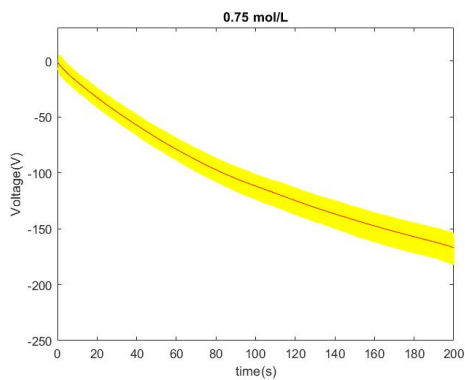


Figure 3.2: Schematic of open circuit configuration.

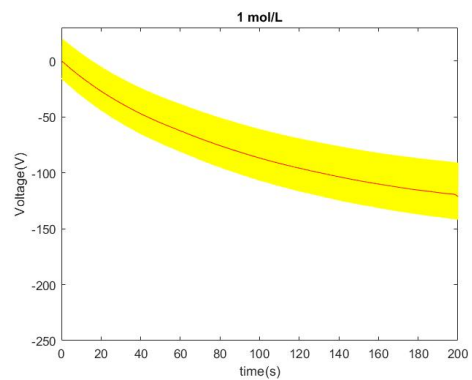
order to underline how much the hydrogel's molar concentration has an influence on the output performances, this type of measurement has been executed using TENGs whose electrodes presents different NaCl quantities. Fig.3.3 shows the graphs obtained starting from the collected data. The graphs in Fig.3.3 show an interesting behavior of the triboelectric devices. In fact, they underline how the PDMS tends to accumulate a negative charge when the TENG is stimulated, reaching so very high negative potential. It is possible to see that the voltage wave have an alternative shape as expected, but a negative exponential seems to be added to it. Seems like that the TENG has a capacitive behavior due to the accumulation of charges on its top surface. The tested TENG is a single electrode one, but since in this configuration it is not directly connected to ground, the



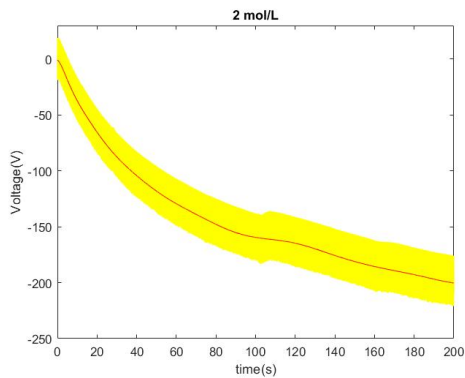
(a) 0.5 mol/L



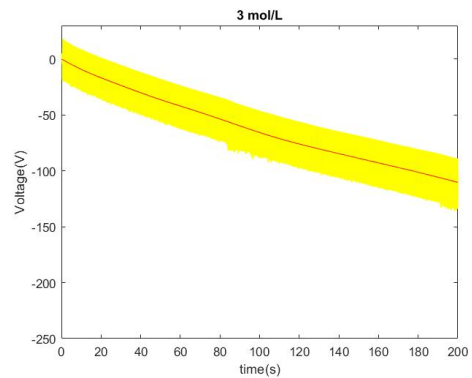
(b) 0.75 mol/L



(c) 1 mol/L



(d) 2 mol/L



(e) 3 mol/L

Figure 3.3: Voltage graphs in open circuit mode.

generated charges on the PDMS surface are not able to be compensated by new opposite charges, so they tend to accumulate increasing the registered negative potential. At each

cycle a certain amount of charge is added to the one already present on the device's surface. After numerous cycles the added charges are less and less, so the potential difference between the TENG and the ground tends to stabilize to a defined value that change based on the type of ionogel used. The trends in time of the different investigated samples are reported in Fig.3.4.

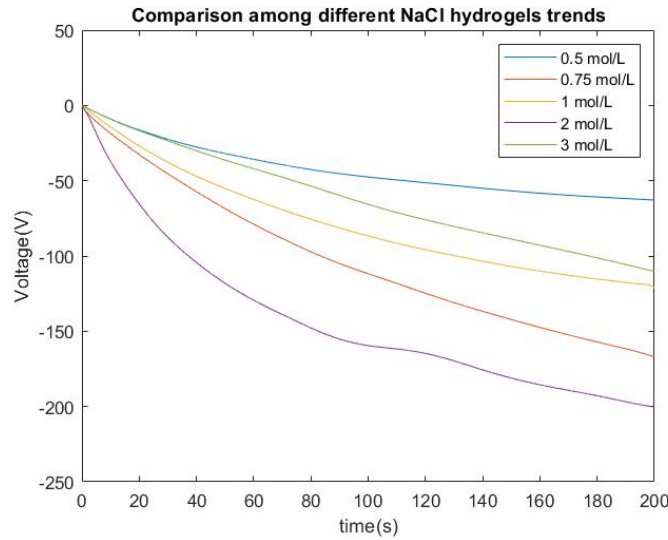
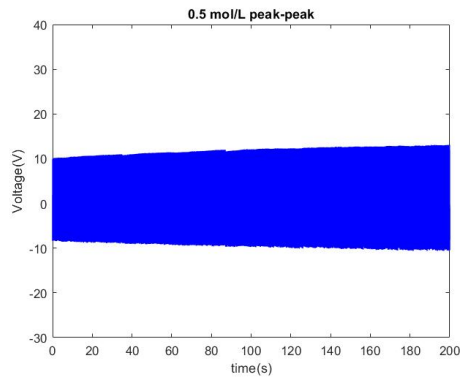
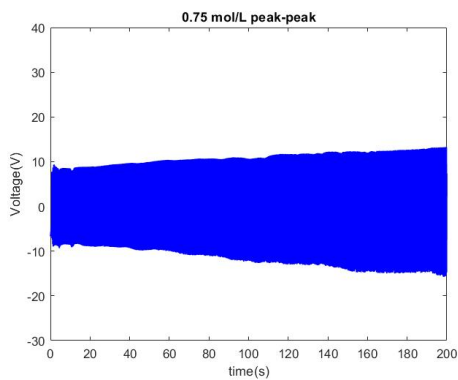


Figure 3.4: Voltage trends of different samples in open circuit configuration.

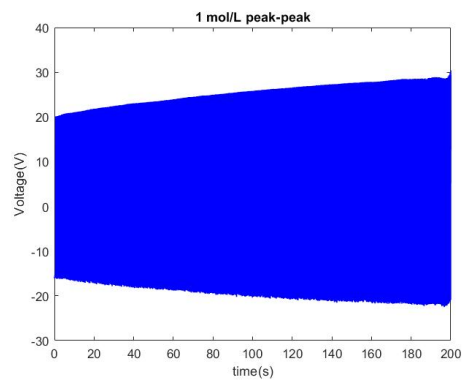
The first trivial consideration to do is that the potential tends to become increasingly negative. This is due to the fact that, since the PDMS is a very negative triboelectric material, when it touches a more positive triboelectric one like steel, which is used for this experiment, it accumulates negative charges. It is interesting to note that there is a similar behavior between the trends, with the only exception of the 3 mol/L sample that seems to have a quite different behavior. It is notable that the voltages reached after only 200 seconds are very impressive. The lowest value is achieved by the sample that exploit a 2 mol/L hydrogel which after 200 seconds arrive to overcome the 200V. However the trends leave to intend that if the measures have been performed for more time the achieved voltages would be more negative. Looking the graph it seems that the maximum voltage reached does not depend on the type of used hydrogel. Probably the shape of the sample and the thickness of the top PDMS layer have much more influence. On the other hand, it is possible that the 0.5 mol/L hydrogel is not able to adequately mirroring all the generated charges on the PDMS and so tends to reach saturation at a higher voltage than the others. Another interesting consideration can be made observing how the peak-to-peak voltage varies in time. This variation can be seen plotting the graphs of Fig.3.3 subtracting the average value of each cycle (so the trend of Fig.3.4). The graphs obtained are shown in Fig.3.5.



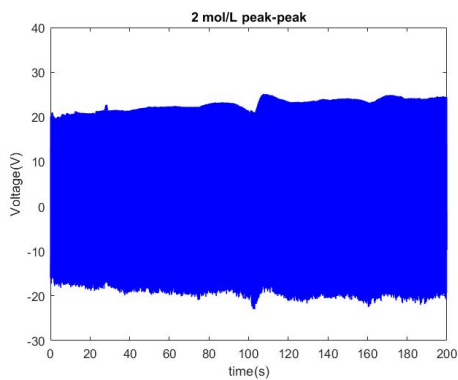
(a)  $0.5 \text{ mol/L}$



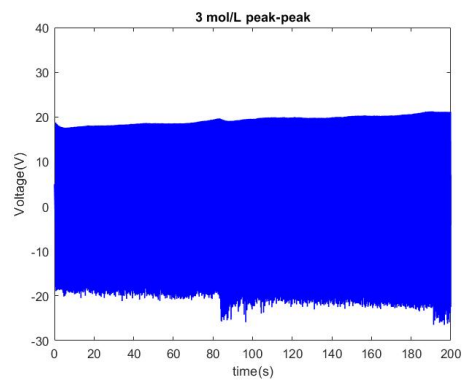
(b)  $0.75 \text{ mol/L}$



(c)  $1 \text{ mol/L}$



(d)  $2 \text{ mol/L}$



(e)  $3 \text{ mol/L}$

Figure 3.5: Voltage variation in time.

A remarkable observation is that the peak-to-peak voltage tends to increase in time in all the considered TENG's samples. The reason of this increasing can be found in the fact that, since at each cycle there is an accumulation of charges on the PDMS surface,

also the voltage peak value increases. This phenomenon is similar to the ion implantation explained in the first chapter, that, indeed, is one way to increase the output voltage. The found result is consistent with other scientific papers about triboelectric devices [15]. Moreover, the tested TENGs exhibited a very good reliability showing a stable output after more than one thousand cycles. This result is more and more valid if we consider that all the other tests described in this thesis have been done with the same samples and no performances degradation have been noted. The last considerations can be made putting in comparison the peak-to-peak voltage values of the tested samples. Since the voltage peak increase with time, but the growth is valid for all the sample, analyzing the voltage values in a specific time range it is possible to have a qualitative indication of how the ionogel's molar concentration affect the electrical output of the TENG. In Fig.3.6 the time interval between 20 and 21 seconds has been chosen. The first remarkable consideration is that there is an appreciable difference between the studied waves. This result is not trivial, in fact this means that the output performances of the TENG depend also to the molar concentration of the hydrogel used as electrode. With a rapid look at the graph it appears clear that being able to reach the lowest voltage value, thanks to charge accumulation, is not directly connected with having the best peak-to-peak value. In fact, observing Fig.3.6 it is easy to recognize that the best voltage output is that of the TENG exploiting 1 mol/L ionogel. What jump directly on the eye is that there is a very big gap between the exhibited peak-to-peak voltage of the 0.5 mol/L and that of 0.75 mol/L hydrogel compared to the others. The voltage of the TENG with 1 mol/L hydrogel, indeed, is almost the double of those which exploits lower molar concentration of salt. Thanks to Fig.3.6(b) it can be seen that low levels of molar concentration are connected to lower voltage outputs. Furthermore a peak in voltage is visible in correspondence of 1 mol/L, instead for higher molar concentrations very similar voltage values are obtained, underlining a sort of saturation. The 1 mol/L appears to be the edge between lower and higher outputs. This is also the molar concentration with the best performances. The small difference between the 0.5 mol/L and the 0.75 mol/L and that between 2 mol/L and 3 mol/L can be connected to TENG structure variations. Despite these small variations, the shape of the trend curve appear quite clear. In the second chapter it has been explained that different salts can be used to obtain a conductive hydrogel. Until now, only the output voltages of NaCl hydrogels have been analyzed, but in order to have an idea of the difference between various salts it has been built a TENG exploiting LiCl. This prototype uses a ionic hydrogel characterized to a molar concentration equal to 1 mol/L as electrode. To investigate its performance it was subjected to the same analysis done for the NaCl samples. Fig.3.7 shows the voltage behavior of this TENG in a time interval of 200 seconds. Also this time it is visible a capacitive behavior even if it seems that the accumulated charge on the PDMS is not a lot. In fact, the potential difference between the TENG and the ground, visible in Fig.3.7(b), is much higher than those obtained in the previous analysis. Since the stored charges are not too much, it is not visible an increasing

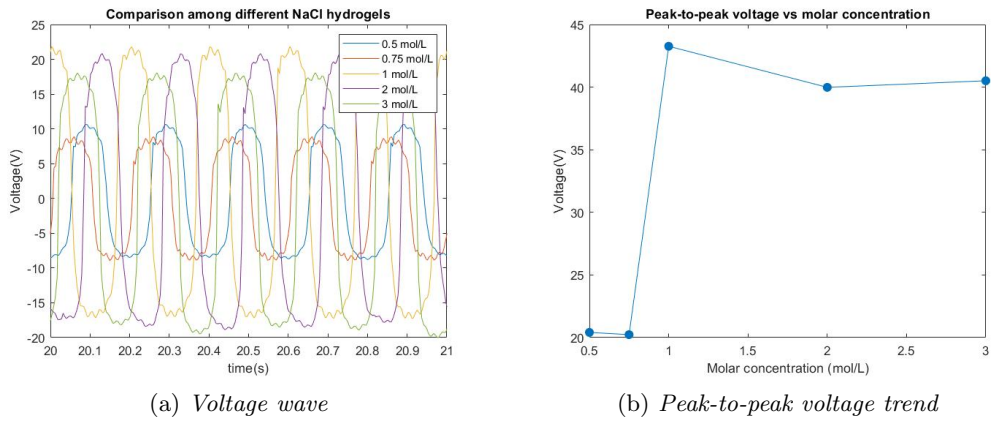


Figure 3.6: Comparison between voltage outputs by different molar concentration ionogels.

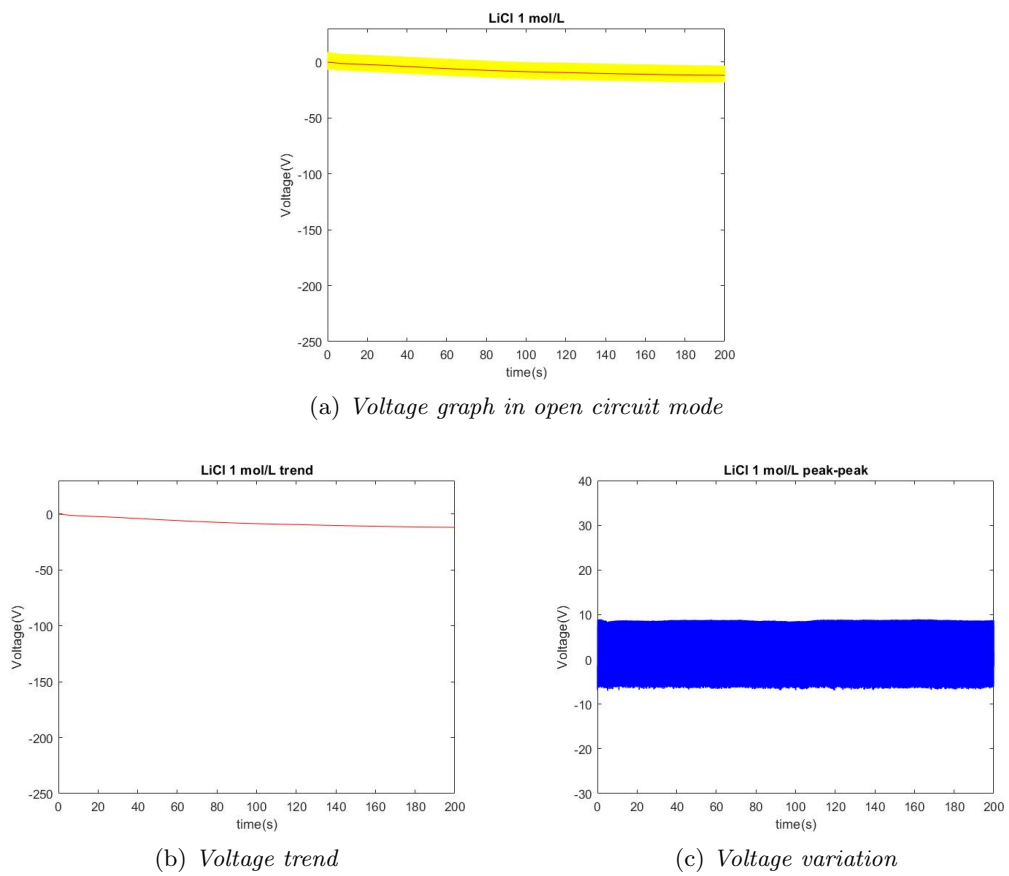


Figure 3.7: LiCl 1mol/L voltage behavior.

in time on the output peak voltage. The peak-to-peak value of this TENG is quite small compared to the already detected ones. In fact, considering the same molar concentration

of salt, the TENG which exploit NaCl shows a peak-to-peak value greater of 40 Volts than that which exploits LiCl. In particular, looking at Fig.3.8, it can be noted that the output voltage connected with the LiCl is lower than that of all the tested NaCl molarities.

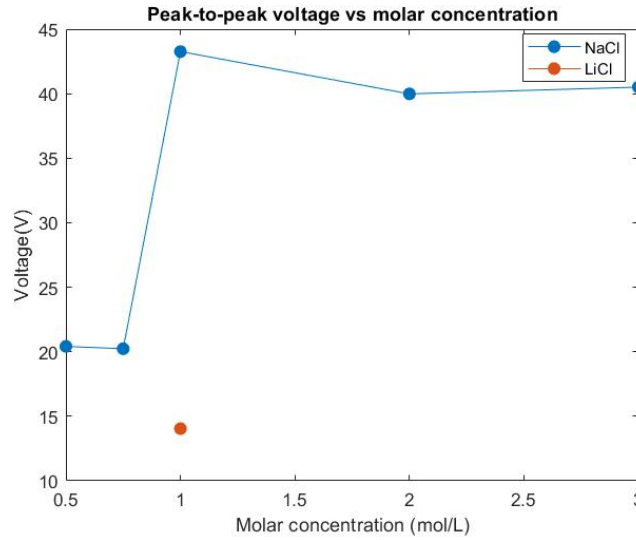


Figure 3.8: Peak-to-peak voltage vs molar concentration.

### 3.2.2 Current analysis

The current measurements have been performed using the electrometer as ammeter and the high precision of the instrument results to be very useful once again. The first set of measures has been done in short-circuit using the configuration shown in Fig.3.9. The ammeter acts like a short-circuit, so the TENG appears to be directly connected to ground without any load. The value of current detected in this configuration is surely the highest one. The shape of current wave is characterized to a series of impulses with peaks in the

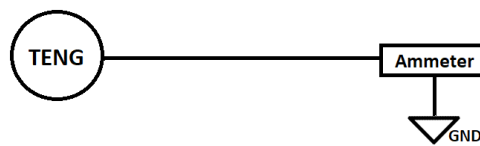


Figure 3.9: Schematic of close circuit configuration.

order of some  $\mu\text{A}$ . Fig.3.10 put in comparison the average peak values of all the TENGs under analysis. The blue curve is linked to NaCl hydrogels and allows to understand how much the molar concentration influences the conductivity of the ionic electrode. It is possible to note that with low values of molar concentration, the detected current is

quite small. Once again the best output is obtained exploiting the 1 mol/L hydrogel. Instead, increasing more the molar concentration the conductivity reduces and so low values of current are obtained. Thanks this short analysis, it seems that once reached the maximum peak, more the molar concentration increase and much less is the current output. Probably, a high quantity of salt leads to less ion mobility that causes small output current. In Fig.3.10 it is marked also the value of peak current reached by the sample which utilizes the 1mol/L LiCl hydrogel as electrode. As for the voltage, also the current of this last TENG shows the worst output.

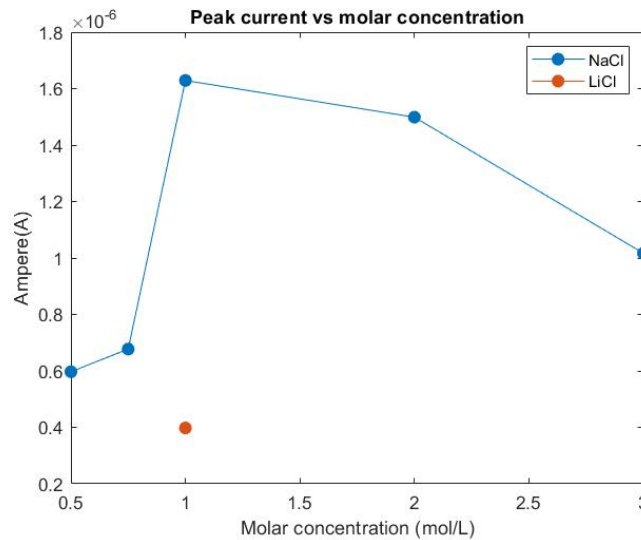


Figure 3.10: Peak current vs molar concentration.

### 3.3 Power analysis

In a real usage, the triboelectric device is connected to an electrical circuit. This last could be used to charge a storage device or to directly supply an appliance. In this part of the thesis it is investigated the behavior of the TENG connected to various resistors in order to have an idea of the best condition of work. To do that, the already mentioned electrometer was connected in parallel to the resistor and forced to act as voltmeter. The tested resistors have values in the range  $1\Omega$ - $1G\Omega$  and each resistor is bigger than the previous one of a factor 10. The schematic of the test circuit is drawn in Fig.3.11. All the measurements have been done with all the TENGs previously mentioned following the aim to understand which is the best molar concentration for the use of the device as direct power supply. Since now, differently to the open circuit configuration, the triboelectric device has the possibility of discharging to ground, the output voltage appears centered on 0V and the TENG does not tend to accumulate negative a charge on its surface. Connecting

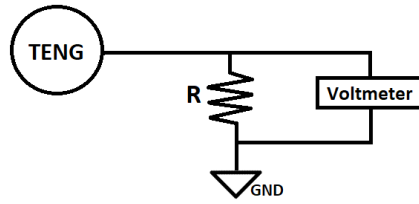
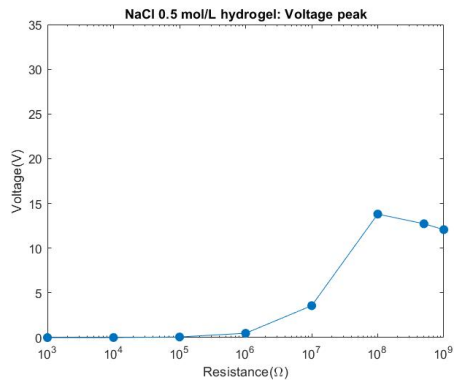
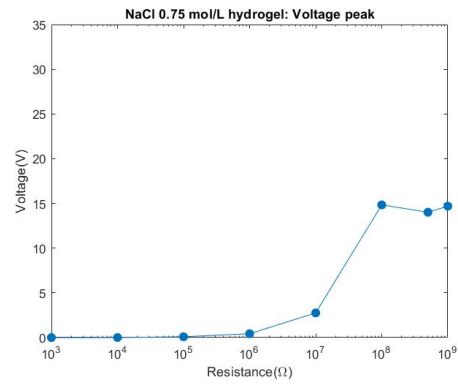


Figure 3.11: Schematic of resistor circuit configuration.

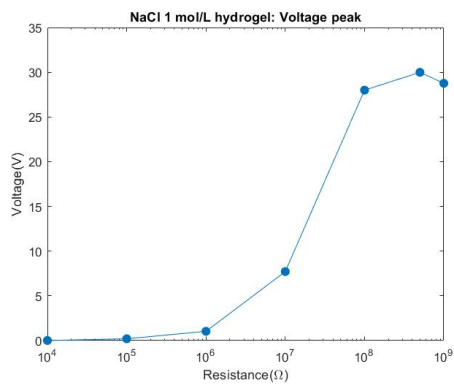
the TENG to different resistors, the first thing that jump to the eye is the fact that, as expected, the voltage output is related to the value of the resistance. In fact, the lower is the resistance and the lower is the peak voltage output. During the experimental session, it has been noted that using resistors in a range from  $1\Omega$  to  $1k\Omega$ , the output is too low to be detected. This means that the resistance range for the detection of the voltage is reduced to  $1k\Omega$ - $1G\Omega$ . As well for the open circuit configuration, also now the output depends on the type of used ionogel. In Fig.3.12 are reported some graphs in which the voltage peak value is marked per each tested resistor. Each chart refers to a precise sample with a different hydrogel. Comparing these plots it is possible to understand which TENG has the highest peak value and for which coupling resistance. As previously mentioned for low values of resistance, also the peak values are lows. Appreciable voltage values are observable starting from  $10M\Omega$ , where the peaks are around 5V. The maximum value of peak voltage is in correspondence of one of the largest resistances, but not of the highest one. In fact after reaching the top value, all graphs tends to decrease a little. The  $100M\Omega$  resistor is linked to the highest voltage peak for almost all the type of TENGs, the only exception is that which exploits the NaCl 1mol/L hydrogel whose shows the maximum value of voltage in correspondence of  $500M\Omega$ . In terms of maximum reached value, there is a big difference between the devices that exploits NaCl 1mol/L and NaCl 2mol/L ionogels compared to all the others. In fact, for these TENG, the maximum value is around 30V, almost the double of other samples' maximums. The last examination for this experimental session is about the output wave shape. It changes, indeed, based on the connected resistor. Small resistance values give impulsive outputs, instead, high resistances lead to a sinusoidal-like outputs. Probably, since a real resistor has not only a resistive behavior, but also a capacitive one, increasing the resistance value, also the capacitive effect increase. This unwanted effect called "parasitic capacitance" is exhibited by all real resistors in greater or lesser manner. To better understand the difference between the output shapes it can be useful to have a look at Fig.3.13. Here three different voltage outputs are reported in a time interval 10-11 seconds. They have been obtained using the TENG with NaCl 0.5mol/L hydrogel and respectively  $1k\Omega$ ,  $100M\Omega$ ,  $1G\Omega$  resistor. These graphs are extremely representative of how, increasing the resistance, the voltage response changes. In order to have a correct analysis of the power connected to the different configurations, also a current analysis



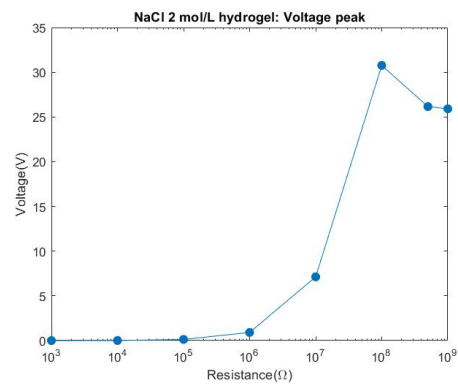
(a) *NaCl 0.5 mol/L*



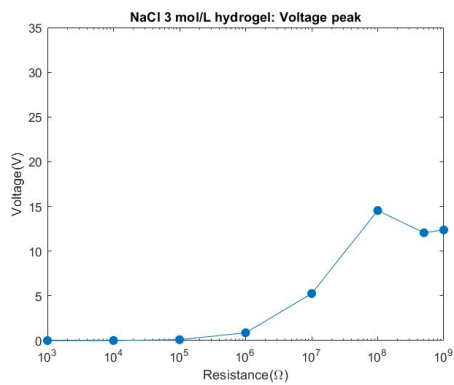
(b) *NaCl 0.75 mol/L*



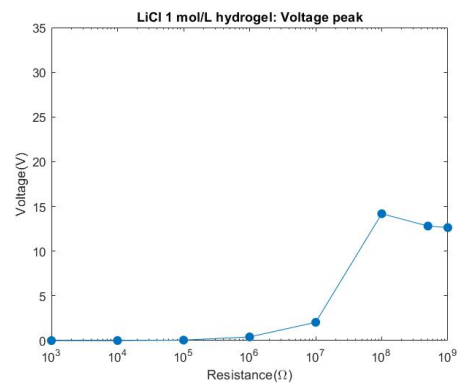
(c) *NaCl 1 mol/L*



(d) *NaCl 2 mol/L*



(e) *NaCl 3 mol/L*



(f) *LiCl 1 mol/L*

Figure 3.12: Voltage peak values for different ionogels.

is needed. Using the circuit drawn in Fig.3.14 the current passing through the resistor is detected. The current measure is done for all the resistors already used for the voltage study. Comparing the collected data with that of the voltage it is possible to understand

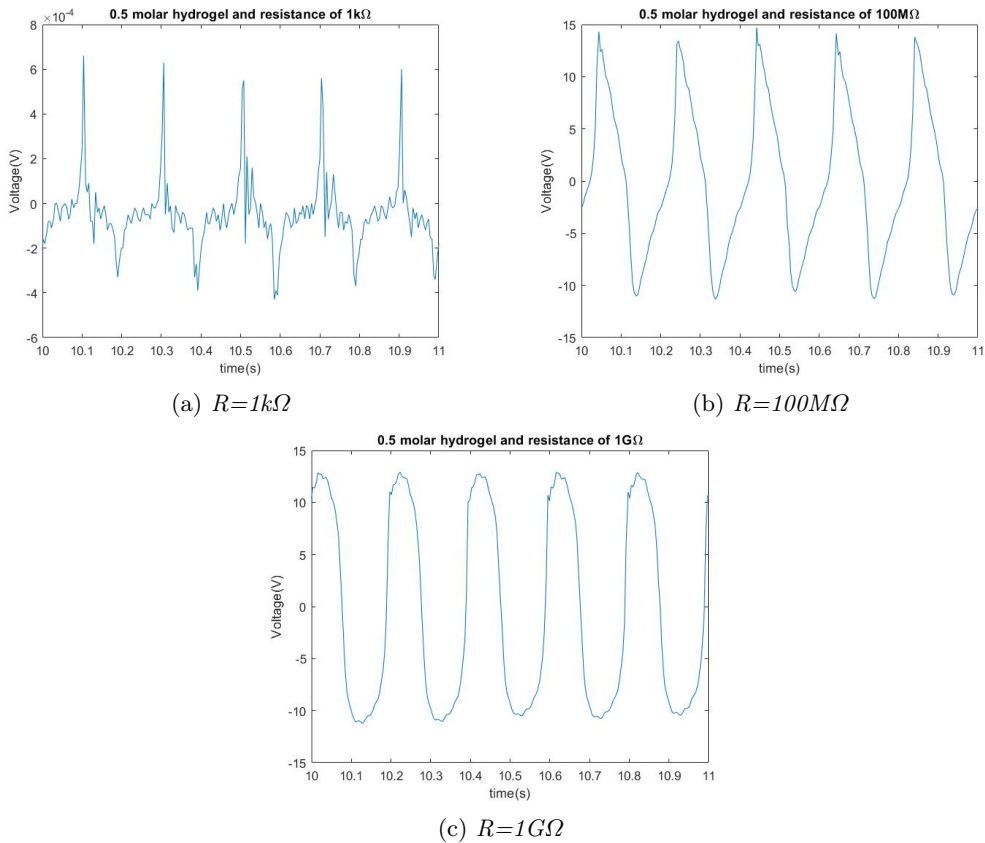


Figure 3.13: Examples of output voltage waves using different resistors.

which is the optimal load for the TENG. Fig.3.15 reports the behavior of the average

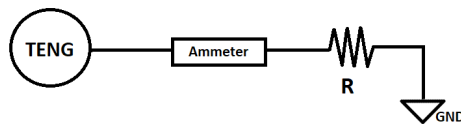


Figure 3.14: Schematic of resistor circuit configuration

peaks current value of all tested samples versus resistance. Each graph refers to a different molar concentration. As expected increasing the resistance value, the value of the peaks tend to decrease. In fact, using resistors in the range  $1\Omega$ - $10M\Omega$ , the current output is more or less the same, but it drastically reduces by increasing more the resistance value. In the range  $1M\Omega$ - $1G\Omega$  the current output is strongly inversely proportional to resistance. In Fig.3.16 are put in comparison the behaviors of both current and voltage versus resistance. These graphs are the union of the plots previously shown. In blue is represented

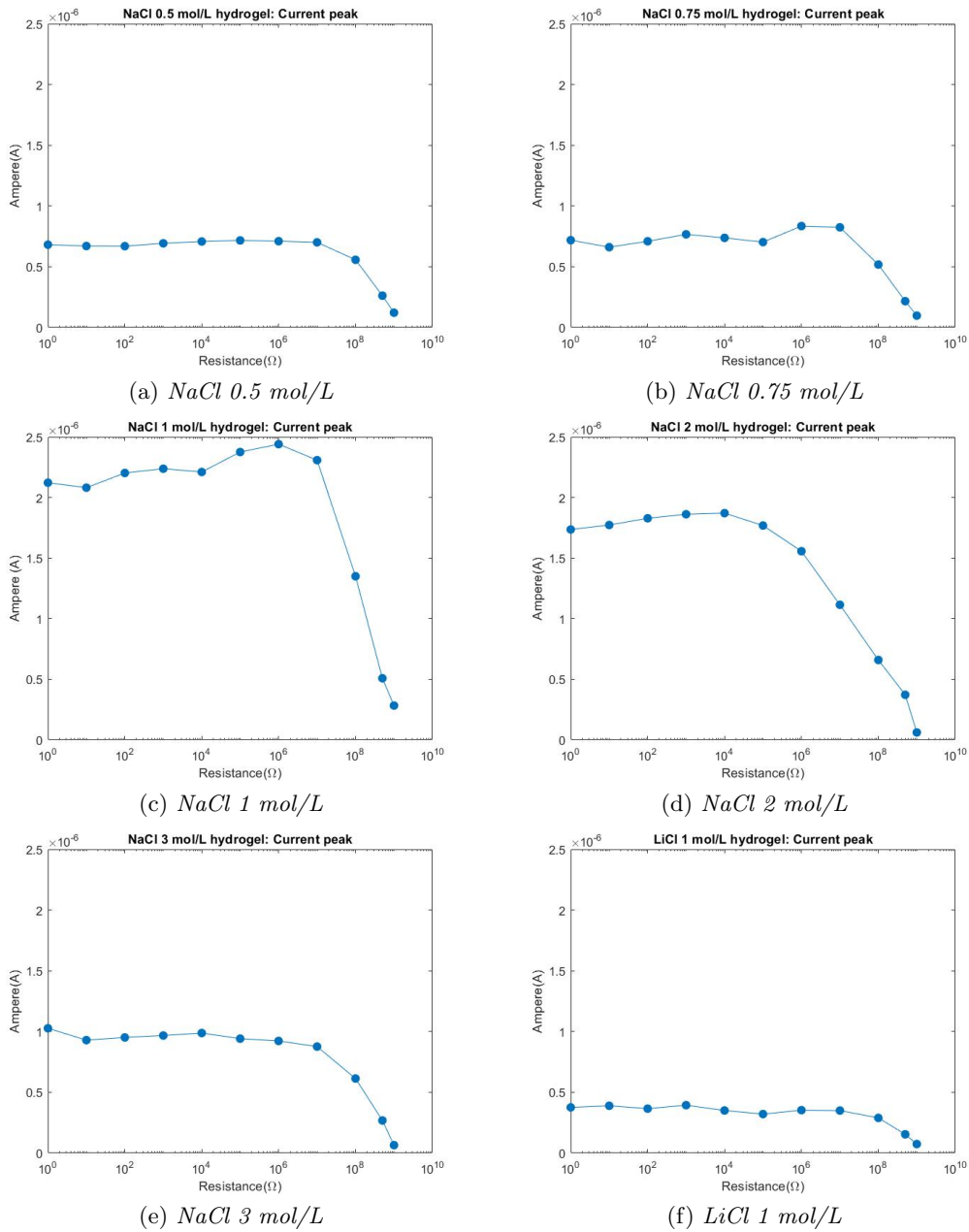


Figure 3.15: Current peak values for different ionogels.

the behavior of the voltage and in red that of the current. After a fast check, it is possible to see that TENGs are characterized by a low current and high voltage output. In fact, peaks of current are of the order of  $\mu\text{A}$  and that of voltage overcome tens of Volts. It is interesting to note that the plot of voltage and that of current are more or less specular, in fact it is evident that increasing the resistance after a certain value, voltage tends to rise

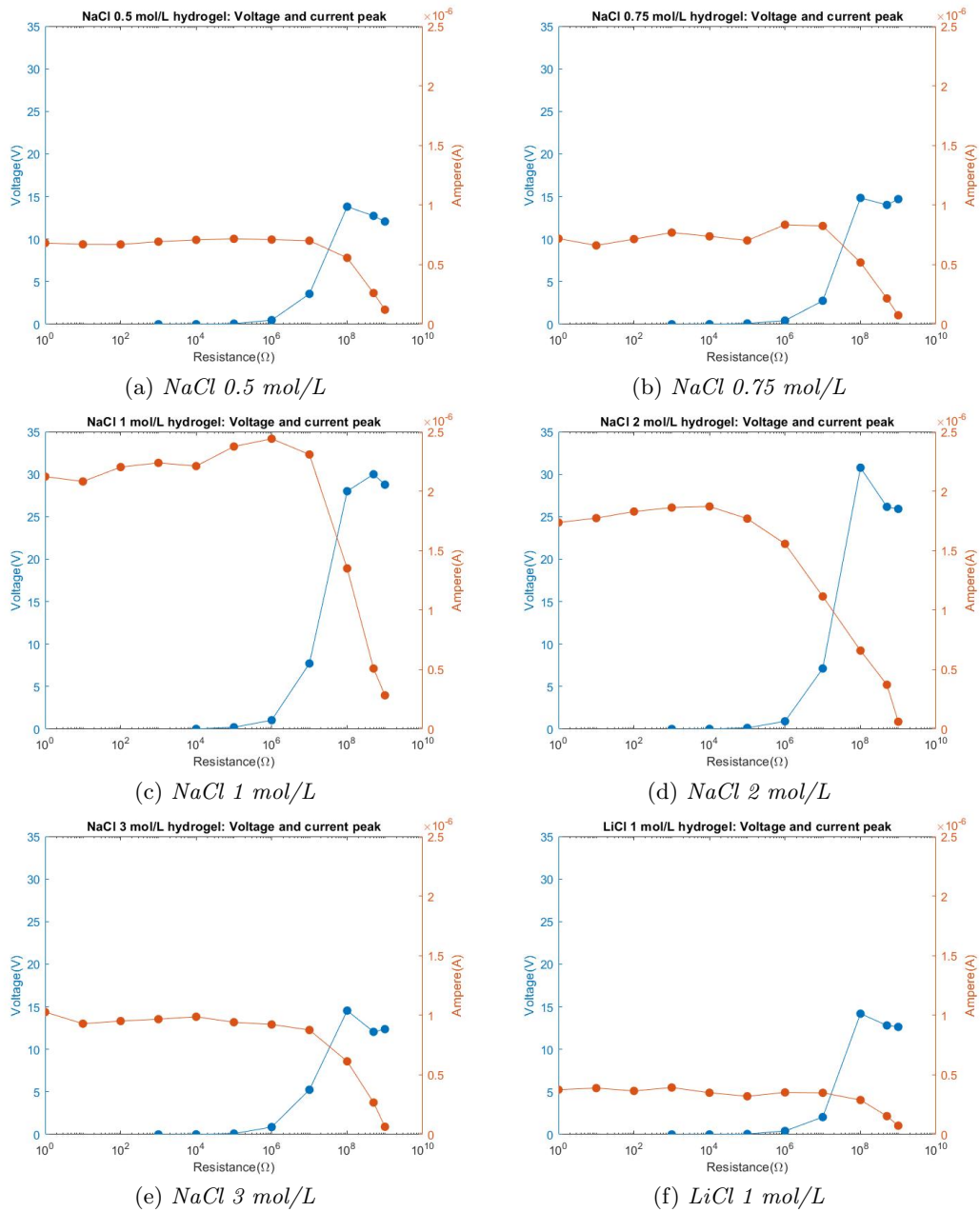
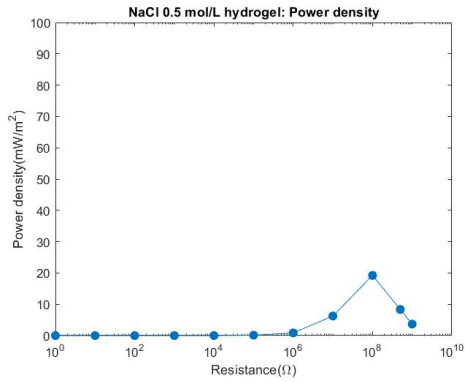


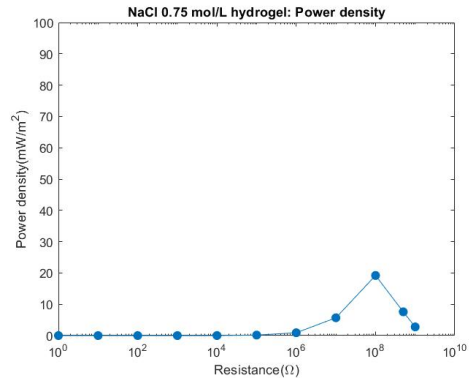
Figure 3.16: Current and Voltage peak values for different ionogels.

strongly and, on the contrary, current tends to sharply decrease. It is possible to recognize three different areas. The first one is in correspondence of resistances smaller than  $1M\Omega$ , where the TENG works like in short-circuit conditions. Instead, for resistances bigger than  $100M\Omega$  the device exhibits a behavior similar to open circuit condition. At the end, in the range  $1M\Omega$ - $100M\Omega$  it is recognizable a transition region, where there is an inversion

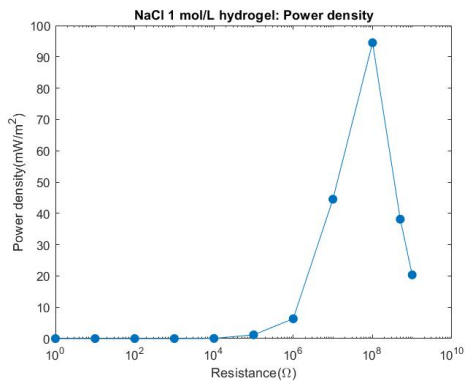
tendency for both current and voltage. In order to manage the produced power in the best way, it is useful to recognize which is the load able to optimize the output performances. To do that, power is computed by making the product between current and voltage peaks. However, the real interesting parameter is the power density that shows how much power is produced by a TENG's square meter. Charts in Fig.3.17 allow to visualize the power density of each tested sample related to the external load. The found values of power density are in line with that of others reviews [30, 10] or rather higher. All the graphs show a behavior with an unique peak in correspondence of  $100M\Omega$ , instead for resistances less than  $1M\Omega$  the power produced is almost negligible. Thus, the impedance matching is reached for a load of  $100M\Omega$  that is the one able to maximize the output power. The other relevant observation is about the amount of power density detected, in fact, without any doubt, the sample exploiting NaCl 1mol/L ionogel is the most performing one. It has a maximum power density of almost  $100mW/m^2$  which is very high compared to the  $20mW/m^2$  of other tested TENGs. In conclusion, the triboelectric device with the 1mol/L ionogel as electrode has demonstrated to have the best performances, starting from current and voltage and ending with the produced power. To sum up, the power density peaks versus molar concentration are reported in Fig.3.18. The graph give rapidly an idea about the power performances of tested TENGs. The gap between the NaCl 1mol/L and the big part of the other TENGs is almost  $69mW/m^2$ , meaning that this molar concentration allows a production of power 4 time higher than the others. On the other hand, the LiCl 1mol/L TENG shows the worst power output, less that any NaCl sample. At the end, it is possible to conclude that the type of salt and its molar concentration have a big impact in the outputs of the triboelectric nanogenerator. Particularly, basing on the experiments performed during this work of thesis, the NaCl exhibited, for all the tested molar concentrations, a greater output than the LiCl and, moreover, the 1 mol/L is resulted to be the best molar concentration for this salt.



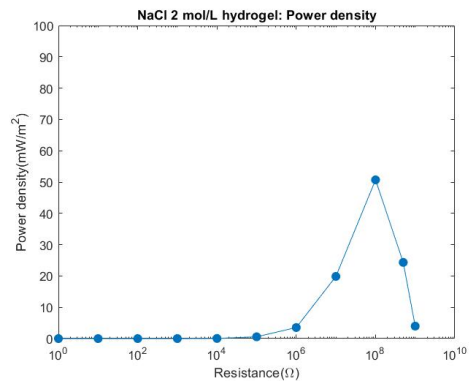
(a) *NaCl 0.5 mol/L*



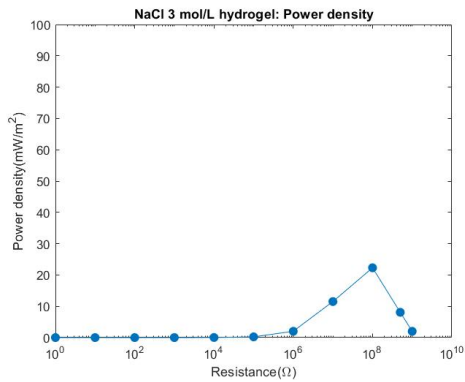
(b) *NaCl 0.75 mol/L*



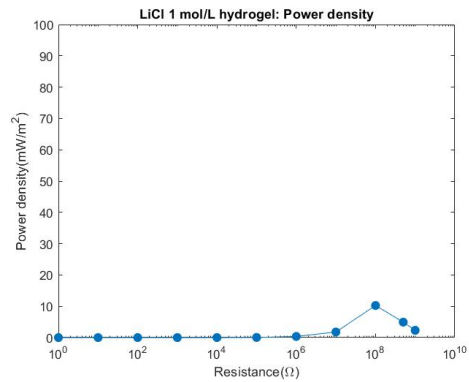
(c) *NaCl 1 mol/L*



(d) *NaCl 2 mol/L*



(e) *NaCl 3 mol/L*



(f) *LiCl 1 mol/L*

Figure 3.17: Power density values for different ionogels.

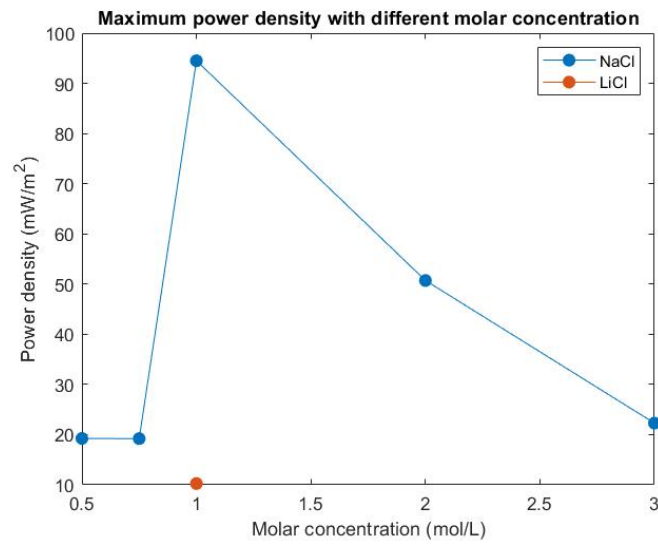


Figure 3.18: Power density peaks versus molar concentration.

---

---

## CHAPTER 4

---

# Conditioning circuit

### 4.1 Power management

Conditioning circuits are one of the most critical parts of the energy harvesting systems. The capacity to harvest power, indeed, strongly depends to the biasing scheme of the transducer. Furthermore, triboelectric devices show a low energy supply efficiency if the outputs are not handled in the best way. Due to their nature, TENGs outputs are characterized by discontinuity, variable frequency and irregular amplitude, so triboelectric devices are not indicated to directly drive most electronic devices. Power management results to be a critical issue for these type of nanogenerators and often it is a technical bottleneck. During the last years, a lot of proposals have been studied trying to maximize and to store energy produced by TENGs. Some of these proposed solutions involve rectification, direct current conversions, electromagnetic transformation and capacitive transformation. Also adaptable interface conditioning circuits have been studied [20], but these type of tools requires active components that need to be supplied. Obviously, choosing this solution, the idea to have a self-powered device is lost, since it is necessary an external power source in order to store the produced energy. Anyway, a study on impedance matching is essential to maximize the output as, in fact, it has been proved in the previous chapter. Equally necessary is the study on power storage. Another conditioning circuit for triboelectric nanogenerator was designed by Tang Zi, utilizing mechanical switches to change the circuit configuration from serial connected to parallel connected capacitors [44]. The drawback of this circuit was the complex mechanical layout, so other circuits like that of Niu were suggested [32]. The problem of circuits based on switches was not only the low efficiency, but also the difficulty to manage the high level of leakages. As already said, also solutions which exploit the electromagnetic transformation have been investigated. They utilize a transformer in order to increase the level of current and simultaneously decrease the level of voltage, obtaining so handleable outputs that can be used to produce

acceptable values of power [14]. Despite the good results achieved, it must be considered that transformers are big structures that are not so easy to be implemented into a circuit. After all these consideration, it is immediate starting to investigate circuits of power management that are both autonomous and efficient. Simple circuits, that do not require any power supply and without any mechanical part have been considered. They are, also, able to be designed in such a way to be flexible and easily implemented into a wearable TENG. Sometimes it is not required a very complex structure to obtain an acceptable results. In the following paragraphs three different conditioning circuits are analyzed, all of them have the simplicity as essential element. The first two are simply rectifiers and the third one is a voltage doubler. They have been used to charge different capacitors and, also, two supercapacitors. The tested circuits are:

- Full wave rectifier;
- Half wave rectifier;
- Bennet's doubler circuit.

In order to better understand the results presented in this chapter, it must be considered that the instrumentation used and the experimental approach are the same of the previous chapter. Particularly, the frequency set for the shaker is 5Hz and the maximum reached acceleration is  $50m/s^2$ .

## 4.2 TENG lumped model

Before starting to show the analysis made using different conditioning circuits, it can be useful to understand in a better way the working mechanism of the triboelectric nanogenerator. In order to do this, it is possible to study a complete model of a TENG [19]. Looking at the nanogenerator as a combination of circuital elements, it is easy to study an high performance biasing circuit. Moreover, having a model of TENG, it is possible to perform simulations using trivial software programs like "SPICE", having so the possibility to know in advance the behavior of a certain circuit. In order to obtain a valid model it is considered a triboelectric nanogenerator with a surface S, a dielectric layer of thickness  $d_{die}$  and permittivity  $\varepsilon_{die}$ . This device have also total triboelectric charge equal to  $Q_{TE}$  and triboelectric charge density  $\sigma_{TE}$ . On top it is consider a moving electrode that periodically touches the dielectric material. The air gap between the moving electrode and the bottom structure is a variable quantity named  $d_{var}$ . It is considered, also, the air permittivity  $\varepsilon_{air}$ . To better understand all the considered parameters, it is possible to refer to Fig.4.1. The electrostatic laws govern the triboelectric device and both the Gauss and Kirchhoff laws are the keys to find a correct model. Calling  $E_{var}$  and  $E_{die}$  the electric field respectively in the air gap and in the triboelectric layer, it is obtained that:

$$E_{die}d_{die} + E_{var}d_{var} = 0 \tag{4.1}$$

$$E_{die}\varepsilon_{die} + E_{var}\varepsilon_{var} = \frac{Q_{TE}}{S} \quad (4.2)$$

and since

$$\frac{Q_{TE}}{S} = \sigma_{TE} \quad (4.3)$$

it is possible to write:

$$E_{die}\varepsilon_{die} + E_{var}\varepsilon_{var} = \sigma_{TE} \quad (4.4)$$

The solution of this equation is:

$$E_{die}d_{die} = \frac{\varepsilon_{TE}d_{die}}{\varepsilon_{die}\left(1 + \frac{\varepsilon_{air}d_{die}}{\varepsilon_{die}d_{var}}\right)} \quad (4.5)$$

The quantity  $E_{die}d_{die}$  is a voltage that in this analysis is called  $V_{TE}$  and shows the voltage on the triboelectric layer's surface. It is easily understandable that  $V_{TE}$  is directed proportional to the charge density  $\sigma_{TE}$ . Assuming that the layer of dielectric is much thinner than the air gap ( $d_{var} \ll d_{die}$ ) and naming  $C_{die}$  the capacitance of the triboelectric layer, it is possible to do an easy simplification:

$$V_{TE} \approx \frac{\sigma_{TE}d_{die}}{\varepsilon_{die}} = \frac{Q_{TE}}{C_{die}} \quad (4.6)$$

This means that  $V_{TE}$  is able to charge the triboelectric capacitance and so to polarize the device. Must be considered that the TENG working mechanism is based on the mutual movement of two layers, this means that the device capacitance varies in time. Moreover, at any cycle, charges are reorganized passing through the external circuit. It is possible to see the TENG as a union of two different capacitors in series: a fixed one and a variable one. The first is composed by the dielectric and the electrode attached to it, in fact, they have the same amount of charge on their surfaces. The variable capacitor, instead, is that consisted by the top and movable electrode and the dielectric layer. A very important thing to consider is that the whole device is electrically neutral at any time. This assumption comes from the charge conservation law, in fact:

$$Q_{TE} + Q_{die} + Q_{var} = 0 \quad (4.7)$$

In particular it can be interesting to note that  $Q_{var}$  and  $Q_{die}$  depend to the mutual position of triboelectric parts and so on time, but, obviously, also to  $Q_{TE}$ . Thanks to the Poisson's equation it is possible to find the voltage generated by a TENG:

$$V_{T-ENG} = - \int_0^{d_{die}} E_{die} dx - \int_{d_{die}}^{d_{die}+d_{var}} -E_{var} dx = -E_{die}d_{die} + E_{var}d_{var} \quad (4.8)$$

In this way it is obtained that:

$$V_{T-ENG} = -\frac{Q_{die}d_{die}}{S\varepsilon_{die}} + \frac{Q_{var}d_{var}}{S\varepsilon_{air}} \quad (4.9)$$

This equation can be divided into two parts, each of them represent a potential difference across a different capacitor, respectively  $C_{die}$  and  $C_{T-ENG}$ . This assumption appears to be more clear considering that:

$$C_{die} = \frac{S\epsilon_{die}}{d_{die}} \quad (4.10)$$

and

$$C_{T-ENG} = \frac{C_{var}}{C_{die}C_{var} + C_{die}} = S \frac{1}{\frac{d_{die}}{\epsilon_{die}} + \frac{d_{var}}{\epsilon_{air}}} \quad (4.11)$$

Looking at equation (4.7), it is possible to write:

$$V_{T-ENG} = \frac{Q_{TE}d_{die}}{S\epsilon_{die}} + \frac{Q_{var}}{S} \left( \frac{d_{die}}{\epsilon_{die}} + \frac{d_{var}}{\epsilon_{air}} \right) \quad (4.12)$$

Made a substitution in equation (4.12) using equations (4.10)(4.11), it is obtained the following result:

$$V_{T-ENG} = \frac{Q_{TE}}{C_{die}} + \frac{Q_{var}}{C_{T-ENG}} = V_{TE} + \frac{Q_{var}}{C_{T-ENG}} \quad (4.13)$$

$V_{T-ENG}$  represent an open circuit voltage obtained by the splitting of polarized tribocharges. This parameter depends only to triboelectric charge and to the thickness of the dielectric layer. It is interesting to note that it does not depend on the air gap if the assumption  $d_{var} \ll d_{die}$  is considered valid. In stationary regime  $V_{TE}$  can be considered as a constant voltage and so can be represented by a voltage source.  $C_{T-ENG}$ , instead, represent the variable capacitance between the two TENG's electrodes. At the end, the TENG lumped model can be seen as a double-ended device made by a fixed voltage source in series with a variable capacitor. This means that it is possible to consider a triboelectric device as a capacitive one. The complete model is shown in Fig.4.1.

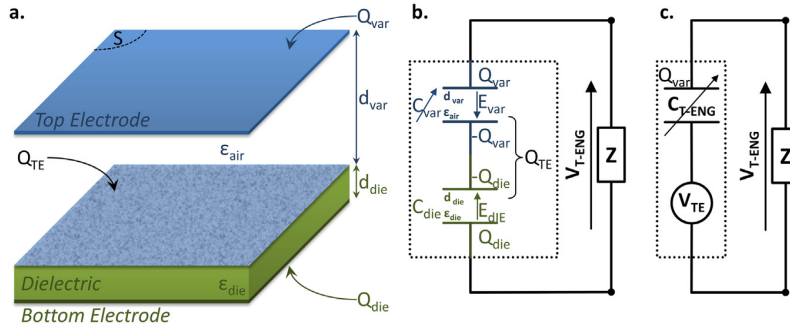
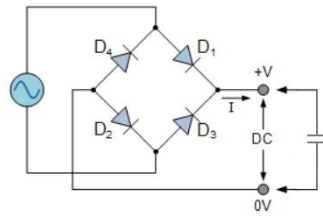


Figure 4.1: Schematic of TENG with parameters[19].

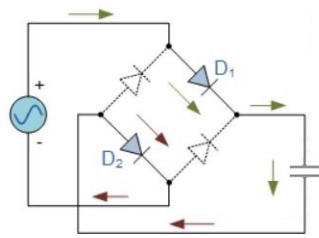
### 4.3 Full wave rectifier

The full wave bridge rectifier has been considered for long time an effective approach to store energy directly from a triboelectric nanogenerator. It is a single phase rectifier,

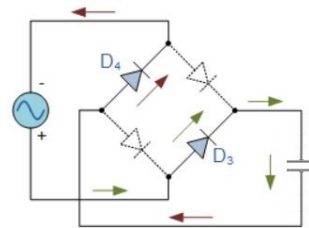
made with four diodes arranged in series pair and connected in closed loop. Its structure is reported in Fig.4.2(a). During each half cycle only two diodes allow the passage of current, so its working mechanism can be better analyzed splitting it into two semi-cycle. During the first half cycle, diodes  $D_3$  and  $D_4$  are reverse biased so do not allow the passage of current, instead  $D_1$  and  $D_2$  conduct and the current can flow into the capacitor, as shown in Fig.4.2(b). On the contrary, during the second half cycle,  $D_1$  and  $D_2$  are "off" and the current flows in the capacitor following the same direction of before but thanks to  $D_3$  and  $D_4$ . The entire mechanism is described in Fig.4.2.



(a) Schematic.



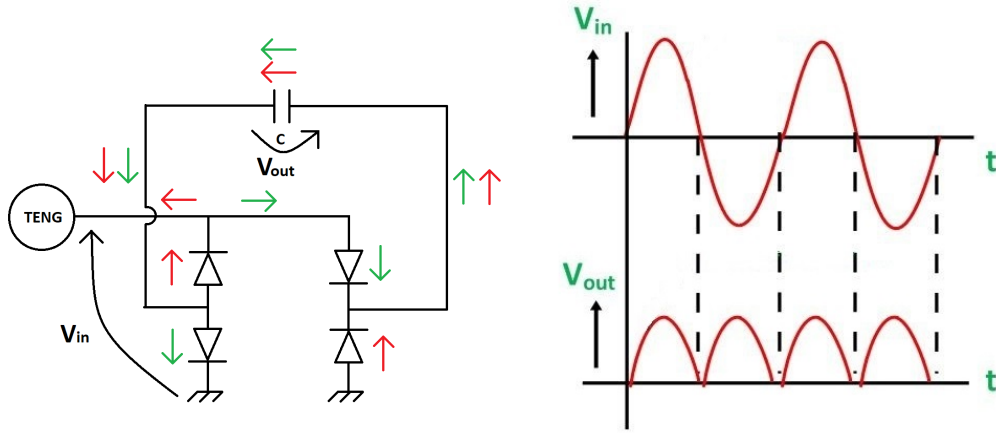
(b) Positive half cycle.



(c) Negative half cycle.

Figure 4.2: Full wave bridge rectifier.

Since the TENG under study is a single electrode one the schematic can be represented as in Fig.4.6, where with green and red arrows are indicated respectively the current's directions during the first and the second half cycle. Must be noted that if it is not reached an impedance match between the rectifier bridge and the TENG, a lot of energy is lost during the storage process. The described circuit has been used to charge different storage device: three capacitors of crescent capacitance, respectively  $1\text{nF}$ ,  $100\mu\text{F}$ ,  $10\text{mF}$  and two supercapacitors of  $33\text{mF}$  and  $0.22\text{F}$ . In Fig.4.4 it is possible to visualize the voltage reached by the tested capacitors into a time interval of 300s. In Fig.4.4(a) can be seen as the full rectifier quickly charge the capacitor of  $1\text{nF}$  until a moderate saturation value is reached. Obviously, the smallest capacitor is the easiest to be charged and despite this, the voltage reached is relatively low:  $1.5\text{V}$ . The more is high the capacitance, the lower is the voltage reached. In particular, it can be observed a big gap between the voltage value achieved by the capacitor of  $100\mu\text{F}$  compared to that reached by all the others bigger



(a) Schematic of used Full wave rectifier. (b) Voltage behavior of used Full wave rectifier.

Figure 4.3: Schematic (a) and output voltage (b) of the used Full wave rectifier.

storage devices. A very interesting analysis is that about the energy stored into the device. In fact, since have been considered different capacitances, the value of reached voltage does not allow an accessible comprehension of the efficiency of the circuit. Only a study on the stored energy can be useful to understand which is the best capacitor to be used and also to know if it possible to use a supercapacitor as device of storage. Moreover, comparing the energy results obtained using the different conditioning circuits it is possible to declare the best one. To compute the total stored energy after  $n$  cycles it is used the following formula:

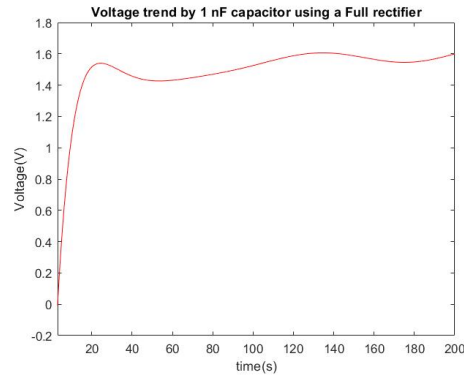
$$E_{tot} = C \frac{V_n^2}{2} \quad (4.14)$$

Another important parameter to consider is the energy per cycle that represent the stored energy after each compression cycle. It can be determined using this formula:

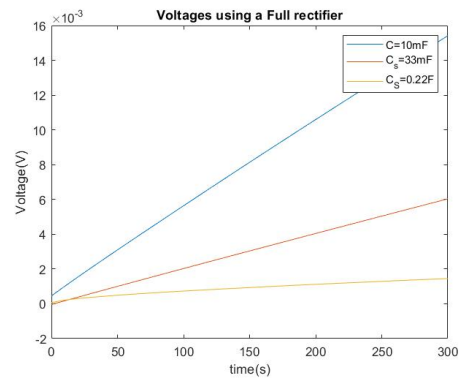
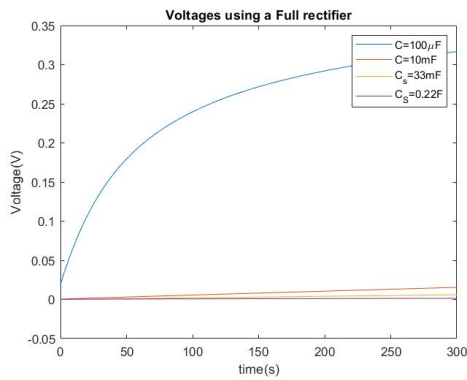
$$E_{cycle} = C \frac{V_{n+1}^2 - V_n^2}{2} \quad (4.15)$$

The graphs of the total energy and the energy per cycle stored into the storage devices previously mentioned using the full wave rectifier are reported in Fig.4.5.

The 1nF capacitor shows the highest value of voltage, but since the capacitance value is very low, the stored energy is also very low. In particular it is the lowest one, with a value close to 0. The maximum energy, instead, is stored into the 100 $\mu$ F capacitor. Observing the graph of the energy per cycle, indeed, for this capacitor a peak at the begin can be identified, where 7.4nJ are achieved, then a progressive decrease can be noted until a small saturated value is reached. This behavior can be deduced having a look to the voltage graph and in particular studying the tangent to the curve. This last

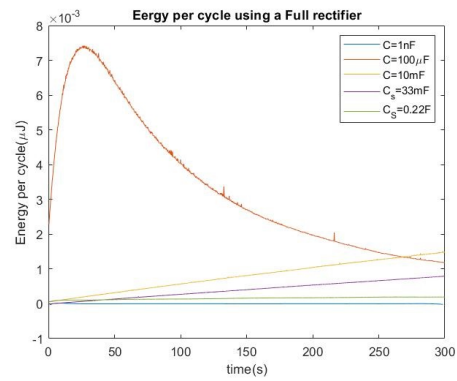
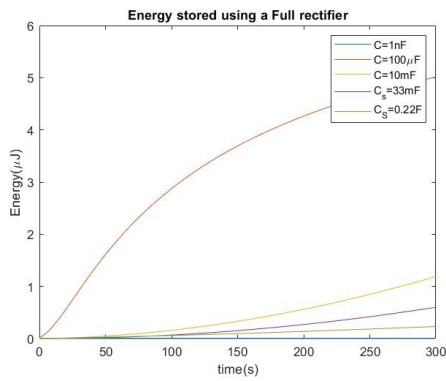


(a)  $1\text{nF}$  capacitor.



(b)  $100\mu\text{F}$ ,  $10\text{mF}$  capacitors and  $33\text{mF}$ ,  $0.22\text{F}$  (c)  $10\text{mF}$  capacitor and  $33\text{mF}$ ,  $0.22\text{F}$  supercapacitors.

Figure 4.4: Voltage using Full wave rectifier.



(a) Total energy.

(b) Energy per cycle.

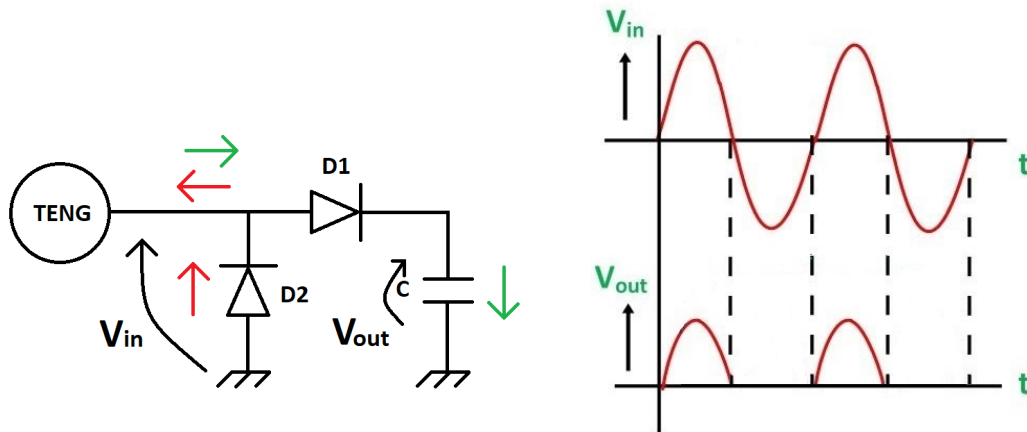
Figure 4.5: Stored energy using Full wave rectifier.

consideration is easily demonstrated thanks to equation (4.15). In the case under study, indeed, the voltage plot grows faster in the first part and then tends to achieve saturation, so at the end, the tangent is almost parallel to x axis. This means that the saturation phenomenon is a very big limit due to the fact that does not allow an efficient storage process. Continuing to examine Fig.4.5, it can be noted that for the bigger capacitors the saturation is not reached and the energy per cycle as well as the total energy continues to increase. However, with equal considered time, bigger capacitors store much less energy respect to the  $100\mu\text{F}$  one, but must be considered that the bigger is the capacitance and the much is the energy that can be stored into a capacitor. Moreover, supercapacitors are interesting because their discharge process is much slower than that of a conventional capacitor. To see the mentioned advantage of big capacitor the time considered is probably not enough. According to the made analysis, the stored energy in the larger capacitors after 300s is in the range  $0.22\text{-}1.2\mu\text{J}$ , taking into account that, at least at the begin, to large capacitance correspond low stored energy.

#### 4.4 Half wave rectifier

The half wave rectifier used in this work of thesis is a little bit different to the conventional one. The schematic of the used circuit is visible in Fig.?? where green and red arrows are used to indicate the current flow's direction during the positive and negative half cycle. The diode D1 is directly connected to the capacitor and allow the passage of current only when it is positive, so it is actuated an half wave rectification. The second diode (D2) is used to have a direct contact of the single electrode nanogenerator with the ground. This connection is fundamental to replenish the charges dissipated when the TENG touches the steel bar.

Having a look at Fig.4.7, it is notable that, also this time, the highest level of voltage is reached by  $1\text{nF}$  capacitor. However, now, the achieved value is much more than that reached using the Full wave rectifier. In fact, after few seconds, the capacitor shows a voltage of almost  $120\text{V}$  and that level corresponds to the saturation. This high voltage is impressive if it is compared to that reached by the others capacitors, but also compared to that reached by the same capacitor using the full wave rectifier. The  $1\text{nF}$  capacitor is not the only capacitor that achieves higher voltages than using the half wave rectifier. In fact, the same speech is valid for all the others storage devices. Observing now the graphs (Fig.4.8) of the total energy and the energy per cycle computed, as for the full wave rectifier, many other considerations can be made. First of all, even if the shape of the curves can resemble that obtained by the full rectifier, this time the achieved values are strongly higher. It is possible to distinguish also the energy stored into the  $1\text{nF}$  capacitor. In fact, observing the blue line in Fig.4.8(a), can be noted that it is the highest one for the first 16 seconds and still remain the higher than most of curves until 140 seconds. This is due to the fast initial charge of this capacitor, but after that saturation is reached, no



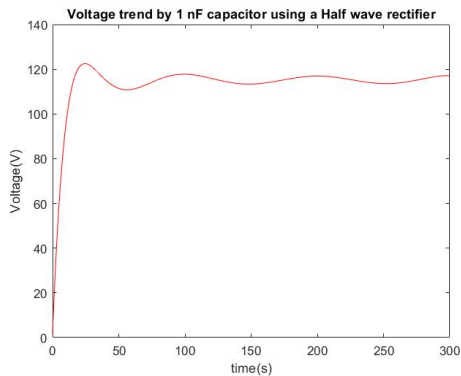
(a) Schematic of used Half wave rectifier. (b) Voltage behavior of used Half wave rectifier.

Figure 4.6: Schematic (a) and output voltage (b) of the used Half wave rectifier.

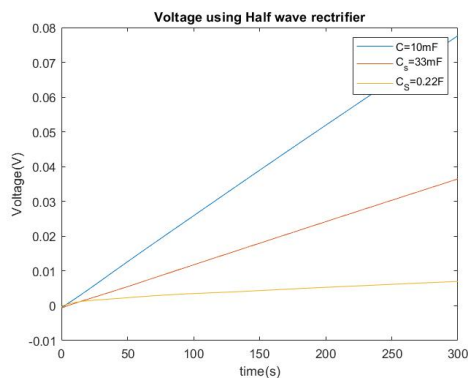
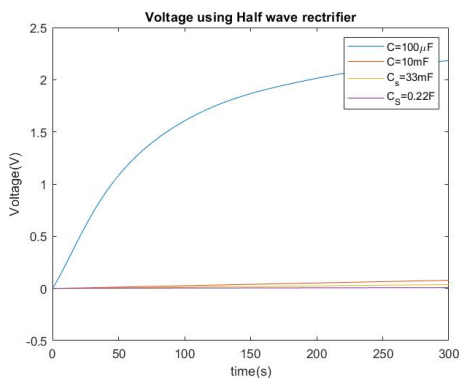
more energy is stored. This phenomenon can be visualized observing the energy per cycle graph. In fact, here, there is a first high peak of  $0.11\mu\text{J}$  followed by a sharply decrease that lead to a  $0\text{J}$  stored per cycle. The mentioned peak is present also using the full wave rectifier but since its height is too low, it is not visible. Instead, since using the half wave rectifier the maximum voltage reached at saturation is almost two order of magnitude bigger, now it is evident. The capacitor with the best performances is once again the  $100\mu\text{F}$  one, with a peak in energy per cycle of almost  $0.35\mu\text{J}$  and a maximum in stored energy of  $238\mu\text{J}$  after 300s. Finally, the bigger capacitors are charged in a similar way of before, so all the already made considerations are still valid. But now they show maximum stored energy after 300s in the range  $6\text{-}30\mu\text{J}$  according to the used storage device.

## 4.5 Bennet's circuit

The study of conditioning circuits that are simple and self synchronized with unpredictable frequency led to the investigation of "charge pump" circuits. They are characterized by high harvested energy per cycle limited only by the nanogenerator's capacitance variation. A very interesting solution, member of this category is the Bennet's circuit. This circuit take its name from the first man that investigated the concept of a doubler of electricity, a machine able to detect small amounts of electrical charges, in 1787 [47]. The rudimentary instrument was made of three conducting plates whose charge increased at each cycle of operation. The system was improved by Queiroz in 2011, changing the mechanical parts in diodes [46]. The schematic of the simplest form of Bennet's circuits is shown in Fig.4.9(a). Its working principle is based on the switching between a series connection of capacitors

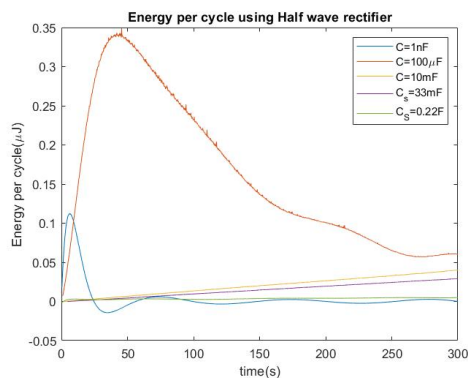
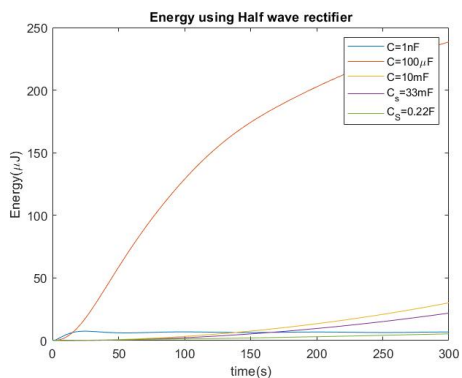


(a)  $1nF$  capacitor



(b)  $100\mu F$ ,  $10mF$  capacitors and  $33mF$ ,  $0.22F$  (c)  $10mF$  capacitor and  $33mF$ ,  $0.22F$  supercapacitors.

Figure 4.7: Voltage using Half wave rectifier.



(a) Total energy.

(b) Energy per cycle.

Figure 4.8: Stored energy using Half wave rectifier.

to a parallel connection configuration. To study the dynamic evolution of charge (Q) and voltage (V) in the following part will be used a powerful geometrical tool thanks to the QV diagram. QV-cycles can summarize the evolution in time of the transducer's biasing taking into account the capacitance variation of the triboelectric device. In order

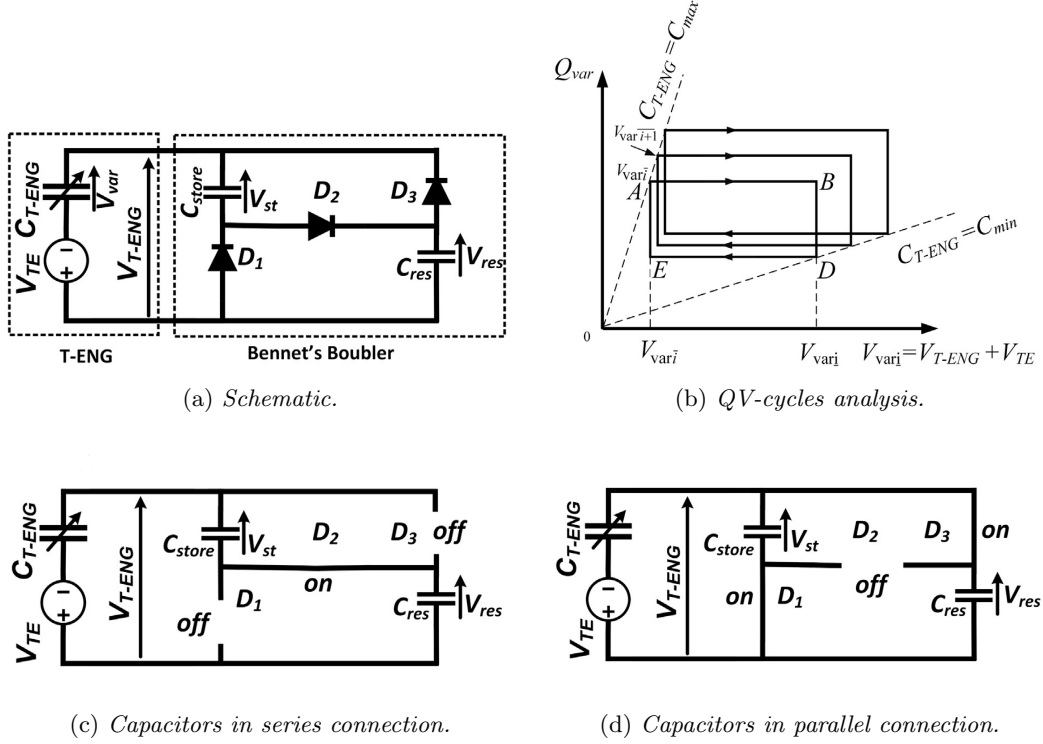


Figure 4.9: Bennet's circuit [25].

to better understand the working mechanism of the Bennet's circuit it is presented a sort of demonstration [25]. For sake of simplicity, but without losing of generality, it is assumed that  $C_{store}=C_{res}=C$  and the diodes are considered ideal. To follow the next part it is necessary referring to the QV diagram in Fig.4.9(b), where with  $C_{max}$  and  $C_{min}$  are called respectively the smallest and largest value assumed by the  $C_{T-ENG}$ , already described in the TENG's lumped model.  $C_{T-ENG}=C_{max}$  when the two triboelectric layer are in contact and  $C_{T-ENG}=C_{min}$  when the air gap is at its maximum. In point 'A' of the QV diagram,  $C_{T-ENG}$  assume the value  $C_{max}$  and in point 'D' it assume the value  $C_{min}$ . When the  $i^{th}$  cycle starts,  $C_{T-ENG}=C_{max}$  and the three capacitors show the same potential difference.

$$V_{store_i} = V_{res_i} = V_{T-ENG_i} = V_i \quad (4.16)$$

In the passage from point 'A' to point 'B',  $C_{T-ENG}$  decreases and  $V_{T-ENG}$  increases. During this time, diodes remain off and do not conduct. The charge into the triboelectric device, instead, remain at the constant value  $Q=C_{max}(V_i+V_{TE})$ .

At point 'B' it is demonstrated in [33] that

$$C_{T-ENG} = 2C_{min} \quad (4.17)$$

and

$$V_{T-ENG} = 2V_i \quad (4.18)$$

The diode  $D_2$  switches on so the capacitors  $C_{store}$  and  $C_{res}$  result connected in series as it can be seen in Fig.4.9(c). At this point, moving from 'B' toward 'D' the TENG supplies, thanks to the generated charge, the two connected capacitors that at the end of this process have an addition of  $\Delta Q_{gi}$ , whose value is:

$$\Delta Q_{gi} = (V_i + V_{TE})C_{max} - (V_{T-ENG_i} + V_{TE})C_{min} \quad (4.19)$$

This amount of charge is transferred both to  $C_{store}$  and  $C_{res}$ . To sum up, in a semi-cycle from  $C_{max}$  to  $C_{min}$  the total charge present in the whole circuit is:

$$-\Delta Q_{gi} + \Delta Q_{gi} + \Delta Q_{gi} = \Delta Q_{gi} \quad (4.20)$$

Analyzing now the second semi-cycle from  $C_{min}$  to  $C_{max}$ , it is needed to start from point 'D'. Since  $C_{T-ENG}$  increases from  $C_{min}$ ,  $V_{T-ENG}$  decreases and so  $D_2$  turns off. The TENG does not change its charge during this process, so the charge into the device remain the same until  $V_{T-ENG}$  became lower than  $V_{store_i} = V_{res_i}$ . This happens at point 'E' and at that moment the diodes  $D_1$  and  $D_3$  turn on obtaining that the capacitors  $C_{store}$  and  $C_{res}$  are connected in parallel and no more in series. This time the charge  $\Delta Q_{gi}$  must be refunded to the triboelectric nanogenerator that now, in fact, shows an amount of charge equal to  $-\Delta Q_{gi}$ . To restore this charge gap, each capacitor of the circuit loses an amount of charge equal to  $\frac{\Delta Q_{gi}}{2}$ . As a result, at the end of each cycle both capacitors  $C_{res}$  and  $C_{store}$  gain  $\frac{\Delta Q_{gi}}{2}$  that comes from:

$$\frac{\Delta Q_{gi}}{2} = \Delta Q_{gi} - \frac{\Delta Q_{gi}}{2} \quad (4.21)$$

Since at the end of one cycle the total amount of charge added to the system is  $\Delta Q_{gi}$ , at the begin of the  $i^{th}+1$  cycle the voltage between the ends of both the two capacitors ( $C_{res}$  and  $C_{store}$ ) is:

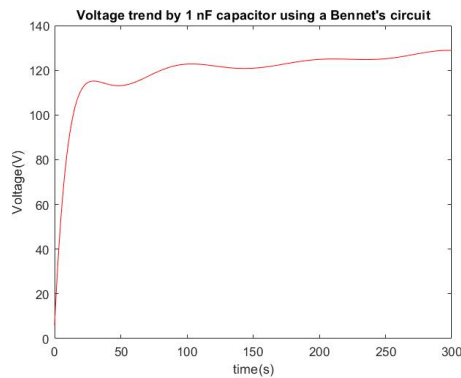
$$V_{i+1} = V_i \left(1 + \frac{(C_{max} - 2C_{min})(C/2)}{(2C + C_{max})(C_{min} + C/2)}\right) + V_{TE} \left(\frac{C_{max} - C_{min}}{2C + C_{max}}\right) \left(1 + \frac{C_{min}}{C_{min} + C/2}\right) \quad (4.22)$$

The big advantage of this type of circuit is that if  $C_{max} > 2C_{min}$ , saturation is never reached and energy is continued to be stored into the two capacitors. This is the aspect that characterize the Bennet's circuit and make it preferable to the half and full rectifier already analyzed. Using the Bennet's circuit, the same storage devices used for the half and full rectifier are been charged.

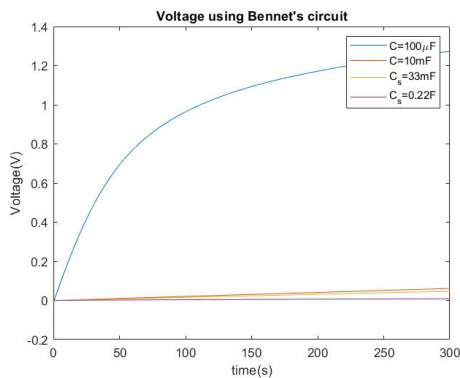
The used configurations are:

- $C_{store}=470\text{pF}$   $C_{res}=1\text{nF}$ ;
- $C_{store}=4.7\mu\text{F}$   $C_{res}=100\mu\text{F}$ ;
- $C_{store}=470\mu\text{F}$   $C_{res}=10\text{mF}$ ;
- $C_{store}=470\mu\text{F}$   $C_{res}=33\text{mF}$ ;
- $C_{store}=470\mu\text{F}$   $C_{res}=0.22\text{F}$ ;

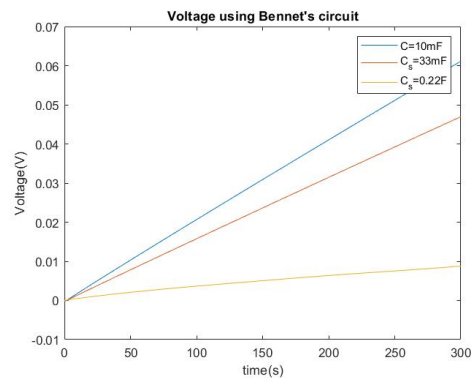
The graph in Fig.4.10 shows the potential difference between the ends of  $C_{res}$  after 300 seconds. Also this time, the 1nF capacitor exhibit the higher voltage with a saturation



(a) 1nF capacitor.



(b) 100µF, 10mF capacitors and 33mF, 0.22F



(c) 10mF capacitor and 33mF, 0.22F supercapacitor.

Figure 4.10: Voltage using Bennet's circuit.

value near to 120V. This value is probably the maximum stood voltage by that type of capacitor. Once again, a very interesting behavior is that of the 100µF capacitor which reached a voltage of 1.24V, much more higher than the other large capacitors. The

voltage showed by the  $100\mu$  using this circuit is a bit lower than that achieved by the same capacitor utilizing the half rectifier circuit described before. Instead, about the large  $10\text{mF}$  capacitor and the two supercapacitors, the reached voltage after 300s is in the range  $0.06\text{-}0.008$  Volts, similarly to the half rectifier. Looking at Fig.4.11, it is possible to see the total energy and the energy per cycle that is stored in all tested capacitors. The shape

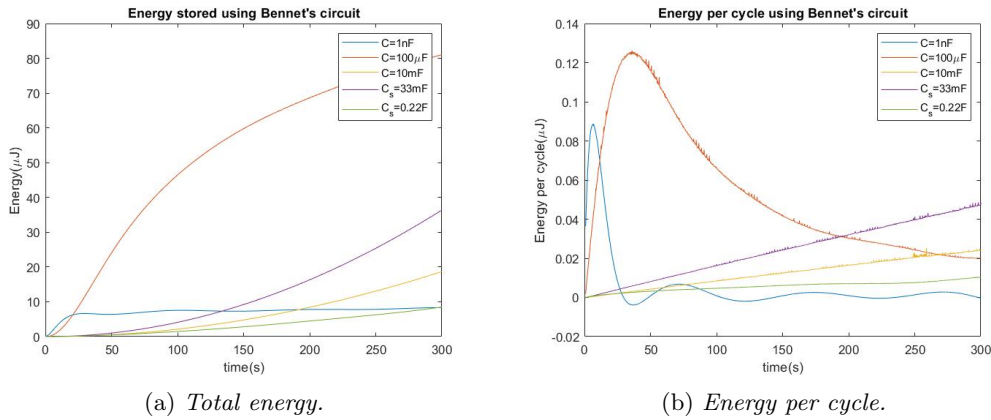


Figure 4.11: Stored energy using Bennet's circuit.

of plots is quite similar to that found exploiting the half and full rectifier. For the  $1\text{nF}$  capacitor, the total stored energy is very little due to the small capacitor's size. A big jump led to the saturation of the voltage, as it is possible to see in the energy per cycle plot, where in blue there is a quite high peak at the begin and then a sharply fall toward  $0\text{J}$  per cycle. About the  $100\mu\text{F}$  capacitor, it shows a total stored energy of almost  $81\mu\text{J}$  after 300s. This last is less than half of the total energy seen using the half rectifier. Moreover, the  $100\mu\text{F}$  capacitor energy per cycle peak is quite low, sign that the rise in voltage is not very fast. The  $10\text{mF}$  capacitor and the supercapacitors, instead, show a behavior similar to that already shown in the half rectifier graph, but this time the  $33\text{mF}$  supercapacitor seems to store much energy than the  $10\text{mF}$  capacitor. For all the results obtained, apart for the  $1\text{nF}$  capacitor, where the limit is probably due to the storage device itself, the time interval considered is not sufficient. In fact, observing the graphs related to the half and full rectifier can be noted that all the capacitors bigger than the  $1\text{nF}$  do not show saturation, but their voltage continue to increase. Since the real advantage of the Bennet's circuit is the overcoming of saturation, it can be appreciate only comparing it to rectifier circuits for enough time. This means that probably could be useful repeating the measurements for a bigger time interval. Until now, it has been understood that, for a short period, the Bennet's circuit handle energy in a way similar, but slightly worse, than the half rectifier.

## 4.6 Comparison among different circuits

The aim of this section is to made a comparison among the previously described conditioning circuits. Some considerations are been already done during the presentation of each circuit. Now, the goal is summarize the concepts and give some extra information in order to find the best circuit to charge a storage device. The first interesting revelation of the performed tests is that, for the purpose of charging a capacitor, the modified half wave rectifier is much more efficient than the full wave one. The difference is tangible especially for the small capacitances. The reason of that can be found in a mathematical [17] way, taking into account that when the TENG is connected to a half wave rectifier, the stored energy per cycle can be defined as

$$\Delta E_{HW} = V_{TE} V_C C_{max} \left(1 - \frac{1 + V_C/V_{TE}}{C_{max}/C_{min}}\right) \quad (4.23)$$

Looking at the equation (4.23), it is possible to recognize a quadratic function whose maximum is in correspondence to a precise value of  $V_C$ . That value is:

$$V_C^2 = \frac{1}{2} V_{TE} \left(\frac{C_{max}}{C_{min}} - 1\right) \quad (4.24)$$

and the maximum converted energy is:

$$\Delta E_{HW}^{max} = \frac{1}{4} V_{TE}^2 C_{min} \left(\frac{C_{max}}{C_{min}} - 1\right)^2 \quad (4.25)$$

Instead, the converted energy per cycle using the full wave rectifier is:

$$\Delta E_{FW} = 2V_C C_{min} \left(\frac{C_{max}}{C_{min}} + 1\right) \left(V_{TE} \frac{C_{max}/C_{min} - 1}{C_{max}/C_{min} + 1} - V_C\right) \quad (4.26)$$

Once again, the equation is a quadratic one, so it exists a maximum for

$$V_C^{max} = \frac{1}{2} V_{TE} \frac{C_{max}/C_{min} - 1}{C_{max}/C_{min} + 1} - V_C \quad (4.27)$$

The correspondent maximum value of energy per cycle is:

$$\Delta E_{FW}^{max} = \frac{1}{2} V_{TE}^2 C_{min} \frac{(C_{max}/C_{min} - 1)^2}{(C_{max}/C_{min} + 1)} \quad (4.28)$$

Making the ratio between the maximum values of energy per cycle of the half wave rectifier over the full wave rectifier it is obtained:

$$r_E = \frac{\Delta E_{HW}^{max}}{\Delta E_{FW}^{max}} = \frac{1}{2} \left(\frac{C_{max}}{C_{min}} + 1\right) \quad (4.29)$$

Since  $C_{max} > C_{min}$  the ratio is positive and so it is demonstrated that the half wave rectifier is capable to provide a maximum energy higher than the full wave rectifier. Basing

on the performed measurements, it seems that also the Bennet's circuit is more indicated than the full wave rectifier to charge a reservoir capacitor. This means that this last circuit is the worse for the purpose of this thesis. Looking at the graphs in the previous paragraphs, the half wave rectifier seems to be the best circuit among the three, but, probably, a more accurate analysis can reveal more details. In Fig.4.12, a magnification of the 1nF capacitor charge curve is reported utilizing both half wave and Bennet's circuit. It is easy to verify that the half wave rectifier allows a much more rapid increase of the voltage. In each cycle, that in the graphs is visualized as a step, it is possible to see a charge of the capacitor followed by a discharge. This last is different based on the type of used circuit. In fact, utilizing the half wave rectifier, during each cycle, the TENG gives an amount of charge to the circuit equal to  $\Delta Q_{gi}$  and the capacitor's charge lost is very little. This is possible thanks to the diode connection of the TENG which allows the taking of restored charges directly from the ground in case of single-electrode TENG, as the device under examination, or from the one of the two triboelectric materials in case of double-electrode TENG. Instead, exploiting the Bennet's circuit, in each cycle the TENG gives to each capacitor a charge  $\Delta Q_{gi}$ , but then both the capacitors lose half of that charge, how it is visible in each discharging step.

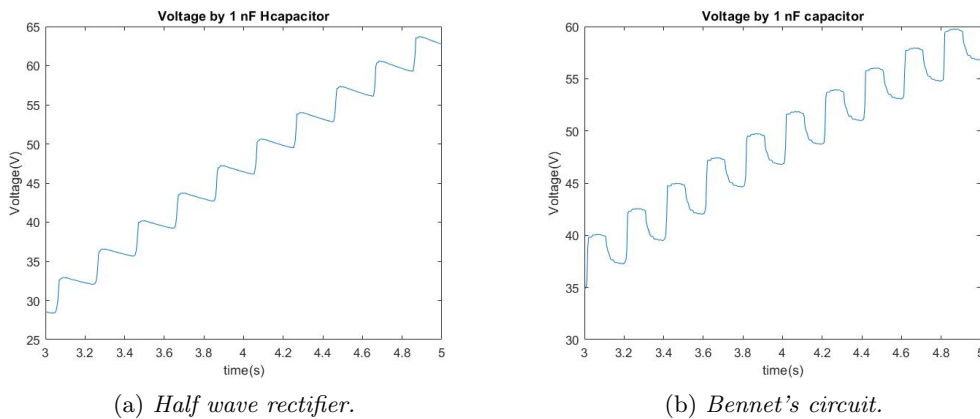


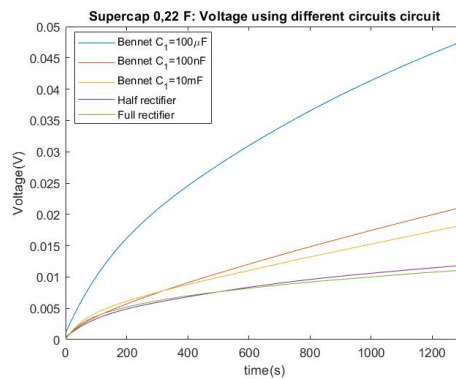
Figure 4.12: Stored energy using Bennet's circuit.

However as already mentioned, the short time interval used for the measurements is not enough to visualize any kind of advantage of the Bennet's circuit over the half wave rectifier. What it is expected to see is that differently to the rectifiers, the Bennet's circuit should not reach the saturation and so should never show a 0J of energy per cycle. In order to verify if this is true, it has been performed a new series of test considering a more longer interval of time. Since each measurement lasts more than 20 min, it has been chosen only one capacitor. The picked one is the 0.22F supercapacitor, in this way it is possible to verify the charging ability on a big supercapacitor which is more versatile in a real use rather than a small capacitor. This supercapacitor has been connected to five

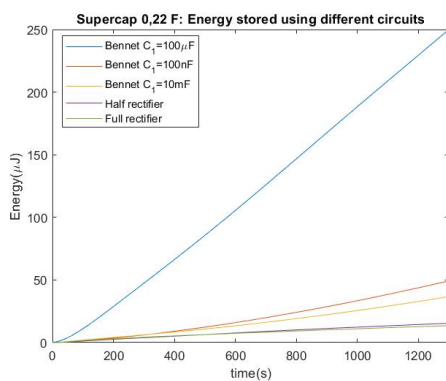
different circuits:

- Full wave bridge rectifier;
- Half wave rectifier;
- 3 different configurations of Bennet's doubler circuit:
  - Bennet1:  $C_{store}=100\mu\text{F}$   $C_{res}=0.22\text{F}$ ;
  - Bennet2:  $C_{store}=100\text{nF}$   $C_{res}=0.22\text{F}$ ;
  - Bennet3:  $C_{store}=10\text{mF}$   $C_{res}=0.22\text{F}$ ;

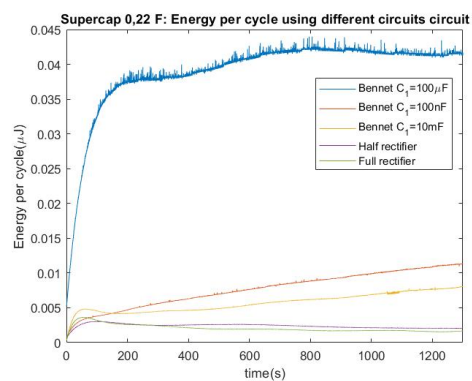
The used TENG is different to that of the previous sections, but since all the following measurements have been done utilizing the same nanogenerator, the obtained results are valid despite they appear different from the previous. In Fig.4.13 it is possible to see the voltage behavior, the total energy behavior and the energy per cycle behavior of  $C_{res}$  using all the mentioned circuits. Be careful that in those graphs the  $C_{store}$  is called  $C_1$ .



(a) Voltage.



(b) Total energy.



(c) Energy per cycle.

Figure 4.13: Voltage and energy stored using different conditioning circuits.

Studying separately the rectifiers and the three configurations of the Bennet's circuit, it immediately appears that the half rectifier is a little more efficient than the full one and, considering a long period of time, the Bennet's circuit is the one with the best performance. In fact, starting from the analysis of the voltage across the supercapacitor (Fig.4.13(a)), it can be noted that until 200 seconds passed, the difference among the half and full rectifier and the circuits named Bennet2 and Bennet3 is very small and the four different plots almost overlap. Then, observing the same plots, it is visible that using the two Bennet's circuits, the voltage continues to increase quite rapidly, instead with the two rectifier the voltage seems to have reached the saturation and so it increases very very slowly. In fact, after 1300 seconds the reached voltage using the two Bennet's circuits is bigger of 54%-90% than that achieved utilizing the rectifiers. In particular, Bennet1 reaches a voltage 54% bigger of the half wave rectifier and 64% bigger of the full wave rectifier, instead, Bennet2 reaches a voltage 78% bigger of the half wave rectifier and 90% bigger of the full wave rectifier. A separate discussion occurs for the Bennet's circuit which exploits the  $100\mu\text{F}$  as boost capacitor (Bennet3). In fact, it jumps on eye that this configuration exhibits the best performance. Looking at the voltage graph, it is easy to recognize that the blue line, which corresponds to that structure, is characterized by a very steep slope and, indeed, it achieves a potential difference of  $47.6\text{mV}$  against the only  $1.1\text{mV}$  of the full wave rectifier. Knowing the evolution of voltage across the capacitor and the value of this last, it is possible to find the total energy and the energy per cycle stored into the device, as already done in the previous sections. Their behaviors are reported into graphs (b) and (c) of Fig.4.13. Looking at the total energy, as expected, when the capacitor is driven by Bennet's circuits the energy stored is more. Particularly, using the Bennet1 circuit, the energy stored into the capacitor after 1300s is equal to  $250\mu\text{J}$  and the sharp slope of the curve gives good hope for a continuous rapid increase in the stored energy. In fact, observing the plots of the Bennet's circuits, it is possible to note a propensity to grow unlike those of rectifiers. The last very interesting analysis is on the stored energy per cycle. Observing Fig.4.13(c), it can be noted that the curves connected with the usage of the two rectifier show a rapid increase at the beginning and then a negative slope, in fact these curves seem to approach the  $0\text{J}$  per cycle. Instead, the plots linked to Bennet2 and Bennet3 exhibit a positive slope and the energy per cycle progressively rises. About the Bennet3 circuit, it shows a very big step at the begin and then the energy per cycle remains almost constant rising slowly. Once again this circuit displays the best behavior, the result is easily understandable observing the gap between the curve of this circuit and those of all the others. A curious discovery is that the performances of the circuit vary based on the used  $C_{res}$  capacitor. All the tested Bennet's circuits obtained best results in terms of efficiency, but both the voltage reached and the energy stored have been strongly influenced by the used boost capacitor. This means that, in order to accumulate the maximum amount of energy, it is necessary to calibrate perfectly the  $C_{res}$  basing on the tested TENG. The short investigation of this work of thesis underlined that the  $100\mu\text{F}$

capacitor always demonstrated to have the best output and so, when it has been used as boost capacitor, it turned out to be the right one to obtain the maximum hoped result. At the end of this analysis, in order to have a visible feedback of the TENG's capability to store energy for a later use, one of the used TENG has been exploited to charge the  $100\mu\text{F}$  capacitor by the Bennet's circuit. Then, the storage device has been connected to a red led through a mechanical switch. In Fig.4.14 it can be seen how, once the capacitor is charged enough, it can turn on the led.

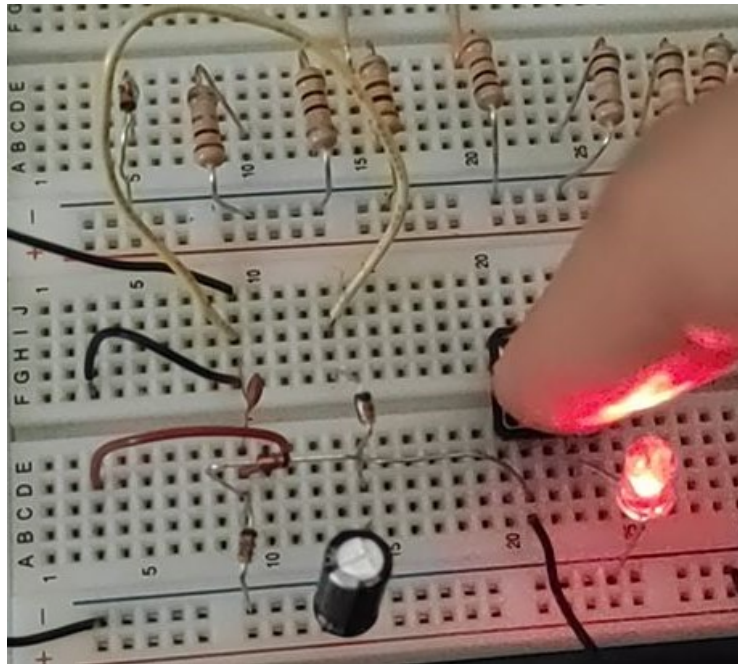


Figure 4.14: Led lighting via TENG.

---

---

## CHAPTER 5

---

# Material influence on TENG's performances

### 5.1 Triboelectric effect

In the first chapter, triboelectric nanogenerators have been introduced and their working mechanism has been explained. The principle on which this type of device is based is the triboelectric effect. It is a type of contact-induced electrification whose effect is well known because it is easily measurable and its consequences are common to see. In fact, when two different materials touch or rub, they electrically charge with opposite polarity. This natural event is so common that it is at the base of the electricity discovery, few centuries ago. The effects of triboelectricity can be observed with an extremely familiar example. In fact, when a plastic pen is rubbed on a fabric like wool or cotton, it results to be electrically charged and so it can attract small pieces of paper. The Greek philosopher Thales of Miletus in 6<sup>th</sup> century b.C. was the first man that observed and reported this phenomenon. He realized that rubbing a small piece of amber, it becomes able to attract small particles. Other very familiar events caused by triboelectrification are the sparks. They are, indeed, due to a rapid electric discharge of two materials previously charged by friction. It must be noted that these phenomena are less evident in humid environment because in this condition, the electrical conductivity of the air tends to increase and triboelectric charging is less favored. What described until now are only the results of triboelectrification, but not the explanation of the phenomenon. Nowadays, giving a definition of triboelectricity is not easy at all. In fact, what is the cause of this effect is not completely understood. Triboelectrification is considered an irreproducible phenomenon because too many factors influence the developed amount of charge. Among them, the characteristics of material surface can be surely mentioned together with the environmental conditions and the nature of contact. In fact, roughness, pre-treatments and damages on the surface strongly influence the charges accumulation. Furthermore, it was demonstrated that the maximum amount of charge is reached in vacuum condition, instead, humidity

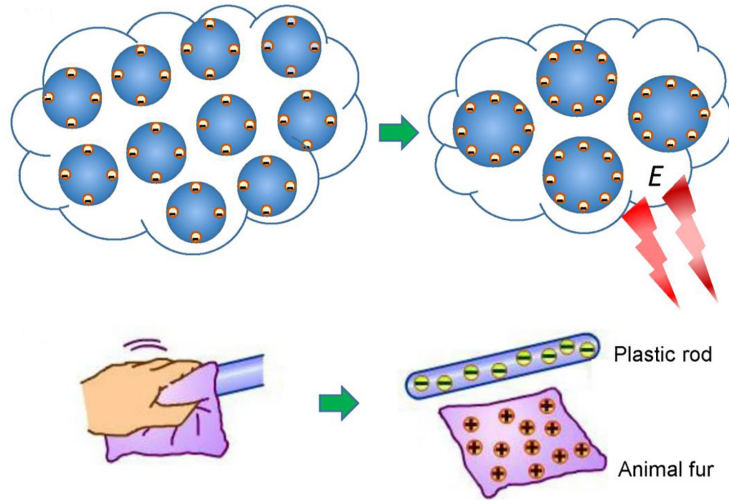


Figure 5.1: Triboelectrification example [9].

deeply reduce the contact electrification. Another important aspect to consider is the contact pressure that has a big impact on charge magnitude. The presence of a large number of parameters that could alter the result, contributed to the difficulty in the determination of a model which fully describes the triboelectric effect. The mechanism of triboelectrification is not completely clear and, nowadays, more than one model tries to present a solution able to include all the possible aspects. In particular, a quantitative model should be extremely useful to know in advance if the contact of two materials leads to a generation of charge and in which quantity. The predictability of the triboelectric effect could be very helpful not only in view of an exploitation of the charge in order to produce electrical power, but also to prevent some very dangerous damages. In fact, there are a lot of cases in which unwanted charges can cause product failure or safety hazards. For example, a spark is particularly unwanted in environments full of flammable vapors like petrol or methane gas. Moreover, in electronic CMOS integrated circuit, MOSFET could be accidentally destroyed due to high voltages produced by static discharge. This means that triboelectric effect must be considered also to protect designed product and human lives. The only sure thing about triboelectricity is that it is strongly linked with the types of material in contact. Furthermore, since this effect is characteristic of all the materials, it is much more difficult to find a model capable to include all of them with all their physical peculiarities. A lot of studies have been done in order to find a correlation between the generated charge and the chemical nature, the work function, the ion density, the charge affinity and also the thermionic emission of materials. The proposed models, until now, base the triboelectrification on electron transfer, ion transfer and material transfer. The first one occurs when the interatomic distance between two molecules of different materials is shorter than the bonding length. So, when two electron

clouds of different atoms/molecules overlap in a repulsive region, an electron transition appears. According to [9] the electron transfer is the main mechanism of charging in solid-solid, liquid-liquid, liquid-gas and liquid-solid contact. Wang, indeed, in this paper proposes a generic model valid for all the materials. On the same time, he suggests to use TENG devices for future studies about the argument. In many other papers presented in literature, a distinction among the types of material put in contact is made. For example, usually, the study is strongly different if it considered a metal or a dielectric and the analysis of triboelectrification between two dielectric materials is generally the most difficult. Particularly, a lot of issues come from the study of organic polymers, where electron transfer seems to be less and less important. There are, also, some models that try to quantify the generated charge by materials' contact [4, 11]. However, often, these models investigate only a small group of materials or, anyway, only a particular category. This means that, until now, empirical analysis is the only method to be sure that one material tends or not to accumulate charges.

**Triboelectric series** In the absence of an efficient way to catalogue materials based on their physical and chemical structure, listing materials according to their tendency to acquire positive or negative charges is the only technique to organize them and to avoid to test all the possible combinations. To do this it is necessary to define a standard method of measurement and use it for a large range of materials. In this way all the tested materials result analyzed under the same well-defined conditions. The obtained list is called triboelectric series and here, all the materials are organized in order of polarity from the most positively charged to the most negatively charged, or vice-versa. One example of triboelectric series has been already shown in the first chapter. According to the position in the series it is possible to have an idea of how effectively charges are exchanged. Since these lists are drawn up in an empirical way, the very interesting parameter to take into account is the distance between two materials that indicates their relative charge polarity. In fact, much more two materials are far each other, much charges are generated. This means that materials near each other tend to not exchange any charge, instead, materials that are at the at the opposites of the series may produce very high voltages and currents. The first triboelectric series was published in 1757 by Johan Carl Wilcke. Then, different laboratories expanded that series or published new ones including also synthetic polymers. Recently the Prof. Zhong Lin Wang's group tried to make a quantitatively standardized triboelectric series [11], it is shown in Fig.5.2 and Fig.5.3. Looking at these type of series, it is possible to choose in advance the materials in order to minimize the generation of charges if this effect could be dangerous. On the other hand, thanks to triboelectric series, materials can be chosen to maximize the amount of produced charge improving so the output performances of a TENG. Obviously, due to the empirical nature of triboelectric series, it is not rare to find little differences among them, caused by the different conditions in which the measurements have been performed.

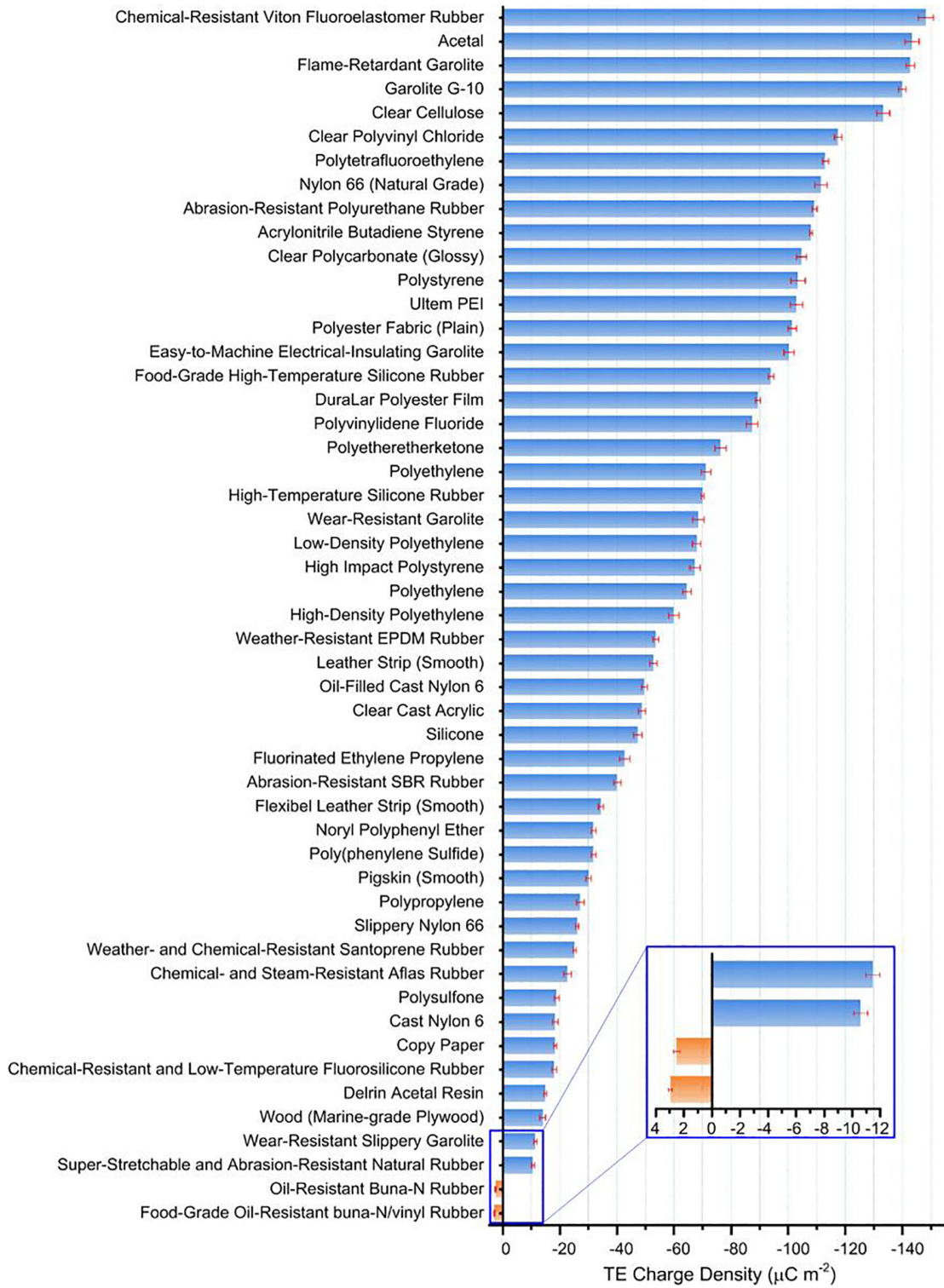


Figure 5.2: Quantified triboelectric series [11].

Table 1 Triboelectric series of materials and their triboelectric charge density (TECD)				
Materials	Abbr.	Average TECD ( $\mu\text{C m}^{-2}$ )	STDEV	$\alpha$
Chemical-Resistant Viton® Fluoroelastomer Rubber		-148.20	2.63	-1.31
Acetal		-143.33	2.48	-1.27
Flame-retardant garolite		-142.76	1.49	-1.26
Garolite G-10		-139.89	1.31	-1.24
Clear cellulose		-133.30	2.28	-1.18
Clear polyvinyl chloride	PVC	-117.53	1.31	-1.04
Polytetrafluoroethylene	PTFE	-113.06	1.14	-1.00
Abrasion-resistant polyurethane rubber		-109.22	0.86	-0.97
Acrylonitrile butadiene styrene	ABS	-108.07	0.50	-0.96
Clear polycarbonate (Glossy)	PC	-104.63	1.79	-0.93
Polystyrene	PS	-103.48	2.48	-0.92
Ultem polyetherimide	PEI	-102.91	2.16	-0.91
Polydimethylsiloxane*	PDMS	-102.05	2.16	-0.90
Polyester fabric (Plain)		-101.48	1.49	-0.90
Easy-to-machine electrical-insulating garolite		-100.33	1.79	-0.89
Food-grade high-temperature silicone rubber		-94.03	0.99	-0.83
Polyimide film	Kapton	-92.88	2.58	-0.82
DuraLar polyester film	PET	-89.44	0.86	-0.79
Polyvinylidene fluoride	PVDF	-87.35	2.06	-0.77
Polyetheretherketone	PEEK	-76.25	1.99	-0.67
Polyethylene	PE	-71.20	1.71	-0.63
High-temperature silicone rubber		-69.95	0.50	-0.62
Wear-resistant garolite		-68.51	1.99	-0.61
Low-density polyethylene	LDPE	-67.94	1.49	-0.60
High impact polystyrene		-67.37	1.79	-0.60
High-density polyethylene	HDPE	-59.91	1.79	-0.53
Weather-resistant EPDM rubber		-53.61	0.99	-0.47
Leather strip (Smooth)		-52.75	1.31	-0.47
Oil-filled cast nylon 6		-49.59	0.99	-0.44
Clear cast acrylic	PMMA	-48.73	1.31	-0.43
Silicone		-47.30	1.49	-0.42
Abrasion-resistant SBR rubber		-40.13	1.31	-0.35
Flexible leather strip (Smooth)		-34.40	0.86	-0.30
Noryl polyphenyl ether		-31.82	0.86	-0.28
Poly(phenylene Sulfide)	PPS	-31.82	0.86	-0.28
Pigskin (Smooth)		-30.10	0.86	-0.27
Polypropylene	PP	-27.23	1.31	-0.24
Slippery nylon 66		-26.09	0.50	-0.23
Weather- and chemical-resistant santoprene rubber		-25.23	0.50	-0.22
Chemical- and steam-resistant aflas rubber		-22.65	1.31	-0.20
Polysulfone		-18.92	0.86	-0.17
Cast nylon 6		-18.35	0.99	-0.16
Copy paper		-18.35	0.50	-0.16
Chemical-resistant and low-temperature fluorosilicone rubber		-18.06	0.86	-0.16
Delrin® Acetal Resin		-14.91	0.50	-0.13
Wood (marine-grade plywood)		-14.05	0.99	-0.12
Wear-resistant slippery garolite		-11.47	0.50	-0.10
Super-stretchable and abrasion-resistant natural rubber		-10.61	0.50	-0.09
Oil-resistant buna-N rubber		2.49	0.23	0.02
Food-grade oil-resistant buna-N/vinyl rubber		2.95	0.13	0.03

Note: STDEV refers to the standard deviation. The  $\alpha$  refers to the measured triboelectric charge density of tested materials over the absolute value of the measured triboelectric charge density of the reference material. The material marked with an asterisk "\*" means it has strong adhesion with mercury, a small drop of mercury is observed when it is separated with mercury. The measured TECD value may be a bit lower than its real value. Source data are provided as a Source Data file.

Figure 5.3: Quantified triboelectric series [11].

## 5.2 Analysis on triboelectric properties of materials

The purpose of this chapter is to verify if changing the contact material of the designed TENG it is possible to improve or to diminish the electrical performances of the triboelectric nanogenerator. The final result of this study is expected to be a sort of triboelectric series in which is possible to pick the material according to the best output and the wanted mechanical and physical properties. Following the advice in [9] the already made TENG has been used as reference to do this type of examination. This means that the PDMS is used as fixed material with which all the others will be compared. Until now, the designed TENG shown in Fig.2.14 has been used in single electrode mode, exploiting steel as contact material. Thus, after the analysis about the variation on TENG's behavior due to the change of the contact material, it could be interesting to detect if there is any change connected to the modification of the TENG operating mode. For this reason, this aspect is investigated in this chapter. In fact, some measurements has been done exploiting the contact-separation mode in double electrode. In this way, it is possible to put in comparison the outputs obtained by single electrode and double electrode working mechanism and so to declare which is the best one. For all the following measurements, a new TENG, similar to that in Fig.2.14, has been used, exploiting a NaCl 1 mol/L hydrogel as electrode. Even if the outcomes presented in this chapter can seem different from that already described in other chapters, the variation is due uniquely to the fact that this nanogenerator has been made in a different time than the previous. However, since the following analysis has been executed utilizing the same TENG, the obtained results are valid and allow to achieve the proposed goal. The configuration in which the measures have been performed is the same described in the third chapter and also the used instruments are the same. The designed TENG has been located on the shaker's top plate that, oscillating at a frequency of 5Hz, allows the periodic contact between the TENG and a suspended steel bar. By attaching layers of different materials on the bar, it is possible to monitor the behavior of the TENG in contact with various substances. It is important to underline that the maximum achieved acceleration of the shaker plate during these measures is  $40m/s^2$ . Moreover, all the measurements described in this chapter have been executed in open circuit configuration for the voltage and in short circuit configuration for the current. This means that the obtained outputs are close to the maximum possible. Thus, if an external circuit is used, the outputs will vary according to the selected load.

### 5.2.1 Single electrode mode

The first made analysis is about how much the material that touches the designed TENG influences the output performances of the nanogenerator itself. To do this, different materials have been attached to the steel bar. Thus, voltage and current outputs have been taken directly from the TENG, exploiting the circuital configuration respectively of Fig.3.2

and Fig.3.9. For this experimental part the following materials have been used:

- aluminum;
- smooth and very thin paper;
- common paper;
- indium tin oxide (ITO);
- steel;
- copper;
- polyvinylidene fluoride (PVDF);
- polyethylene terephthalate (PET);
- polyimide (Kapton).

Having a look at the triboelectric series in Fig.1.2 and Fig.5.3 it is easy to understand that in the previous list, the materials are organized according to their polarity. Aluminum should be the most triboelectric positive among the tested materials and, instead, Kapton should be the most triboelectric negative. It is notable that, differently to all the other materials, ITO is not included into a lot of triboelectric series. One of the few papers where it appears in a series, has been written by Sungwoo Hwang and et al.[34] in 2016. Fig.5.4 is taken by their article and it is possible to see that ITO is located between PET and aluminum. However, it is important to keep in mind that the used triboelectric nanogenerator is made in PDMS so also this material should be taken into account. Particularly, PDMS results to be the most triboelectrically negative material among the mentioned, but it is not very different from Kapton. This means that all the tested materials are theoretically more triboelectrically positive than the PDMS. What it is expected to find is that the PDMS should collect negative charges in each configuration.

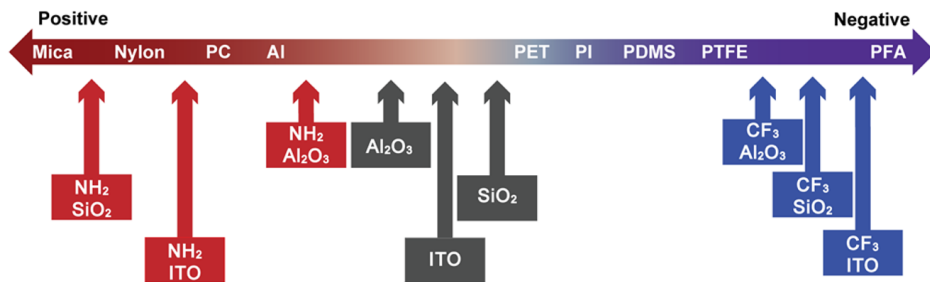


Figure 5.4: Triboelectric series containing ITO [34].

**Voltage analysis** Making a voltage analysis, it is evident that the PDMS tends to accumulate charges showing a capacitive-like behavior similar to that visible in Fig.3.3. It is notable that the rate at which it accumulates charge varies depending on the material that touches it. In the graph reported in Fig.5.5(a), it appears clear that, exploiting ITO as contact material, PDMS tends to charge much more faster. In fact, after 50 seconds a voltage of -56V is detectable on the PDMS. In order to understand the difference in charging rate, just think that when ITO is used, the PDMS achieves, in 50 seconds, a voltage almost 44V lower than all the other configurations. In Fig.5.5(b) the same graph is reported, but this time the curve which refers to ITO has been eliminated in order to allow a better vision of the differences among all the other materials that show a more similar behavior. Analyzing this chart, it can be noted that almost all the tested materials

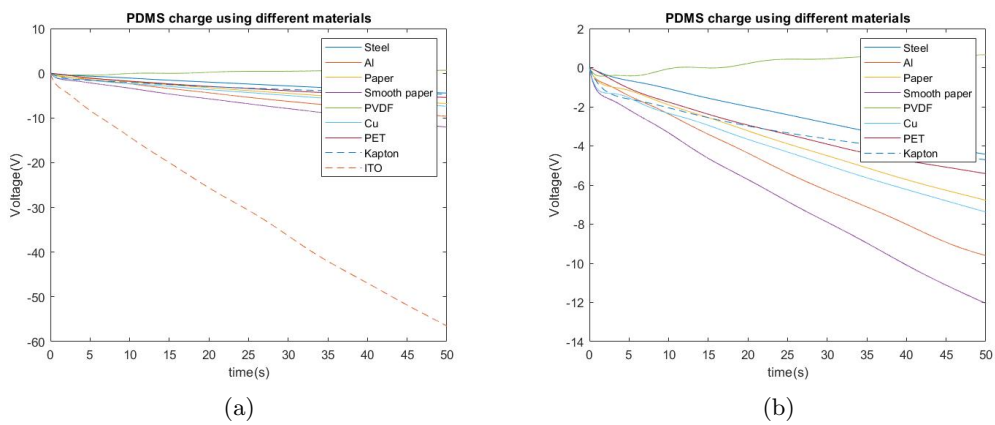


Figure 5.5: Charging behaviors of PDMS using different materials.

tend to negatively charge the PDMS. In fact all the curves, apart from that connected with PVDF, show a negative slope and so a negative voltage is detected which decreases in time. The only exception is the PDVF plot. In fact, in this case the curve has a positive slope, meaning that this material induces a positive charge in the PDMS. Nevertheless, if it is considered that after 50 seconds only a voltage of 0.66V has been detected, it is easy to imagine that the stored charge into the PDMS is not a lot. Looking at the triboelectric series in Fig.5.3, it is easy to verify that the PDVF and the PDMS are very near and this means that, even if the PDMS is more triboelectrically negative, there is not so much difference in their polarity. Thus, a small variation in the PDVF surface is sufficient to change its triboelectric properties just enough to be more negative polarized than the PDMS. After the investigation about the accumulated charge on the TENG surface, surely it is interesting to evaluate the voltage sinusoidal output. In fact, talking about nanogenerators, it is the desired and exploitable quantity. In order to examine the differences due to the usage of separate materials, all the output voltages have been put in sequence and are visible in Fig.5.6. The graph, indeed, is divided into 9 parts, one per

each tested materials.

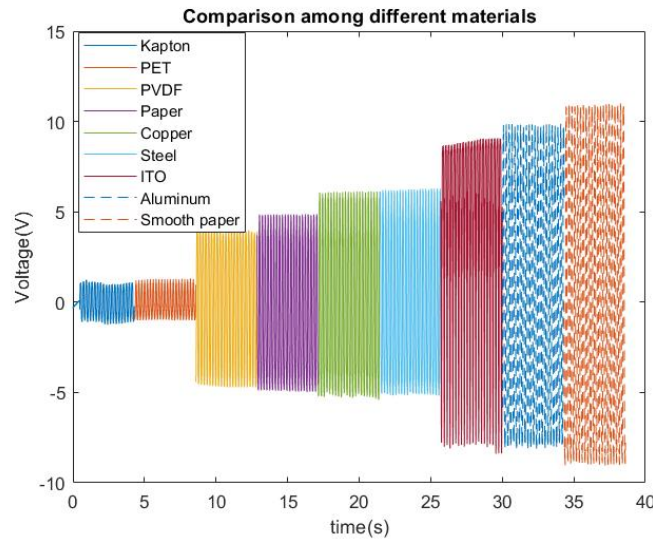


Figure 5.6: Single-electrode TENG voltage output using different materials.

Looking at Fig.5.6, some consideration can be immediately made. In fact, the curves corresponding to PET and Kapton are rapidly recognizable at the beginning of the graph. They present the lowest peak values. On the other hand, the smooth paper would seem to have the highest peak value. The exploitation of ITO and copper seem to have more or less the same effect on the TENG output voltage. Instead, the dissimilarities among the other waves are not very well defined in this figure. It must be considered that, as already discovered thanks to Fig.3.5, the peak voltage tends to increase in time during the stressing. Taking into account this effect, it has been obtained the bar chart in Fig.5.7 which provide a more clear vision. Here there are reported the average peak-to-peak values of the voltage output waves measured from the TENG in contact with the tested materials. These values have been organized in way to have a sort of list of materials. In fact, observing this graph it is possible to recognize a triboelectric series. It is interesting to verify if the found relative positions comply those reported in the triboelectric series displayed before. Starting from the bottom, it can be noted that PDVF bar is set in a different position than the others. This choice has been made in order to underline the relative polarity of the material which the bar refers compared to PDMS. In the case under analysis since PDVF is the only one that leads to a different charge on the silicone surface, its bar is positioned toward the negative direction. As regard peak-to-peak magnitude, Kapton and PET are almost equal and present the lowest value with only 1.7V generated. Considering that these materials are very near to PDMS in Fig.5.2, the obtained result can be considered extremely valid. The commented values are followed, after a big gap, by the output obtained using PVDF as contact material, with a peak-to-peak value of

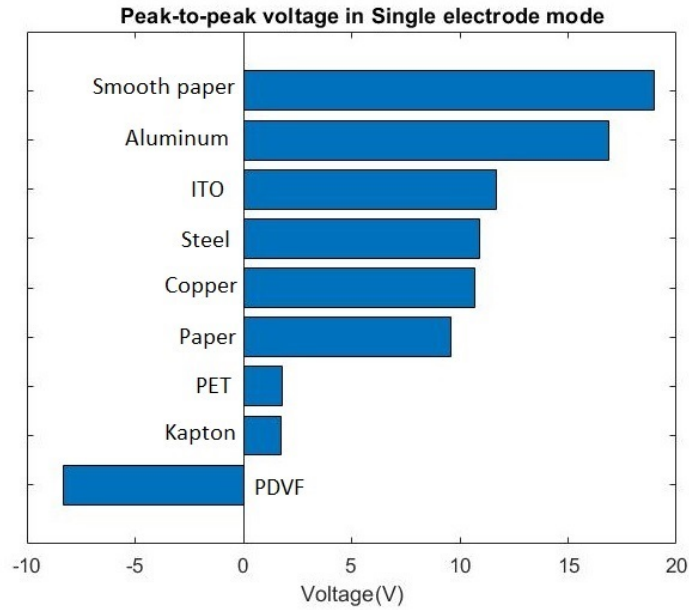


Figure 5.7: Comparison among peak-to-peak voltage values.

about 8V. A peculiar situation is found for the paper. In fact, depending on the type of used paper, the output voltage can be the highest detected or in the middle of the graph. Particularly, utilizing the common paper it is obtained a peak-to-peak value of 9.5V, in the middle between those obtained by the PDVF and the copper. Instead, thanks to the smooth and thin paper, the voltage output achieved by the TENG is the highest one, with a peak-to-peak value of almost 19V. Neither of the two values obtained exploiting the paper can be considered in the correct position according to the triboelectric series of Fig.1.2. This probably means that, especially with this material, the surface roughness and the superficial variations have a big impact on the output performances. Following in the description of Fig.5.7, after paper, from the bottom to the top, there are in sequence copper, steel and ITO. Particularly, the first two materials show a very similar behavior, instead the ITO allows to obtain an output voltage some volts higher. A remarkable value is achieved by the TENG when aluminum is used as contact material. In fact, in this configuration, the reached peak-to-peak value is of almost 17V confirming the fact that aluminum is one of the most triboelectrically positive materials.

**Current analysis** The current investigation has been performed in short-circuit configuration, using the electrometer as ammeter. As happened for other current waves already described, also now they appear like a series of impulses. Depending on the material with which the designed TENG comes in contact, the output current vary a lot. Using materials

triboelectrically similar to PDMS, current peaks are of the order of tens of nanoampere. This is valid exploiting both Kapton and PET. A particular behavior is that of the current wave obtained by the TENG stimulated with PVDF. In fact, in this case, the wave shape appears different from all the others. To better understand this, PVDF current wave is put in comparison with the aluminum one in Fig.5.8. As it is possible to see, in all the tested configurations, the highest peaks are positive, with the only exception of that which exploit PVDF. In fact, in this last the higher peaks are negative. This divergence is due to the fact that when the PVDF is used, PDMS tends to charge positively (as explained in the paragraph of the voltage analysis) and so, the flux in which the majority of charges moves has an opposite direction compared to all the other cases. To conclude this anal-

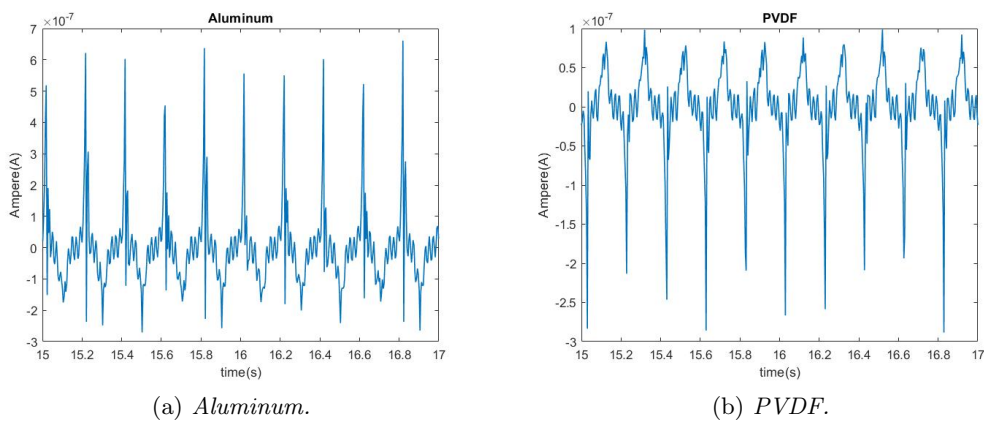


Figure 5.8: Aluminum (a) and PDVF (b) current wave.

ysis, the detected current peak values of the different configurations have been organized in a graph similar to that of Fig.5.7. The aim is to verify if the series found in this way matches perfectly or not that of Fig.5.7. The collected data of current are displayed in Fig.5.9. Although the bar heights are different in the two graphs, the series of materials is almost the same. Particularly, the two fit together perfectly apart from the steel that led to current peaks lower than expected. Except for this small imperfection, the current and voltage performances in a TENG are strongly connected to the triboelectric materials used.

### 5.2.2 Double electrode mode

Typically, single electrode TENGs are considered the triboelectric nanogenerators with the worst performances. Double electrode TENGs, instead, tend to have higher outputs. In order to made a comparison between these two working modes, now it is presented a performed analysis about double electrode TENGs. In this work of thesis, the double electrode TENGs are made in a very rudimentary way, simply using the same configurations already presented in the paragraph before. The designed single electrode nanogenerator of

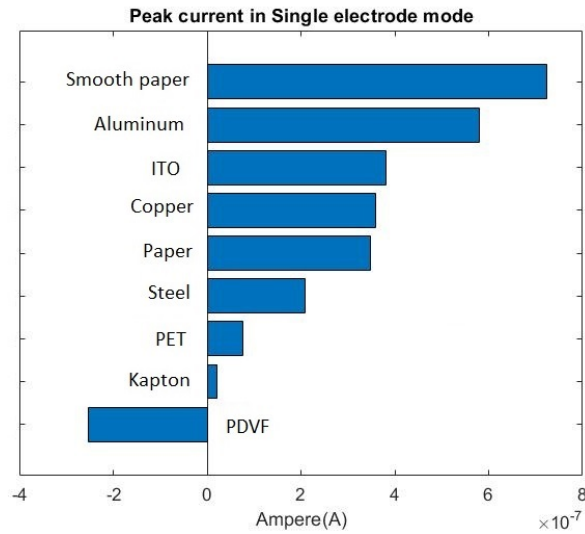


Figure 5.9: Comparison among peak-to-peak current values.

Fig.2.14 constitutes half of the device and the material with which it comes in contact acts as second electrode. In fact, if one end of the electrometer is connected to the second material instead to be connected to ground, current and voltage of a double electrode TENG are detected. Of course, the described structure cannot be considered a finished device, however the performed analysis could be a preliminary study in order to understand the behavior and the possible advantages of one working mode compared to the other. Since the half formed by the designed single electrode TENG is fixed, the only variable in this investigation is the contact material. For this role, almost all the materials previously used are employed. In the earlier study, the suspended bar located above the shaker has been directly used in order to have a contact with the steel, but now, since it is impossible to connect a cable to the bar, the analysis with the steel is avoided. For the sake of clarity, the tested contact materials are listed here:

- aluminum;
- smooth and very thin paper;
- common paper;
- indium tin oxide (ITO);
- copper;
- polyvinylidene fluoride (PVDF);
- polyethylene terephthalate (PET);

- polyimide (Kapton).

Only some of the mentioned materials are conductive: aluminum, ITO and copper. For all the others it is necessary to attach a conductive electrode on the back side in order to monitor the generated charges on the material. To do this a thin layer of gold is deposited on Kapton, on PDVF and on the two types of paper. PET, instead, is deposited onto ITO. This choice has been made because the PET layer is transparent and, especially, ITO is an almost transparent conductive material, even if it remains slightly opaque. The foil obtained by the superposition of PET and ITO is shown in Fig.5.10. The transparency is evident since it is possible to see completely the hand that stand the sheet. Thus, the combination of PDMS, PET and ITO can be perfect in order to build a transparent double electrode TENG, allowing any type of visual information transmission. In order



Figure 5.10: Conductive foil made of PET and ITO.

to made a comparison between the performances of single-electrode and double-electrode TENG, also now the measurements have been performed in open circuit for the voltage and in short circuit for the current. In the first case, the electrometer is able to detect the potential difference between the PDMS and the other used material. Instead, in the second case, the same instrument (that this time acts like an ammeter) allows the flowing of charges between the two triboelectric materials and so can monitor the current value. In this section, the descriptions of the individual measurements are less detailed because the considerations to be highlighted are extremely similar to those already made for the

single electrode configuration. The voltage waves tracked by the voltmeter are reported

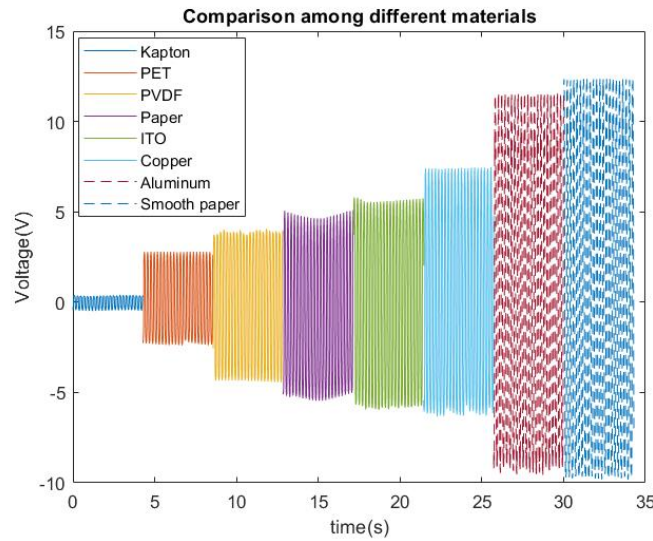


Figure 5.11: Double-electrode TENG voltage output using different materials.

in figure Fig.5.11. In this figure, all the detected waves are put in sequence. On the left, it is recognizable a sinusoidal curve characterized by a very small peak value. This is the wave connected to the use of Kapton as second triboelectric material. The second smallest peak is that shown by the TENG which exploits PET. This output, despite is one of the smallest, is considerably higher than that obtained using the Kapton. On the other hand, the maximum output voltage seems to be that linked with the smooth and thin paper. In fact this wave have a very high peak value which is able to slightly exceed even that produced by aluminum. According to the few examinations made until now, it would seems that the differences in performance due to the exploitation of various materials are still valid. In particular, the polarity and the mutual position in the triboelectric series continue to have a great relevance in the voltage output. In order to verify in which manner this is true and if the whole study made for the single electrode mode continues to be solid also for the double electrode one, on the basis of the above investigation, the collected data have been organized in two summary graphs. They are presented in Fig.5.12. The charts in Fig.5.12 are similar to those of Fig.5.9 and Fig.5.7 which refer to single electrode TENG. The analogy among those figures makes comparison easy. All the mentioned graphs can be associated to a triboelectric series and it is remarkable that the relative position of the material analyzed is always the same. This result is relevant because underlines how, despite the used working mode, the materials which form the TENG have always the same influence, tending to increase or decrease the outputs. However, comparing the outcomes of the single electrode mode with those of the double electrode one, what can be noted is that in the second case, some outputs are higher. However, the discrepancy is not very

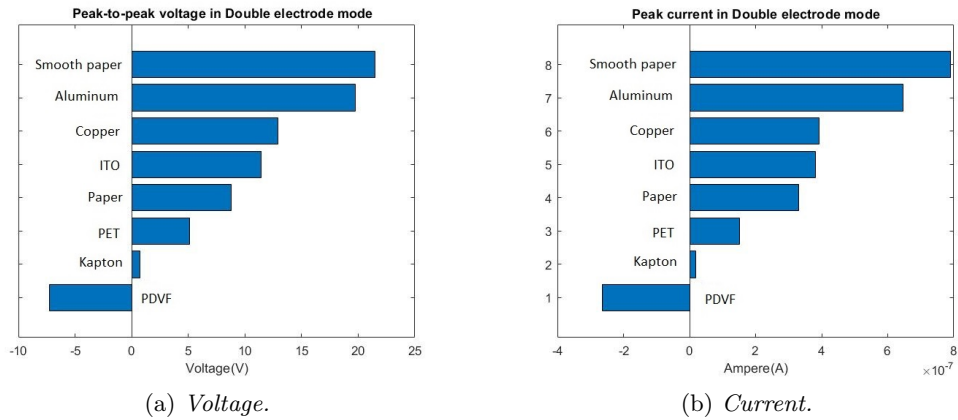


Figure 5.12: Comparison among voltage (a) and current (b) output values using double-electrode TENG.

relevant. For instance, the TENG which exploits the smooth paper shows a peak-to-peak voltage of 21.5V in double electrode against the 19V in single electrode. Particularly, it seems that as more the used material is far from the centre of the triboelectric series, more the difference between single electrode and double electrode mode appears to be relevant. This is due to the fact that materials located in the middle of the triboelectric series tend not to accumulate charges on their surface and so they have a lower influence in the output. In conclusion, double electrode TENG would be beneficial compared to single electrode one, but the real advantage must be evaluated basing on the real usage and the cost-effectiveness of the device.

---

## Conclusion

The aim of this thesis work was the design and the fabrication of an energy harvesting system exploiting a triboelectric nanogenerator (TENG). This recent, but very promising technology can be efficiently used in a wide range of applications from the civil to the military environment. In fact, thanks to their easy integration with the uniform, TENGs can offer an alternative supply for the wearable electronics belonged to soldier's equipment, enabling also a consistent lightening of the load carried by warfighters. For all these reasons, the wanted device would have to be flexible and suitable to be used into a wearable context. All these purposes have been respected and a perfectly working prototype has been obtained. The designed nanogenerator comes out thanks to a meticulous attention on the chosen materials. A well known silicone, the polydimethylsiloxane (PDMS), together with a water-based polymeric structure, the hydrogel, allowed the realization of a flexible, soft, stretchable, low cost, resistant, transparent, bio-compatible and biodegradable device. Following these conditions, the presented work resulted, in its first part, in an analysis about the usage of ionic-hydrogels (ionogel) as conductive electrodes. In order to highlight how the dissolved percentage of salt (essential ionogel component) influences the performances of the triboelectric device, different hydrogel samples, characterized by different molar concentrations of salt, have been tested. The trial revealed that the 1 mol/L of NaCl is the best molar concentration for a ionogel that should be used as TENG electrode. The device characterization continued with a study on the matching impedance and on the maximum produced power density. The obtained results are worth and show a maximum power density of almost  $100mW/m^2$  in correspondence of an external resistance of  $100M\Omega$ . Then, the study about an effective conditioning circuit capable to handle power and to store energy into capacitors and supercapacitors has been carried on. Among the three tested circuital configurations, the half wave rectifier is resulted the one able to perform the fastest charge, but the Bennet's circuit demonstrated to overcome the limit of capacitor's saturation, allowing a slower but continuous charging with a consequent storing of much more energy in time. Finally, a study on the triboelectricity and on the triboelectric series proved that it is possible to improve the TENG's outputs exploiting the contact with the most triboelectrically positive materials.

---

## Bibliography

- [1] *Venkateswaran Vivekananthan, Arunkumar Chandrasekhar, Nagamalleswara Rao Aluri, Yuvasree Purusothaman, Gaurav Khandelwal and Sang-Jae Kim.* Triboelectric Nanogenerators: Design, Fabrication, Energy Harvesting, and Portable- Wearable Applications. 2020
- [2] *Dong Wook Kim<sup>1</sup>, Ju Hyun Lee<sup>2</sup>, Jin Kon Kim<sup>2</sup> and Unyong Jeong.* Material aspects of triboelectric energy generation and sensors. 2020
- [3] *Army AL and T Staff.* [asc.army.mil/web/access-log-the-energy-circuit](http://asc.army.mil/web/access-log-the-energy-circuit) The Energy Circuit. A roundup of projects and efforts to power change in Army energy. 2020
- [4] *Haiyang Zou, Litong Guo, Hao Xue, Ying Zhang, Xiaofang Shen, Xiaoting Liu, Peihong Wang, Xu He, Guozhang Dai, Peng Jiang, Haiwu Zheng, Binbin Zhang, Cheng Xu, Zhong Lin Wang.* Quantifying and understanding the triboelectric series of inorganic non-metallic materials. 2020
- [5] *Diana Cafiso.* DLP-3D printable cellulose-based hydrogels. 2020
- [6] *Dong Wook Kim, Ju Hyun Lee, Jin Kon Kim, Unyong Jeong.* Material aspects of triboelectric energy generation and sensors. 2020
- [7] *Rajesh Uppal.* Military transforming from wearables into Smart and Intelligent textiles that combine sensing, actuation, communication and processing into the fabric. 2020
- [8] *Jiaqing Xiong and Pooi See Lee.* Progress on wearable triboelectric nanogenerators in shapes of fiber, yarn, and textile. 2019
- [9] *Zhong Lin Wang, Aurelia Chi Wang.* On the origin of contact-electrification. 2019
- [10] *Chunlong Fang, Tong Tong, Tianzhao Bu, Yuanzhi Cao, Shaohang Xu, Youchao Qi, and Chi Zhang.* Overview of Power Management for Triboelectric Nanogenerators. 2019
- [11] *Haiyang Zou, Ying Zhang, Litong Guo, Peihong Wang, Xu He, Guozhang Dai, Haiwu Zheng, Chaoyu Chen, Aurelia Chi Wang, Cheng Xu, Zhong Lin Wang.* Quantifying the triboelectric series. 2019
- [12] *Sofia Scataglini, Giuseppe Andreoni, Johan Gallant.* Smart Clothing Design Issues in Military Applications. 2019
- [13] *Ding Zhang, Yuanhao Wang, Ya Yang.* Design, Performance, and Application of Thermoelectric Nanogenerators. 2019

- [14] *Kun Zhao, Yuanhao Wang, Lu Han, Yongfei Wang, Xudong Luo, Zhiqiang Zhang<sup>5</sup>, Ya Yang<sup>1</sup>*. Nanogenerator-Based Self-Charging Energy Storage Devices. 2019
- [15] *Lijie Sun, Shuo Chen, Yifan Guo, Jianchun Song, Luzhi Zhang, Lijuan Xiao, Qingbao Guan, Zhengwei You*. Ionogel-based, highly stretchable, transparent, durable triboelectric nanogenerators for energy harvesting and motion sensing over a wide temperature range. 2019
- [16] *Qingbao Guan, Guanghui Lin, Yuzhu Gong, Jingfeng Wang, Weiyi Tan, Dequan Bao, Yina Liu, Zhengwei You, Xuhui Sun, Zhen Wen and Yue Pan*. Highly efficient self-healable and dual responsive hydrogel-based deformable triboelectric nanogenerators for wearable electronics. 2019
- [17] *Ali Ghaffarinejad, Javad Yavand Hasani, Dimitri Galayko, Philippe Basset*. Superior performance of half-wave to full-wave rectifier as a power conditioning circuit for triboelectric nanogenerators: Application to contact-separation and sliding mode TENG. 2019
- [18] *Ting Liu, Mengmeng Liu, Su Dou, Jiangman Sun, Zifeng Cong, Chunyan Jiang, Chunhua Du, Xiong Pu, Weiguo Hu, and Zhong Lin Wang*. Triboelectric-Nanogenerator-Based Soft Energy-Harvesting Skin Enabled by Toughly Bonded Elastomer/Hydrogel Hybrids. 2018
- [19] *Ronan Hincheta, Ali Ghaffarinejad<sup>b,c</sup>, Yingxian Lub, Javad Yavand Hasanic, Sang-Woo Kima, Philippe Basset<sup>b</sup>*. Understanding and modeling of triboelectric-electret nanogenerator. 2018
- [20] *Yongshan Hu, Qiuqin Yue, Shan Lu, Dongchen Yang, Shuxin Shi, Xiaokun Zhang and Hua Yu*. An Adaptable Interface Conditioning Circuit Based on Triboelectric Nanogenerators for Self-Powered Sensors. 2018
- [21] *Canhui Yang and Zhigang Suo*. Hydrogel ionotronics. 2018
- [22] *Jiangman Sun, Xiong Pu, Mengmeng Liu, Aifang Yu, Chunhua Du, Junyi Zhai, Weiguo Hu and Zhong Lin Wang* Self-Healable, Stretchable, Transparent Triboelectric Nanogenerators as Soft Power Sources. 2018
- [23] *Kofi Sarpong Adu-Manu, Nadir Adam, Cristiano Tapparelo, Hoda Ayatollahi, and Wendi Heinzelman*. Energy-Harvesting Wireless Sensor Networks (EH-WSNs): A Review. 2018
- [24] *Joseph Swanner, Jo Bito, Gregory Nichols, Xuanke He, Joel Hewett, and Manos M. Tentzeris*. Homeland Defense and Security Information Analysis Center, Oak Ridge, U.S.A. Georgia Institute of Technology, Atlanta, U.S.A. Integrating Multiple Energy Harvesting Systems for Department of Defense Applications. 2018
- [25] *Ali Ghaffarinejad, Javad Yavand Hasani, Ronan Hinchet, Yingxian Lu, Hemin Zhang, Armine Karami, Dimitri Galayko, Sang-Woo Kim, Philippe Basset* A conditioning circuit with exponential enhancement of output energy for triboelectric nanogenerator. 2018
- [26] *Seung-Bae Jeona, Sang-Jae Parka, Weon-Guk Kim, Il-Woong Tcho, Ik-Kyeong Jin,*

- Joon-Kyu Han, Daewon Kim, Yang-Kyu Choi.* Self-powered wearable keyboard with fabric based triboelectric nanogenerator. *2018*
- [27] *Xiaofeng Wang, Yajiang Yin, Fang Yi, Keren Dai, Simiao Niu, Yingzhou Han, Yue Zhang, Zheng You.* Bioinspired stretchable triboelectric nanogenerator as energy-harvesting skin for self-powered electronics. *2017*
- [28] *Yeon Joo Kim, Jaejun Lee, Sangwon Park, Chanho Park, Cheolmin Park and Heon-Jin Choi.* Effect of the relative permittivity of oxides on the performance of triboelectric nanogenerators. *2017*
- [29] *Xiong Pu, Mengmeng Liu, Xiangyu Chen, Jiangman Sun, Chunhua Du, Yang Zhang, Junyi Zhai, Weiguo Hu, Zhong Lin Wang.* Ultrastretchable, transparent triboelectric nanogenerator as electronic skin for biomechanical energy harvesting and tactile sensing. *2017*
- [30] *Yang Wang, Ya Yang and Zhong Lin Wang.* Triboelectric nanogenerators as flexible power sources. *2017*
- [31] *Joel J. P. C. Rodrigues, Senior Member, IEEE, Dante B. R. Segundo, Heres A. Junqueira, Murilo H. Sabino, Rafael M. Prince, Jalal Al-Muhtadi and Victor Hugo C. de Albuquerque* Enabling Technologies for the Internet of Health Things. *2017*
- [32] *Fengben Xia, Yaokun Panga, Wei Lia, Tao Jianga,b, Limin Zhanga, Tong Guoa, Guoxu Liua, Chi Zhanga,b, Zhong Lin Wang.* Universal power management strategy for triboelectric nanogenerator. *2017*
- [33] *P. Basset, E. Blokhina, D. Galayko, Wiley, Hoboken.* Electrostatic kinetic energy harvesting. *2016*
- [34] *Kyung-Eun Byun, Yeonchoo Cho, Minsu Seol, Seongsu Kim, Sang-Woo Kim, Hyeon-Jin Shin, Seongjun Park, and Sungwoo Hwang.* Control of Triboelectrification by Engineering Surface Dipole and Surface Electronic State. *2016*
- [35] *Yunlong Zi, Simiao Niu, Jie Wang, Zhen Wen, Wei Tang & Zhong Lin Wang.* Standards and figure-of-merits for quantifying the performance of triboelectric nanogenerators. *2015*
- [36] *Richard Trenholm.* Wearables at war: How smart textiles are lightening the load for soldiers. *2015*
- [37] *Naziha Chirani, L'Hocine Yahia, Lukas Gritsch, Federico Leonardo Motta, Soumi-Chirani, Silvia Fare.* History and Applications of Hydrogels. *2015*
- [38] *Richard Trenholm.* Wearables at war: How smart textiles are lightening the load for soldiers. *2015*
- [39] *Sofia Scataglini, Giuseppe Andreoni, Johan Gallant.* A Review of Smart Clothing in Military. *2015*
- [40] *Maria Assunta Navarra, Chiara Dal Bosco, Judith Serra Moreno, Francesco Maria Vitucci, Annalisa Paolone and Stefania Panero.* Synthesis and Characterization of Cellulose-Based Hydrogels to Be Used as Gel Electrolytes. *2015*

- [41] *Joe Briscoe, Steve Dunn.* Piezoelectric nanogenerators – a review of nanostructured piezoelectric energy harvesters. *2015*
- [42] *Mikaela Börjesson and Gunnar Westman.* Crystalline Nanocellulose — Preparation, Modification, and Properties. *2015*
- [43] *Sihong Wang , Yannan Xie , Simiao Niu , Long Lin , Chang Liu , Yu Sheng Zhou , and Zhong Lin Wang.* Maximum Surface Charge Density for Triboelectric Nanogenerators Achieved by Ionized-Air Injection: Methodology and Theoretical Understanding. *2014*
- [44] *W. Tang, T. Zhou, C. Zhang, F.R. Fan, C.B. Han, Z.L. Wang.* Nanotechnology 25. *2014*
- [45] *Zhong Lin Wang.* Triboelectric nanogenerators as new energy technology and self-powered sensors – Principles, problems and perspectives. *2014*
- [46] *A.C.M. de Queiroz, M. Domingues.* The doubler of electricity used as battery charger, IEEE Trans. Circuits Syst. II Express Briefs. *2011*
- [47] *O. Sahin, O. Kayacan, E. Yazgan Bulgun Dokuz Eylul University Engineering Faculty, Izmir; Turkey.* Smart Textiles for Soldier of the Future. *2005*
- [48] *A. Bennet XXVII.* An account of a doubler of electricity, or a machine by which the least conceivable quantity of positive or negative electricity may be continually doubled, till it becomes perceptible by common electrometers, or visible in sparks. *1787*
- [49] *en.wikipedia.org/wiki* Polydimethylsiloxane.
- [50] *www.thoughtco.com* What Is Cellulose? Facts and Functions.